Structural performance of a three dimensional bio-based parametric structural element, through additive manufacturing

Master Thesis

L.M.J. Roex

Eindhoven, December 2023

Final version 1.0

Title	Structural performance of a three dimensional bio-based parametric structural element, through additive manufacturing
Subtitle	Master thesis
Date	21-12-2023
Place	Eindhoven
Author	L.M.J. (Luc) Roex
Student number	1637533
Email address	l.m.j.roex@student.tue.nl luc@roex.nl
Department	Built Environment
Master	Architecture, Building and Planning
Master track	Structural Engineering and Design
Chair	Innovative Structural Design
Graduation committee	Ir. A.P.H.W. Habraken Assistant Professor Innovative Structural Design Dr. Ir. S.P.G. Moonen Associate Professor Innovative Structural Design Ir. A.D. Deetman MSc Concrete & Masonry Structures

Preface

Addressing environmental problems and thereby improving the construction industry has always interested me. In course Resource Efficient Structural Engineering and Design given by Ir. A.P.H.W. (Arjan) Habraken all these aspects came together. The reduction of material use and the use of bio-based materials provided opportunities for research topics. Exploratory discussions with Ir. A.P.H.W. (Arjan) Habraken soon led to the research topic, 3D printing of bio-based materials.

This research project is part of the Resource Efficient Structural Engineering and Design (RESED) workshop within the Innovative Structural Engineering and Design chair. This project focuses on 3D printing of a parametric structural element consisting of bio-based material to reduce environmental pollution and create opportunities for structural design. This graduation project was carried out together with Franka Pels Rijcken and is part of the master track Structural Engineering and Design (SED) within the master Architecture, Building and Planning (ABP) at TU/e.

I would like to thank my supervisors for their feedback and support during the project. At the beginning of the project, we did not know where this project would end because of its innovative nature. I'm thankful for the time you gave me to establish the topic of my thesis project and to develop it. I would also like to mention a few personal contributions from you for which I am particularly grateful: Ir. A.P.H.W. Habraken - that I was allowed to be part of your thesis studios, for sharing your views on different topics and for the weekly feedback which was very helpful. Ir. A.H. Deetman - for sharing his knowledge on robots. Dr. Ir. S.P.G. Moonen - for being involved and sharing his knowledge on bio-based materials.

In addition to my supervisors, I would like to thank fellow student Franka Pels Rijcken for collaboration during the thesis project. Sharing your knowledge, brainstorming and discussing the topic often brought me new insights. The experience I gained from you and your advice were helpful in bringing this project to a successful conclusion.

I would like to thank the two former TU Delft students C. Bierach and A. Alberts Coelho. for getting us started with printing a bio-based material. I would also like to thank the SED lab staff and especially H.M.L. Lamers for his support and involvement during the production and testing phase of the project. Finally, a special thanks to my fellow students. D. Janssen and R.T. Damoiseaux for their helping hands during the printing process.

Luc Roex

Eindhoven, December 2023

Abstract

This research project focused on the structural performance of an optimized three-dimensional parametric structural element (column) consisting of bio-based material. The manufacturing of this one-meter-high column is by means of additive manufacturing. During this research, different materials, printability and material properties were investigated and documented. Whereby different aspects of the research question were approached and the necessary basis was created to answer it.

The research was started with a literature review on what types of forms of additive manufacturing exist. Based on this study and the knowledge available within TU/e about 3D concrete printing, the choice was made to print on the basis of the DIW method. A further literature search was then carried out to find out what type of bio-based mixtures are printable using this method. This research resulted in two highly promising printable wood mixtures based on cellulose and lignin as designed by C. Bierach and A. Coelho in 2022. The first mixture consists of cellulose, lignin, methylcellulose and water. This mixture is 100% bio-based. The second mixture consists of cellulose, lignin and woodglue. This is mixture is not fully bio-based because the glue is polyvinyl acetate-based.

In the materials research phase, these two mixtures were simulated. It was soon found that the mixture with methylcellulose did not show much promise, as it went mouldy and extruder resistance was not optimal. As a result, all focus was put on the mixture with woodglue. In the mixture of by C. Bierach and A. Coelho, the percentage of woodglue of 65,4% appeared to be too high compared to the other added materials. The result of the material research was two new highly promising printable mixtures. In one mixture, the percentage of woodglue was reduced to 43,3% and the other mixture consisted of bio-glue. The binder (woodglue or bio-glue) combined with Valida L,3% were mixed with cellulose and lignin to form a homogeneous paste with high viscosity and adhesion, resulting in smooth and well-structured extrusions.

Of these two promising mixtures, compressive strength and flexural strength were tested. Despite the fact that the mixture with woodglue had higher values, it was chosen to proceed with the bio-glue-based mixture. This was chosen to comply with the principle of bio-based printing. Next, the effect of adding fillers in the mixture with bio-glue was examined. This resulted in three new mixtures and these were also tested for compressive and flexural strength. Based on the end element (column), the mixture representing the highest value for compressive strength was chosen. The mixture with the highest value for compressive strength was the bio-glue mixture with the addition of bentonite.

The focus of the final design was on stacking the elements to arrive at a one metre high column, where the resistance to buckling should be as high as possible until it collapses globally. This column was tested for buckling as this is the main failure mechanism for a slender structure loaded in axial compression. Parameters and the optimization target were used to set up the numerical model in the parametric modelling software Rhino, via a script written in grasshopper. While changing the geometric parameters, the script searches for an optimized structure to accommodate an axial compression force. This resulted in a final design where the buckling resistance is as high as possible.
Once the optimized column design was found, the print path that could be used to make the column was determined. Robot Components was used to visualize all the actions of specified robot. This resulted in RAPID code, which was loaded into Robot Studio to simulate the full print path and fabricate the structure.

A total of one column was fabricated. During testing in the printing phase, it was found that with this mixture (bio-glue + bentonite), a maximum of 6 layers can be printed vertically on top of each other. As a result, the column consists of 36 elements of 6 layers. After all elements cured, the elements were manually glued together one by one until the height of one metre was reached. After the glue cured, small imperfections in placing the elements on top of each other were observed due to manual gluing.

The cured bio-based column was tested in axial compression in the compression testing machine. At a force of 46,82 kN, the column failed. The main failure mechanism of the axial compression test was global buckling. The calculated force in the numerical model was 41,81 kN, after which an average factor difference of 1,12 was found between the test and numerical results for the axial force.

After this research project, it can be concluded that it is feasible to create a bio-based optimized column design through additive manufacturing. It has good potential in the construction industry, but further research and refinement of the properties is needed for structural applications.

Index

1. Introduction

The world is increasingly faced with the consequences of global warming of the atmosphere, such as heavier rain fall and flooding on one hand and prolonged droughts and wild fires on the other. Fossil fuels, the main source of increased atmospheric CO_2 levels need to be phased out. Alternative clean sources of energy need to be introduced at a large scale. We all should be climate conscious, as the limits are gradually being reached. The construction industry is responsible for approximately 39% of total CO_2 emissions worldwide, contributing significantly to environmental pollution [1]. This pollution involves greenhouse gas emissions, waste generation, energy consumption and material depletion. In the construction industry, there are two types of categories of energy that can be encountered. The first category is operational energy, which is the energy required for the day to day running of the building such as cooling, ventilation, heating etc. [2]. The second category consists of embodied energy [2]. This includes the energy needed to construct and maintain the building and the energy needed to produce and transport the materials [3]. Reducing the consumption of both energy in the construction industry also reduces the CO_2 emissions released into the atmosphere duo to construction activity. In the Netherlands, the government has set a goal (in the climate agreement) for the Dutch economy to be fully circular by 2050. Reducing CO_2 emissions only works if other countries also participate. Hence, the UN Paris Climate Accord was signed by almost all countries in the world [4].

In recent years, many efficient and innovative technologies have been developed to minimize the operational energy use of buildings [5]. This research focuses only on embodied energy. Reducing the embodied energy consumption of buildings is still a major challenge. However, bio-based and low-carbon materials have been used to reduce the consumption of embodied energy in buildings, which produce more CO_2 emissions. A bio-based material is a material made from plant or other biomass sources rather than from fossil fuel sources. These materials can be used in a wide range of applications, including the production of plastics, textiles, paper, and fuels. Because bio-based materials can be replaced more quickly and do not rely on limited fossil fuel supplies, bio-based materials are usually considered to be more sustainable than traditional materials. Additionally, the production of bio-based materials can often result in fewer greenhouse gas emissions than the production of traditional materials. Bioplastics, bamboo, hemp, and wood are a few types of bio-based materials [6].

The transition to a low-carbon economy is essential to address the environmental crisis. Therefore, this project will introduce a new bio-based material and print a columns as a structural element from this material using additive manufacturing, also known as 3D printing. To print this structural element (design), the printing parameters and mechanical properties must be determined by testing, see figure 1. Additive manufacturing can be used to automate the manufacturing process and to create structures with a large degree of freedom. Through additive manufacturing, higher levels of precision can be achieved which could lead to reduced physical labor, waste production and increased construction speed [7]. Apart from the fact that bio-based materials have been successfully introduced into the construction industry and have been used for numerous structural applications, society's perception of the reliability and robustness of these types of building materials has not yet changed. Experimental testing of bio-based materials is needed to know the mechanical properties and ensure structural safety.

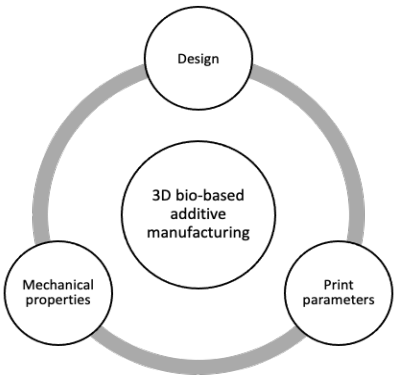

Figure 1. Additive manufacturing

The goal of this project is to design a 3D parametric structural element consisting of bio-based material. The 3D structural element will be realized by additive manufacturing. This project is part of the Innovative Structural Engineering and Design (ISD) field and focuses on a new printable bio-based material and integrating architectural and structural design. The research question of this project is formulated as follows:

''How can a three dimensional parametric structural element (column), consisting of bio-based material, be printed by additive manufacturing and what is its structural performance?''

To answer this main question, a step wise process was established, see figure 2. All steps in this process must be completed after which the main question can be answered. The process consists of two main parts. The first part deals with creating the final printable mix for the final structural element. This process was performed in close collaboration with Franka Pels Rijcken. After carrying out this process, the ways with Franka are separated. The second process comprises creating the final structural element.

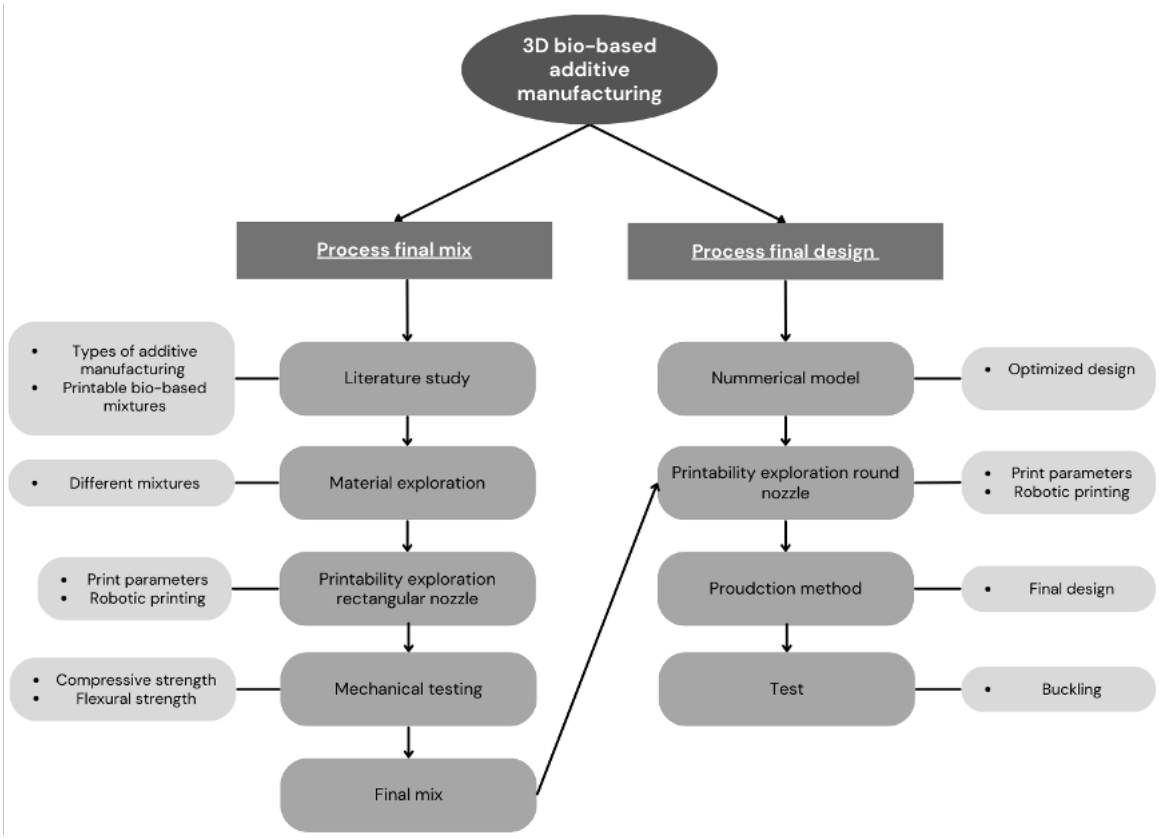

Figure 2. Graduation process

2. Literature review

2.1 Additive manufacturing

Additive manufacturing, also known as 3D printing, is widely used in various industries such as automotive, manufacturing and construction. It has great potential to be applied in the construction industry by reducing labor, cost, energy and material waste. As presented by D. Camacho [8], there are already several examples of constructions in the construction industry based on cement, polymer and clay. Around the world, companies are already using 3D printing technology to fabricate entire buildings.

It is a process that uses a digital model to print a 3-dimensional (3D) construction part layer by layer. It is called "additive" manufacturing because it adds material to make the object, rather than removing material through processes such as cutting or carving. It can be used to make a wide range of objects, including complex shapes and geometries that are difficult or impossible to make with traditional manufacturing methods.

All 3D printers for additive manufacturing currently work with layers. The thinner the layer, the higher the product definition and the closer the digital model will be to the physical model. The difference between different 3D printers is the raw material and the process by which the layers are created and bonded together. These are the basic elements that determine the accuracy, speed (manufacturing process), mechanical properties and definition of the printed part.

Additive manufacturing, as proposed by I. Gibson [9], is based on a digital model developed with CAD software and derived from the model used for product design. The basic principle is that a three-dimensional Computer-Aided Design (3D CAD) can be produced directly. If a change needs to be made to the design, only the digital model needs to be adjusted. The steps which are in the additive manufacturing process are shown in figure 3.

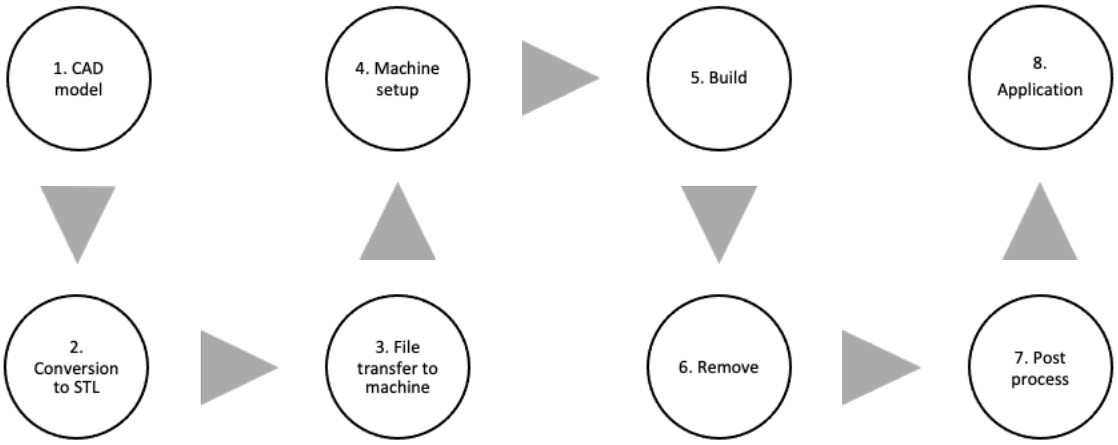

Figure 3. Additive manufacturing process [9]

Types of additive manufacturing

Additive manufacturing methods using bio-based composite as feedstock are classified into five different categories [10], see figure 4. The categories are: material extrusion, powder bed fusion, photopolymerization, binder jetting and sheet lamination. Applications, material composition and properties should be considered to determine the method to be employed for the fabrication of each product.

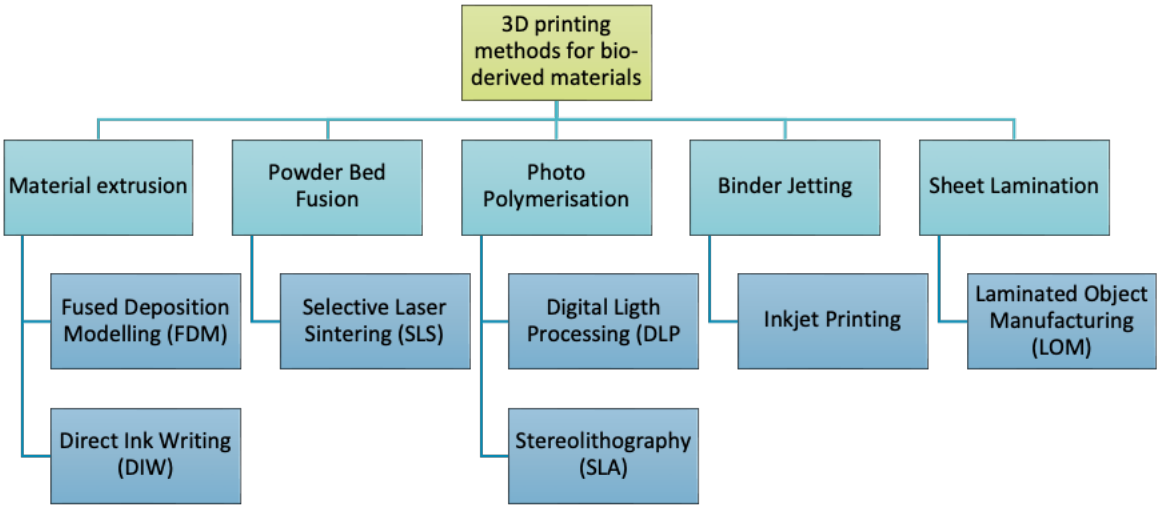

Figure 4. Methods and types of additive manufacturing [10]

Material extrusion

Extrusion-based 3D printing methods, such as FDM and DIW, are some of the most widespread methods. These methods use the principle that a viscous liquid or molten material (basically the ink) is extruded through a nozzle that can travel in X, Y and Z directions. Based on the CAD model of the product, the nozzle follows a path defined by the 3D printing software. Layer by layer, the final product is built up in the vertical direction (see figure 5) [11]. For optimal printing results, the ink must quickly turn into a solid or have solid-like behaviour after extrusion. This can be achieved by [12]

1. Quick melt-to-solid transitions (this is used for e.g. Acrylonitril-Butadieen-Styreen (ABS), PolyLactic Acid (PLA), etc.).
2. Shear-thinning or thixotropic behavior, in which the ink flows under the extrusion pressure but becomes more viscous once the pressure is removed.
3. Cross-linking, which is the interconnecting of different polymer chains.

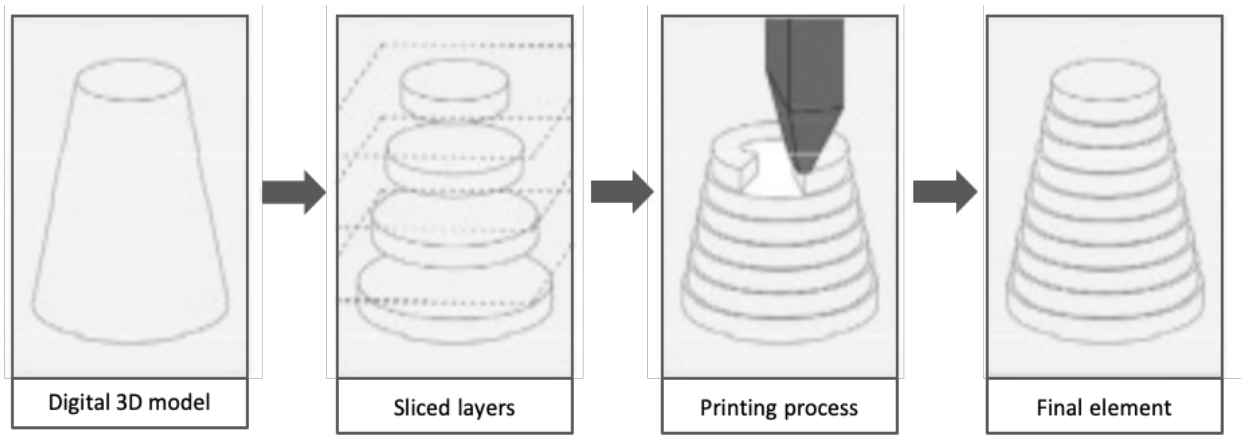

Figure 5. Material extrusion process workflow [11]

Fused Deposition Modelling (FDM)
FDM, see figure 6, uses a filament as raw material (conventionally made from a thermoplastic) that is often replaced by a biodegradable polymer, such as PLA [10]. Bio-based composite filaments can be produced from the combination of PLA pallets with natural fibers (hemp, coconut, flax, cellulose, etc.) The ink in the form of a solid filament is rolled into hot nozzle (usually temperatures up to 200 °C), where it is melted (to become flowable) and extruded using a motorized pinch roller system. The FDM process is feasible for printing with biomaterials that are thermoplastic in nature, but not suitable for other types of temperature-sensitive biomaterials.

Direct Ink Writing (DIW)
DIW, see figure 7, is an extrusion-based 3D printing method, also known as liquid deposition modeling (LDM). This uses a viscous substance as a raw material such as gels and pastes. It is used to extrude clay and concrete in the construction industry or art. It is also applied for biomedical applications in tissue engineering, protheses and implants with cellulose-based gels [10].

Powder bed fusion
Methods based on particle fusion, see figure 8, uses a container filled with a layer of powder (usually metal or plastic) as the base material. It reacts to an energy source (laser) that heats the particles above their melting temperature. When heated, the particles melt together without melting. This is why it is called a sintering process and not a melting process. The working platform then moves and the laser travels along the path that describes that specific layer and fuses the particles where necessary. This process is repeated until all the layers of the final product are built up and fused [13].

Photo polymerisation
This process is known as the founding process in the field of additive manufacturing. The photo polymerization methods uses light to initiate the polymerization process. A UV or laser beam moves over a bath of photo polymerizable liquid. Upon contact with the beam, the liquid polymerizes, forming a solid. When a layer of the product is finished, the platform on which the product is placed lowers itself into the liquid bath and the new layer can be printed. Stereolithography (SLA), see figure 9, was the first process to become commercially available in the 1980s [12].

Binder jetting
Binder jetting or inkjet printing, see figure 10, is a 3D printing process in which small ink droplets (1-100 picoliters) are applied to a printing surface. The droplets then harden on this surface to form a 3D structure. Hardening is done through the same mechanisms as that were described for extrusion-based methods [12].

Sheet Lamination (SHL)
This methodology is based on stacking two dimensional sheets in order to form a three dimensional object. The materials which could be used are various (for e.g. paper or cardboard). Before the sheets are bond together, the upper sheet will be cut into the desired shape. This cutting is done by a laser. Because each layer is cut in the desired shape, the waste material can be removed manually after the print is finished. In order to bind the layers, an adhesive is used [14]. When finished, the production table is lowered and the process is repeated for the next layer. The technique is less suitable for solid surface finish and is sensitive for damage in case of complicated geometries. Figure 11 shows an image of the Laminated Object Manufacturing (LOM).

Figure 6. Fused Deposition Modelling (FDM) [12]	Figure 7. Direct Ink Writing (DIW) [12]	Figure 8. Selective Laser Sintering (SLS) [15]
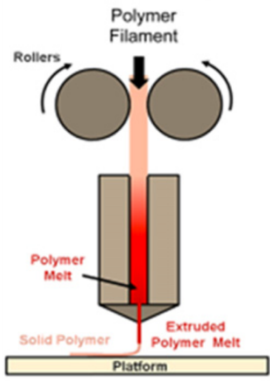	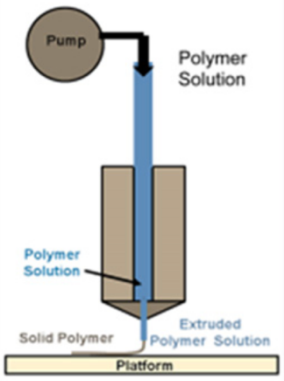	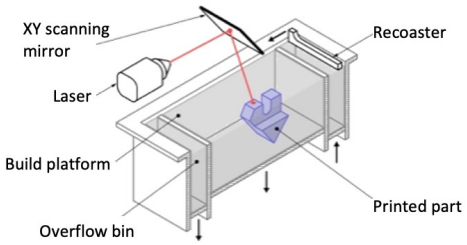
Figure 9. Stereo-lithography (SLA) [12]	**Figure 10. Inkjet Printing [12]**	**Figure 11. Laminated Object Manufacturing (LOM) [16]**
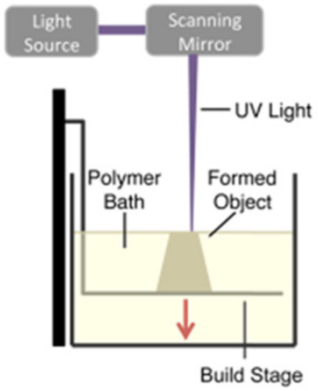	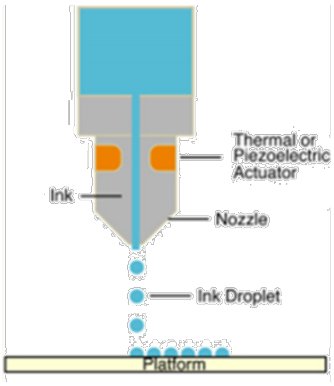	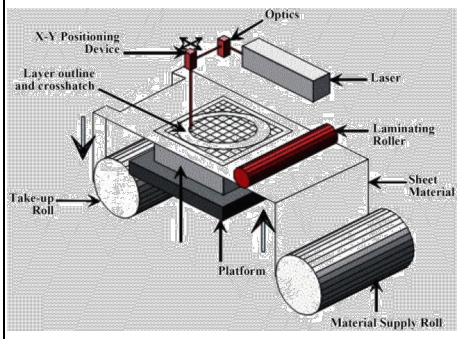

For this research, the first category of additive manufacturing is chosen, namely material extrusion (DIW). This is chosen because the research on which this project is based was also related to extrusion-based 3D printing. This is also chosen because the TU Eindhoven has a lot of knowledge regarding extrusion-based 3D printing with concrete and clay.

2.2 Printable bio-based materials with DIW method

2.2.1 Non-structural

Materiom

Materiom is an open-source database bio-based material recipes including recipes for 3D printing. Making these recipes public accelerates the development concerns bio-based material recipes. Materiom lowers barriers in the new materials market and aims to give communities the means to nourish themselves. To achieve this goal, they collaborate with makerspaces (companies and local communities). These companies are supported in developing new bio-based materials based on the characteristics of the natural resources available in the respective regions where the companies operate. The open-source database makes it easy to produce products by following the recipes, see table 1 and figure 12. 3d printed element [17]. By enabling makerspaces to develop bio-based materials, local communities can be nourished, local production can be encouraged. Local production is seen as a sustainable alternative to centralized production [18].

Table 1. Mix: Printable mussel shell

Ingredients	Quantity (g)	Figure 12. 3D printed element [17]
Water	3,6	
Sodium alginate	0,3	
Mussel shell powder	6,1	

Wood and methylcellulose

There has been much development in additive manufacturing technologies in recent years, but only a few attempts have been made to use bio-based materials such as wood for 3D printing. In this research, M. Rosenthal [19] has looked at creating a printable paste-like mixture. The mixture consists of ground beech sawdust and methylcellulose dissolved in water (see table 2). The physical properties are influenced by the binder-to-water ratio and the size of the wood particles.
The results of the study show that LDM is a promising technology for 3D printing wood. Compared to FDM, the maximum wood content in the mixture increases from 40% to 90%. Since the wood-based binder methylcellulose was used, the 3D printed element (see figure 13 consists of 100% of the renewable raw material wood.

Table 2. Mix: Wood and methylcellulose

Ingredients	Quantity (-)	Figure 13. 3D printed element [19]
Water	-	
Methylcellulose (MC)	MC/Water 1:20	
Wood fraction (mesh size 0.25mm)	MC/Wood fraction 1:85,5	

Wood and adhesive

In this study, M. Kariz, M. Sernek and M.K. Kuzman [20] studied the different proportions of wood powder as a component in adhesive mixtures for 3D printing. Polyvinyl acetate (PVAC) and urea-formaldehyde (UF) adhesives were used as binders. The optimal mixture (see table 3. mix: wood and adhesive) was determined by measuring the corresponding extrusion forces. Simple blocks were 3D printed (see figure 14) and their bending properties were determined. The study shows that the bending strength depends on the amount of wood powder in the mixture and on the type of adhesive. The results of the study show that it is possible to use wood powder in mixtures containing adhesive for 3D printing. The mechanical strength of the 3D printed element from PVAC adhesive is insufficient and needs to be improved. The 3D printed element of UF adhesive showed strength that is sufficient only in non-structural applications. To make the technology suitable for a wider range of applications, the mixture and the 3D printing process must be further optimized.

Table 3. Mix: Wood and adhesive

Ingredients	Quantity (%)	Figure 14. 3D printed element [20]
UF adhesive	15%	
Wood powder (beech wood)	85%	

2.2.2 In the future structural

Omlab

Omlab (circular bio-based research and design studio), in collaboration with the water sector, housing companies and education, is conducting research into a future-proof alternative to 3D structural printing. Here Omlab does not use minerals, fossil raw materials or chemical additives but focuses on tertiary raw materials (formerly waste) derived from waste material from sewage and water treatment plants. The mix (see table 4) contains chalk from water softening treatments, kaumera (bio-polymer) from sewage treatment, cellulose, water and alginate. The paste of the mixture looks like that of clay and is extruded by the 3D printer. The printed material is then air-dried and looks like 3D printed concrete (see figure 15).
The material can be applied to 3D print stackable building elements for indoor and outdoor use.

Table 4. Mix: Omlab

Ingredients	Quantity (%)	Figure 15. 3D printed element [21]
Water	60	
Chalk	30	
Cellulose	5	
Kaumera	5	
Alginate	<1	

Cellulose and lignin, separately, have been continuously exploited as reinforcing fibers and fillers, respectively [22]. However, as a single combined compound, there are not many references available and the state-of-art thesis research in this area was published by T. Liebrand [23]. A follow-up to this thesis research was conducted by C. Bierach [24] and A. Alberts Coelho [25]. Both students focused on exploring wood as a natural alternative raw material for additive manufacturing and its potential for architectural applications by experimenting with different ratios of the two elements.

The experiments were based on soda lignin and bleached kraft cellulose sheets as raw material, pulped and mixed with water and binders at different ratios to create a printable paste. The recipes were evaluated in terms of homogeneity, bonding, viscosity and water absorption through manual and visual tests, graded and compared, indicating the most promising materials to be further explored. From the 12 recipes initially explored, two were considered adequate and further tested on a cold extrusion process with the robot, simulating a liquid deposition modelling AM process.
Mix 3: methylcellulose (see table 5) had been chosen because this mix is 100% bio-based and compared to the other mixes scored well on the points mentioned above. Mix 10: woodglue (see table 6) had been chosen because this mix had the best mechanical properties and scored well on the points mentioned above.

Next, the optimization of print settings was investigated. Print settings are related to material properties and can affect the feasibility and quality of the design to be produced. Layer height and width, print speed and flow were changed and different shapes (circles and triangles) were produced to test the influence of the shape on the material and print settings.

Finally, both students printed an element. One student printed a corner of a window frame and the other student printed a structural node, see figure 16 and 17. The conclusion of this study confirmed that the building blocks of wood can be used as feedstock for additive manufacturing. Further studies and improvements are still necessary to apply this 3D printed material for structural elements.

Table 5. Mix: Methylcellulose

Ingredients	Quantity (g)
Lignin	30
Cellulose	3
Water (80°)	65
Methylcellulose	5

Figure 16. 3D printed methylcellulose [24,25]

Table 6. Mix: Woodglue

Ingredients	Quantity (g)	Figure 17. 3D printed woodglue [24,25]
Lignin	10	
Cellulose	1	
Woodglue	30	

Blast studio

Blast stands for biological laboratory of architecture & sensitive technology. The design studio was founded in 2018 by Pierre de Pingon, Martin Detoeuf and Paola Garnousset. The studio's goal is to explore how nature and technology can be brought into dialogue to transform the discarded material of cities into artifacts and architecture.
Urban waste such as coffee cups, pizza boxes and packaging boxes, sawdust and other wood waste is recycled. Then a special technique converts the waste into a biomaterial that can be taken over by living organisms such as mycelium (root network of fungi) and plants. Once the desired product is printed, the mycelium consumes the pulped paper cups and grows to take over the whole column, producing mushrooms that can be picked off and eaten. Next, the root structure of the mycelium is dried into a supporting architectural element with natural insulating and fire-retardant properties. With the mixture shown in table 7, furniture, artifacts (see figure 18 and architectural pieces can be 3D printed without the need for formwork.

Table 7. Mix: Mycelium

Ingredients	Quantity (-)	Figure 18. 3D printing process [26]
Water	- (unknown)	
Mycelium	- (unknown)	
Urban waste (cardboard)	- (unknown)	

Living soil – soil inks

The research team at the University of Virgina (UVA) has invented a sustainable and innovative technique to 3D print structures created from soil implanted with seeds [27]. Among other things, this technique can be used to create walls and roofs that flourish with plants.
The green walls and roofs created with this technique are extremely useful and can perform various functions, such as -natural insulation, green spaces for people, flood prevention and pollinators for other animals. The process also eliminates many unnecessary materials that have large emissions and contributes to the circular approach to building and design.
The prototypes built by the studies initially look like ordinary ground structures. But over the course of a few days, they sprout and become covered with greenery (see figure 19).

The mixture (see table 8) consists of local soils and plants mixed with water. By combining soil and seeds into 3D printable (soil inks) greenery could be built into the fabric of architectural elements rather than just laid on top. The seeds used to plant in the ground are stonecrops, this is a succulent that hardly needs water to survive. If a printed element is not needed or is not of the right quality, the material can be recycled and reused for the next print.

Table 8. Mix: Living soil

Ingredients	Quantity (-)	Figure 19. Growing greenery on the printed wall [28]
Local soils	- (unknown)	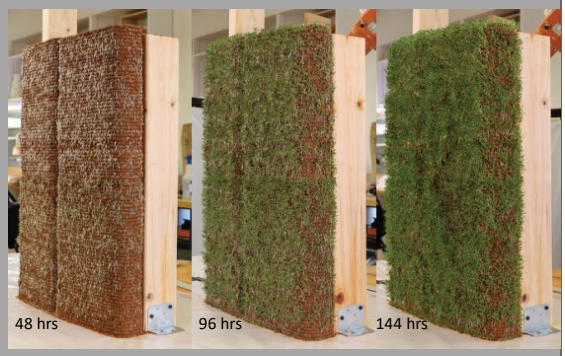
Plants (stonecrop)	- (unknown)	
Water	- (unknown)	

2.2.3 Structural

Tecla house 3D-printed from locally sourced clay

Tecla is a combination of the words technology and clay. Designed by architecture studio Mario Cucinella Architects, the low-carbon home prototype was built and constructed by 3D printing specialist WASP using clay from a nearby riverbed (see table 9). Printed in Massa Lombarda (Italy) the house is 60 square meters with a height of 5,2 meters [29]. It consists of two connected dome-shaped volumes with a 3D printed outer wall of clay constructed from 350 stacked layers (see figure 20). The clay was applied to not only provide structural stability, but also act as a thermal barrier.
The house was built using a multi-level modular 3D printer that uses two synchronized arms, each with a 50-square-meter printing area that allows modules to be printed simultaneously. This technology allows residential modules to be built within 200 hours without construction waste [29].
The envelope geometry can be adjusted and modified to work with different types of raw earth and respond to different climate conditions.

Table 9. Mix: Tecla house

Ingredients	Quantity (-)	Figure 20. 3D printing process [30]
clay from a nearby riverbed	- (unknown)	

Soil and agricultural waste – Gaia house

In October 2018, the Gaia House was printed in the town of Massa Lombarda (region of Emilia-Romagna) that is made of biodegradable materials [31]. The Italian developer of 3D printing technology WASP (World's Advanced Saving Project) built the Gaia house to show the possibilities of a modular 3D printer (hanging on a crane) that can make houses of different sizes and formats.
The Gaia house has 3D printed exterior walls that were applied layer by layer with a series of triangular cavities between the interior and exterior layers. The vertical cavities in the outer wall are filled with rice husk for insulation. Although the biodegradable material is suitable for supporting the overhanging roof, the main load-bearing elements for the overhanging roof consist of wooden columns placed along the inside of the structure. In total, the Gaia house is 30m^2 [32].
The mixture (see table 10 and figure 21) of the house consists of a natural mud mixture made from soil taken from the surrounding land, as well as waste materials from rice production, such as chopped straw and rice husks.

Table 10. Mix: Gaia house

Ingredients	Quantity (%)	Figure 21. 3D printing process [33]
Soil (30% clay, 40% silt and 30% sand)	25	
Straw chopped rice	40	
Rice husk	25	
Hydraulic lime	10	

The focus of the remaining part of this research is on TU Delft's mixes. The methylcellulose and woodglue mixes are the reference mixes for the study. These mixes were chosen because they are promising bio-based mixes and much knowledge has already been gained by C. Bierach and A. Coelho. C. Bierach and A. Coelho were open to sharing their acquired knowledge. This allowed the material properties of the mixes to be improved. Material properties can be improved by investigating different binders besides lignin and cellulose, such as nanocellulose, and looking at different additives such as bentonite, and larger fibers.

2.3 Materials

There are several ways to make a printable material. In this case (see figure 22), a gel is prepared from a raw material combined with a binder and possibly with a liquid. These ingredients are mixed until a homogeneous gel is formed. A responsible for structural rigidity is then added. Mixing is done again until a homogeneous composite mix is formed.
Nowadays, three basic requirements for 3D printed elements are widely accepted: 1) excellent extrudability to ensure a continuous paste; 2) sufficient build behavior to resist structural deformation; 3) sufficient strength to compensate for external damage.

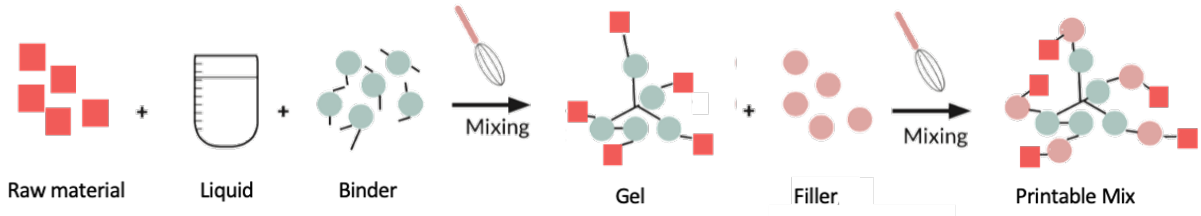

Figure 22. Creating printable mix

Cellulose

Cellulose is the most abundant polymer in nature. It has been used by humans for thousands of years in a wide variety of fields, from clothing and paper production to energy generation. In combination with lignin and hemicellulose, it forms the building block of wood. Softwood samples contain 33-42% cellulose, while hardwood contains 38-51% of the composition [34]. The wood cell wall is a regular structure composed of cellulose microfibrils organized into crystalline and amorphous regions [10]. These are formed by the long string-like molecules of cellulose. It is then inserted into a brittle material matrix (lignin) and linked together using the smaller molecules of hemicellulose [35].
Cellulose is also a structural component in plants, reinforcing cell walls in a lignin matrix [36]. All plants contain cellulose and are designed to support their own weight and withstand adverse weather and environmental conditions [10]. The cellulose fibers are good in tensile strength and give the wood its flexibility.

About 33% of cellulose is made from sugar compounds produced by photosynthesis. It can also be made from recycled raw materials such as cardboard, sawdust and lignocellulose-containing agricultural waste [37].
Cellulose from wood, bark, grasses, cotton and seaweed can be used to make paper. Because cellulose is used in various industries, it is considered an alternative to oil-based raw materials. Cellulose-based composite materials can compost by naturally returning nutrients to the environment. This allows inorganic carbon compounds to be stored, reducing greenhouse gas emissions [37]. Therefore, cellulose is one of the most organic compounds in the world [38].

3D printing offers great opportunities to quickly construct a wide range of customized structures. Cellulose, lignin and hemicellulose the three most common natural polymers and main components of plant raw materials, possess a large potential for bio-based products because of their advantages. Cellulose has many favorable properties, such as its abundance across the globe, it is environmentally friendly, renewable and its low cost [39]. The integration of cellulose, lignin and hemicellulose as the main bio-based raw materials offer new opportunities for 3D printing of high-performance 3D objects/elements. Cellulose and cellulose derivatives are promising bio-based raw materials for 3D printing and offer a practical way to make durable structures [40]. Table 11 describes the properties of cellulose and its derivative-based raw materials for 3D printing [41]. It shows that cellulose or cellulose derivatives play different functions in the 3D printing process. The simultaneous use of cellulose and cellulose derivatives as 3D bio-based raw materials can provide excellent performance, as some properties of the original single component can be retained and unexpected interactions can occur between the multiple components in the final 3D products.

Table 11. Properties of cellulose and its derivatives [41]

Type cellulose	Derivatives	Properties
Cellulose	-	Thickening, good shear thing under pressure (good thixotropic behavior)
Cellulose esters	Cellulose acetate (CA)	Formability and glossy appearance; Enhancing bio-feedstock viscosity etc.
Cellulose ether	Methylcellulose (MC)	Enhancing bio-feedstock viscosity
	Carboxymethyl cellulose (CMC)	Viscosity thickening and thixotropic rheology, etc.
Microcrystalline cellulose (MCC)	-	Poor solubility and thickening
Nano cellulose	Cellulose nanofibrils (CNF) / Valida L,3%	Providing appropriate rheological properties; Giving a gel-like and high consistency; Crosslinking to form network structure; Increasing the yield stress, storage modulus or elastic recovery, etc.
	Cellulose nanocrystals (CNC)	Surface grafted with printed polymer; As a natural crosslinker; Good shear thinning under the pressure; Reducing viscosity or storage and loss moduli, etc,

Lignin

After cellulose, lignin is the most abundant polymer in nature. Lignin is an important natural constituent in the structural cell walls of plants and wood [42]. Lignin is a hardening agent that holds cellulose fibers together and a natural stiffener of cellulose in nature. It also serves as a binder that binds polysaccharides together to give strength [43]. Lignin provides great physical strength and rigidity to the tissue and cell structure of plants and individual fibers [44].

Lignin is composed of three basic blocks (called monomers) whose concentrations vary depending on the source [45]. The percentage of lignin in softwood is 25-35% and in hardwood 16-24%. Grasses such as sugarcane (2-3%) and hemp (less than 4%) contain less lignin. Grasses they are therefore a great source for the paper industry after their fibers are decomposed efficiently [46]. The different chemical composition, see figure 22 [47], explains the different behaviors and why one type of lignin is better suited for a specific use than another.

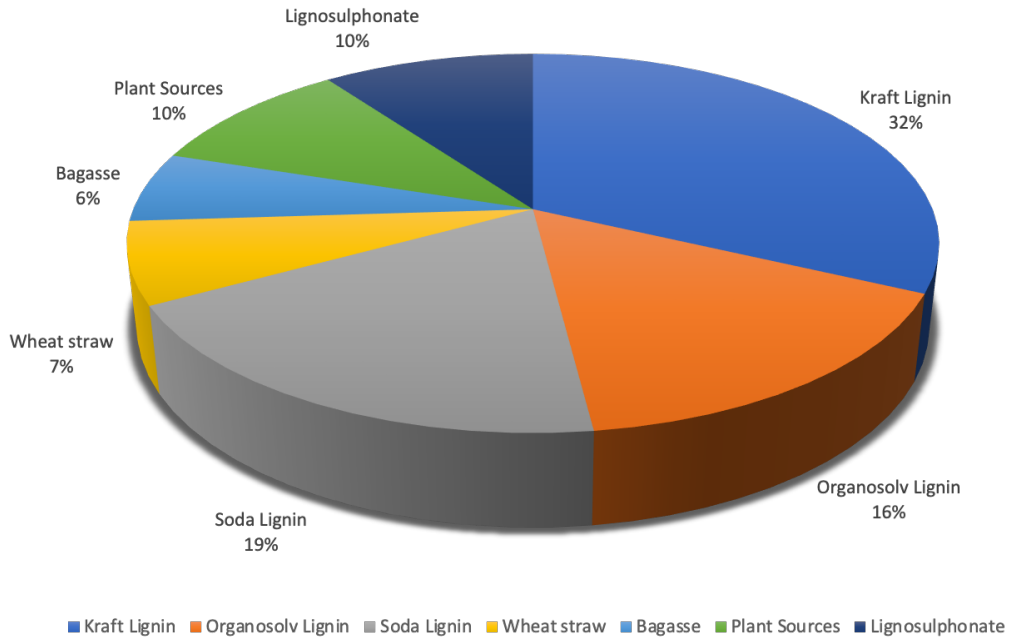

Figure 23. Lignin application from various sources [47]

More than 50 million tons of lignin are produced each year worldwide as a byproduct of biorefineries, 98% of which is burned to generate energy. Only 2% of lignin is used for other purposes, mainly in applications such as dispersants, adhesives and fillers [36].

Two categories of lignin come from the wood/cellulose pulping process, the lignosulfonates, and kraft lignin. Lignosulfonates account for about 88% of the total lignin produced, and kraft, lignin accounts for about 9% of the total. The remaining production of about 2% corresponds to organosolv or biorefinery lignin [48].

For several years, lignin has changed from a waste material to a raw material for valuable products. The attributes of lignin are high abundance, low cost, biodegradability and reinforcing capacity [36]. Lignin is a versatile element that has potential in the bio-based materials industry and can even compete with common polymers. It can be modified and engineered to improve affinity with thermoplastics. [49]. Moreover, it can be combined with natural fibers as a natural binder to combine hydrophilic fibers and hydrophobic matrices and participate in the development of bio composite materials.

Binder

Binders facilitate cohesion of components in a material with the goal of improving its texture, hardness or specific properties. Examples of binders are methylcellulose and woodglue.

Methylcellulose

Methylcellulose is a natural polymer derived from cellulose. Cellulose is a polymer of glucose containing hydroxyl groups (-OH) that can be substituted with methoxide groups (-OCH3) to produce methylcellulose [50]. In pure form, it is a white powder that dissolves in cold water but not in hot water. In hot water, it forms into a gel-like consistency. Like cellulose, it is non-digestible, non-toxic and non-allergenic. Traditionally, it has been used as an additive in the production of cement, mortar and glue in construction. It improves workability, stability, cohesion, homogeneity and increases the viscosity of mixtures [51]. This makes it suitable as a printing material and also because it is easily stackable.

As a binder for additive manufacturing materials, methylcellulose has been investigated in numerous and diverse bio-based composites. In Rosenthal's [19] study, it was mixed with beech wood powder, resulting in a smooth mix that was used to extrude test samples. Mixing methylcellulose with lignocellulose results in a load-dependent material. It flows as a viscous paste under load and behaves as a solid material once the force is removed. In Li's [52] research, it was used in the biomedical field to improve the viscosity of alginate-based hydrogels. In Peeters' [53] research, a quantity of wood (85% of its dry weight) was mixed with methylcellulose and bentonite to print a vase, considered the largest 3D printed object at the time. In Viere's [51] research, the ratio of methylcellulose to water is 1:20 to 1:33,3 depending on viscosity. Methylcellulose is mixed with heated water at 80 degrees, above the gelling point, to improve solubility. Continuous stirring until it cools results in a homogeneous mix with which to print.

Woodglue

Most common wood adhesives used in construction and wood production are based on polyvinyl acetate (PVAc) and urea formaldehyde (UF) [20]. PVAc is a synthetic polymer obtained by the polymerization of vinyl acetate. It is available in solid form (powder or granules), but mainly as latex or in an aqueous emulsion (it is insoluble in water). UF is a polymeric synthetic resin. It consists of chains of a compound between formaldehyde and urea.

In the field of additive manufacturing, PVAc and UF adhesives have already been investigated. The adhesives were mixed with wood powder in various proportions between 12,5% and 25%. The result was a homogeneous mix with which test samples were printed. The results indicate that the strength and stiffness of the binder directly affect the material. The greater the difference between the mechanical properties of binders and fillers, the less influence the wood content has on the performance of the element [20].

Bio-glue

Today's society relies heavily on glued wood products for such things as structures, flooring and furniture. Almost all adhesives on the market are based on fossil raw materials and many also contain UF. The health risks of UF adhesives (carcinogenic and allergenic properties) have already raised concerns. With society's rapid increase in environmental awareness, it is becoming increasingly important to look for greener and more sustainable alternatives. Studies resulted in promising directions including lignin, tannin and starch. But because adhesives based on synthetic polymers perform better, especially in terms of water resistance, those of natural origin played a secondary role. The growing interest in the use of biopolymers from renewable sources, such as wood/forest, corn and grains, has led to significant developments toward the use of biopolymers in green wood adhesives [54].

Filler

Fillers are needed to increase the volume of the bio-based material and/or add weight or mass. Fillers are also used as additives. Additives are usually used in the mixtures to obtain specific properties, such as improving stiffness and to aid processing to produce an economical final product.

Wood powder

Finely ground wood containing particles of similar grain is called wood powder. In practice, the definition of wood powder is particles passing through a sieve with a mesh size of 850mm [55]. Many researchers have moved on from these definitions and classified wood powders more concisely. Wood is one of many lignocellulosic materials and A. Barakat [56] and C. Mayer-Laigle [57] have classified them according to different categories, see table 12. Table 12 describes particle size classification in a general sense, which includes wood and lignocellulosic materials.

Table 12. Size classification wood powder [56,57]

Classification	Ultrafine	Fine	Intermediate	Course	Wood powders in 3D printing
Size range (μm)	<20	50 - 500	1000 – 10000	>10000	14 – 2000

Wood powders have been investigated as fillers in 3D printing. The powders investigated were from common commercial hardwood and softwood species. M. Kariz and N. Ayrilmis [58] used 237 mm beech wood. On the other hand, M. Rosenthal [19] used 250 mm and 400 mm beechwood powder. Spruce with dimensions of $800e^{2000}$ mm was used by K. Henke and S. Treml [59] in the 3D printing process. Y. Tao [60] used 14 mm aspen wood powder. H. Bi [61] used 150 mm poplar wood powder for their research on 3D printing. Finally, K. Chawla [62] used 50 mm wood powder obtained from sawdust in their study.
Researchers have used different types of binders in combination with wood powders including urea formaldehyde (UF), gypsum, methylcellulose, polyvinyl alcohol (PVA), polyactic acid (PLA), sodium silicate and cement for object printing [55].

Bentonite
Bentonite is a naturally occurring type of clay with great swelling capacity when in contact with water. It is a nontoxic clay type from volcanic ash, typically found in the United States [63]. The main component of bentonite is hydrated water-containing aluminum silicate with the elements magnesium and calcium or sodium. Bentonite can be applied in several ways; in this case it is applied as an additive to the mixture.

Below are some examples of completed studies where bentonite has been applied as a filler:

1. From the study by C. Bierach [24]and A. Alberts Coelho [25], it can be concluded that bentonite provides better adhesion between both surfaces and layers. This improves the stability of the multilayer structure. It also increases the resistance to pressure when touched.

2. In study by J. Peeters [64] at the Umea School of Architecture, bentonite was added as an additive in the mix. The study described the experience of developing a wood-based mix with methylcellulose as a binder and bentonite as an additive. Bentonite mixed with cement in small amounts, it increases the viscosity of the material and improves extrudability in the additive manufacturing process.

3. RISE worked with the WASP team at RISE in Umea, Sweden, to develop a biodegradable mixture. The final mixture consisted of sawdust, water, wool paper glue and bentonite. Bentonite was used to make the mixture elastic and help harden the material recipe [24].

4. In the study performed by M. Chen [63], bentonite was introduced to control the rheological parameters, thixotropy, and creep of 3D-printed calcium sulfoaluminate (CSA) cement composites to achieve a stable 3D structure. From this, the following was concluded: 1) the excellent performance of a 3D structure could be achieved by incorporating bentonite; 2) based on the results of the creep period, the addition of bentonite could reduce the deformation of a 3D structure over time; 3) the compressive strength of 3D-printed CSA cement composites increased, which resulted in excellent structural performance and reduced porosity.

Natural fibre

Vegetable fibers are fibers extracted from plant sources such as hemp, jute, banana, almond, etc. Plant fibers are divided into four basic categories, namely fibers from the inner bark, seed fibers, leaf fibers and fruit fibers [65] see table 13.

Inner bark fibers are fibers obtained from the inner layer of plants examples are flax, kenaf, ramie, hemp and jute. These fibers can be used as a blending material (reinforcing agent) for the mix. Seed fibers are fibers obtained from the outer shell of the seed examples are almond skin fiber and silk fiber. These fibers are used in the preparation of biomedical scaffolds. Abaca and sisal are examples of leaf fibers, these fibers are used in the preparation of thermoplastic composites in civil engineering structures. Coir is a fruit fiber extracted from the outer husk of the coconut and improves mechanical and surface properties.

The excellent biodegradability biocompatibility, mechanical properties see table 13, thermal properties and surface properties are some of the reasons that plant fibers are used in current additive manufacturing process [66,67].

Table 13. Mechanical properties of natural fibers [66,67]

Grouping	Fibre Source	Tensile strength (Mpa)	Young modulus (Gpa)	Elongation at break (%)	Denisty (g/cm^3)
Bast	Flax	345-1035	27.6	2.7 – 3.2	1.5
	Kenaf	930	53	1.6	-
	Ramie	560	24.5	2.5	1.5
	Hemp	690	70	1.6	1.48
	Jute	393 – 773	26.5	1.5 – 1.8	1.3
Seed	Silk	300-600	8-12	13-20	1.37
Leaf	Abaca	400	12	3 – 10	1.5
	Sisal	511 – 635	9.4 – 22	2 – 2.5	1.5
Fruit	Coir	175	4 – 6	30	1.2

Some of the previous studies emphasized that incomplete or reduced adhesion, choking of the material in the additive manufacturing process led to increased processing time or problems that need to be addressed for defect-free production. The study by M. Saadi [68] showed that a fiber volume fraction greater than 5% led to nozzle clogging and thus manufacturing failure. Nozzle clogging is a challenge that DIW method often faces when printing fiber-reinforced mixes.

The raw materials, binders and fillers described above are shown in table 14

Table 14. Materials

Raw material	
Cellulose	Lignin
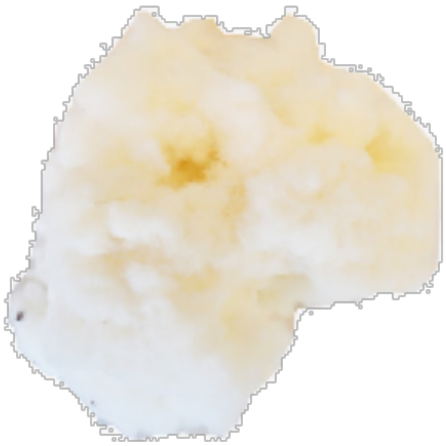	
Liquid	
Water	Valida L,3%
	

Binder		
Methylcellulose	Woodglue	Bio-based glue
		
Filler		
Saw dust	Bentonite	Flax fibre
		

3. Material exploration

The purpose of the material exploration phase is to understand how cellulose and lignin react with binders. Quantities are determined through ratios and observations during material mixing. Material properties are assessed to compare and evaluate recipes, with the most promising recipes being developed in this chapter. For each binder, the expected outcome is a recipe for a stable bio-based mixture, with optimal viscosity and binding properties for extrusion by a DIW process.

3.1 Preparations

3.1.1 Materials suppliers

In discussion with R. Gosselink, C. Bierach and A. Coelho and through own research, the materials described below were ordered.

Cellulose

Kraft

The cellulose used in the project is a product of the kraft pulp process. The cellulose is supplied as sheets of paper and is bleached. The pulp is valued for its strength and reinforcing properties. Other good properties of the pulp are biodegradable, renewable and recyclable material [69].

Company – Storaenso

Valida L,3%

Valida is a renewable material natural cellulose and contains the smallest component of cellulose fibrils. Valida is fibrillated cellulose in water suspension. It is derived from wood pulp from sustainably managed forests. It is a pre-hydrated bio-based multifunctional additive with a thixotropic character and unique rheology profile. In adhesive applications, Valida improves drying time, stability, particle settling and the balance between sagging and leveling. The strong shear thinning profile makes Valida easy to process and improves extrudability [70].

Company – Sappi

Soda lignin

Lignin is from the sodium hydroxide type. Sodium lignin is a biocompatible polymer that can be synthesized from the hydrolysis of sodium lignin, a byproduct of wood pulp. Sodium lignin has a basic structure consisting of phenolic acid and hydroxyl groups. These two components are responsible for hydrogen-bonding interactions with other molecules, allowing it to form strong bonds with other materials such as polymers (e.g., cellulose) [71].

Company – WEPA

Methylcellulose

Methylcellulose is from the E461 food grade type. It is a purified cellulose that dissolves in cold water and forms a gel in hot water. It has the unique property (suitable for 3D printing) of forming a gel when heated above 45°C that becomes liquid again when cooled (approx. 15°C) [72].

Company – Special Ingredients Europe

Woodglue

Woodglue is from a polyvinyl acetate base, water resistant (EN 204 D2 classification). It is the most commonly used glue with water dispersion. PVA consists of a water-based emulsion of a common type of glue, variously referred to as woodglue, white glue, carpenter's glue, school glue or PVA glue [73].

Company – Praxis

Bio-based glue

Bio-based glue (VA 104) is glue based on a polyvinyl alcohol solution. Polyvinyalcohol also known as PVA is a water-soluble synthetic polymer. According to contact person S. de Jong, the adhesive is 100% biodegradable. This is a commonly known characteristic of a bio-based material and therefore the VA 104 glue is considered a bio-glue.

Company – Intercol BV

Saw dust

The sawdust was supplied by Ir. A. Habraken. The type of sawdust was unknown, but it could be used to see what effect adding sawdust has on the mix.

Company – TU/e

Bentonite

Portaclay A 90 is produced from a natural Sodium-bentonite. This is a very plastic clay which is very suitable as an additive. Portaclay A 90 is produced by grinding this clay to a constant grain size and moisture content. The mean constituent is the clay-mineral montmorillonite. The standardized quality of Portaclay A 90 is guaranteed by means of an ISO 9001 certified quality management plan. The raw materials and production are closely monitored to ensure a constant quality with regard to its chemical composition and grain size [74].

Company – Silex

Flax fibre

Flax was chosen as the fiber reinforcement since this fiber was in stock in the SED lab at Eindhoven University of Technology. The flax type is flaxtape-50 unidirectional flax fiber tape from Eco-Technilin. It is an environmentally friendly and sustainable alternative to traditional composite reinforcements such as fiberglass. It was also chosen because of its combination of high strength and stiffness plus its frequent use in natural-fiber reinforced composites [75].

Company – Easy composites

The materials described above are shown in table 15. For the information of the relevant contacts, see Appendix 1 Contact information.

Table 15. Overview materials

Item number	Material	Item number	Material
1	Bentonite	6	Flax fibre
2	Valida L, 3%	7	Methylcellulose
3	Bison woodglue	8	Saw dust
4	Lignin	9	Bio-based glue (VA 104)
5	Kraft cellulose		

3.1.2 Equipment

The experiments are conducted in the Structures Laboratory at Vertigo on the TU/e campus in Eindhoven. In this laboratory, temperature and humidity are controlled and measured. The temperature averages 20.2 – 20.5 °C and the average relative humidity (RH) is 59.7 – 60.3% during the period used. Table 16 shows the equipment used throughout the process.

Table 16. Overview equipment

Item number	Equipment	Item number	Equipment
1	Whipped cream syringe	9	Pipet
2	Hot plate	10	Syringe
3	Pan	11	Mixer
4	Scale	12	Blender
5	Scoop	13	Rubber spatulas
6	Pots	14	Petri dishes
7	Measuring cups	15	Makita
8	Beakers		

3.1.3 Process

The process of the material experiments is shown in figure 24. For an extensive mixing process of each mixture, see Appendix 2 Mix process.

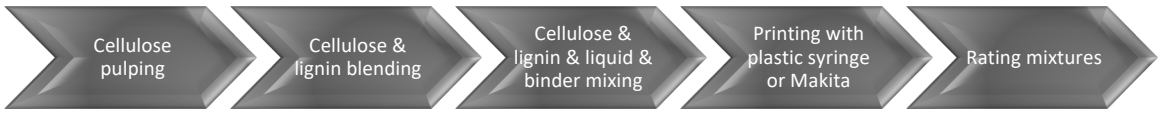

Figure 24. Material research process

Cellulose pulping

Cellulose must first be blended separately to separate the fibers and increase the contact area. The most effective pulping method for cellulose is to reduce the large sheets to small 20x20 mm shreds and process them in small quantities with a blender, see figure 25.

Figure 25. Cellulose pulping

Cellulose & lignin blending

The increased contact area increases fiber coverage with the lignin polymer, which is added in the blender. It also promotes bonding between matrix and fibers.

Cellulose & lignin & liquid & binder mixing

A mixer is then used to mix the liquid and binder until homogeneous distribution. Experiments are being conducted with different types of binders. At this homogeneous distribution, cellulose and lignin are added to create a matrix with a uniform fiber distribution.

Printing

If the mixture is printable, it is printed by manual extrusion with a plastic syringe. By repeating the process described above several times and constantly adjusting the proportions of raw materials and their quantities, a printable mix is created.
Next, a small amount of the most promising mixtures is manually printed with the Makita. For the working of the Makita, see section 4.1.3.

Rating mixture

A criterion set with five parameters, see figure 26, was developed and used to evaluate the different mixtures. Here a distinction is made between the fresh state and the hardened state of the mixtures. The evaluation is based on manual assessment and eye observations.
Each criterion is assigned a value from -2 to 2 for negative, indifferent, or positive performance, respectively. All values are added together, this provides a complete semi-quantitave comparison between all the different mixtures. The mixtures with the highest potential are further compared and evaluated by mechanical testing.

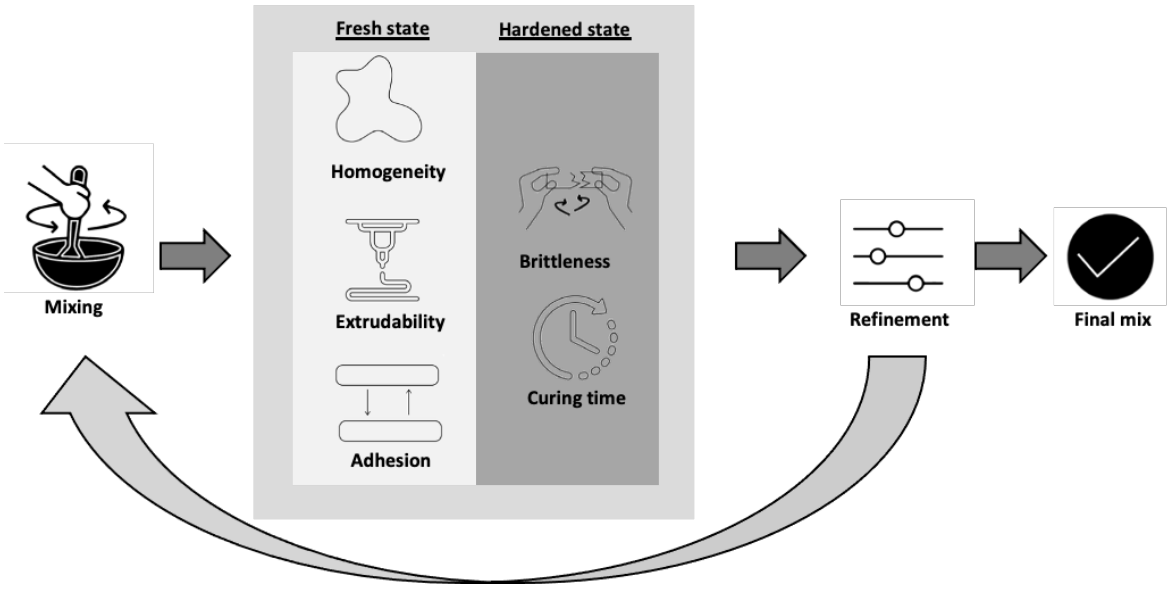

Figure 26. Criteria to be assessed

Fresh state

- Homogeneity
  Homogeneity refers to a completely uniform paste for a high-quality print with optimum performance. A homogeneous paste has a uniform color and consistency and contains no clumps.
- Extrudability
  Extrudability is a combination of adhesion and viscosity. The mixture is pushed out of a nozzle. Experiments are being conducted with a plastic syringe operated manually and, at a later stage, with a caulking gun. If the mixture is too dry, it will not extrude. Material to be pushed out from a nozzle. If the material is too dry, it will not extrude.
- Adhesion
  Adhesion refers to sticking and bonding between layers. The higher the adhesion, the stronger the layered structure. Ideal for additive fabrication is moderate to high adhesion. The mixture is sticky but without blocking movable parts and interfering with equipment operation.

Hardened state

- Brittleness
  Brittleness refers to the ease with which a cured mixture can be broken by touching it and applying a small force to it. The aim is plastic failure (score 2) instead of brittle failure (score -2).

- Curing time
  Cure time refers to the complete curing of a printed part. In this study, different curing methods are investigated, oven curing, room temperature curing and climate room curing. Different types of covers are also examined, see table 17.

Table 17. Cover type

Glass cover	Wooden cover	Plastic cover	No cover
	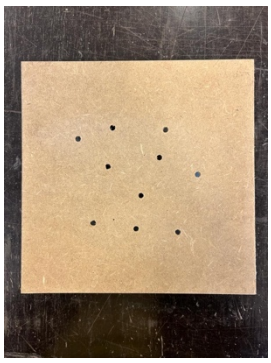		

3.2 Mixtures TU Delft

The first phase of the material consists of reproducing the two mixtures developed by C. Bierach and A. Coelho in 2022. The two former students from TU Delft discovered that the raw materials (lignin and cellulose) can be combined with the binders (woodglue or methylcellulose) and possibly with water to get a printable mixture. The reproduction of the recipes can be fully explored because all the materials are the same as in Delft. The only difference with Delft is that they made the cellulose small with a coffee grinder and in this study the cellulose was made small with and blender.

3.2.1 Methylcellulose mix TU Delft

Manufacture process

Cellulose was first reduced into smaller particles and then mixed with lignin and methylcellulose to separate the fibers and improve coverage with the polymer and binder. Water at 80°C was added and the mixture was mixed continuously to form a homogeneous and moderately viscous mix.

From the experiments conducted in this phase, a ratio of 1:6 between lignin and methylcellulose as well as the ratio of 1:10 between cellulose and lignin proved to be the most promising recipe. See table 18 for the materials in the mix.

The mixture is produced hot and the temperature drops during the process. The mixture requires a complete and slow cooling process of at least 24 hours in a closed plastic container covered with plastic film to achieve the optimum consistency.

Table 18. Methylcellulose mix TU Delft

Material 1 (Raw material)	Material 2 (Liquid)	Material 3 (Binder)	Material 4 (Filler)
• Cellulose (3g) • Lignin (30g)	• Water (65g)	• Methylcellulose (5g)	• -

Photos of process are shown in figure 27. On the left, the freshly printed material can be seen. The printed material showed high moisture content and no optimal adhesion. Top right shows the mixture after it has been mixed and bottom right shows the hardened state of the printed material. It can be seen that the hardened material has gone mouldy.

Figure 27. Pictures methylcellulose mix TU Delft

Rating

Scores were assigned to the printed material in the fresh state and hardened state. These scores are shown in table 19. The properties of the fresh sate were tested during printing and the properties of the hardened state (curing without cover) were tested after 8 days.

Table 19. Material rating methylcellulose mix TU Delft

Fresh state				Hardened state		Total
Homogeneity	Extrudability	Adhesion		Brittleness	Curing time	
1	1	1	*Non oven*	-2	1,5	**2,5**
			Oven 40℃	-2	2	**3**

Result

Several iterations were carried out to maximize the amount of lignin and cellulose and minimize the water content to optimize material properties while retaining the amount of binder (see appendix 3 Assessing mixtures). Lignin improved viscosity and adhesion, but it also increased friability and turned it into a dry mix. An increased amount of fibre reduced homogeneity and formed lumps. Reducing the water content resulted in a dry mixture and reduced extrudability of the material.

Despite many iterations, we failed to get a good printable mixture, which is reflected in the low scores. Moreover, the cured material went mouldy after several days and this happened also in the mixture of TU Delft (see figure 27 bottom right). To counteract moulding, a print was cured in the oven. This print did not go mouldy, but during testing it turned out to be much too brittle. Also, no fibres were visible in the print, which probably burned away in the oven.

Due to the low scores and the moulding of the printed material, it was decided to discontinue with this mixture.

3.2.2 Woodglue mix TU Delft

Manufacture process

Cellulose was first made small and then mixed with lignin to separate the fibers and improve coverage with the polymer. Water and woodglue were added and the mixture was mixed continuously to a homogeneous and viscous mix. Good adhesion was immediately noticed.

From the experiments conducted in this phase, a ratio of 1:3,33 between lignin and woodglue as well as the ratio of 1:10 between cellulose and lignin proved to be the most promising blend. See table 20 for the materials in the mix.

Table 20. Woodglue mix TU Delft

Material 1 (Raw material)	Material 2 (Liquid)	Material 3 (Binder)	Material 4 (Filler)
• Cellulose (3g) • Lignin (30g)	• Water (20g)	• Woodglue (100g)	• -

Photos of the process are shown in figure 28. The freshly printed material is shown on the left. The printed material showed lower moisture content than methylcellulose and excellent adhesion. Top right shows the mixture after it was mixed and bottom right shows the cured state of the printed material.

Figure 28. Pictures woodglue mix TU Delft

Rating
Scores were assigned to the printed material in the fresh state and hardened state. These scores are shown in table 21. The properties of the fresh sate were tested during printing and the properties of the hardened state (curing without cover) were tested after 10 days.

Table 21. Material rating woodglue mix TU Delft

Fresh state				Hardened state		Total
Homogeneity	Extrudability	Adhesion		Brittleness	Curing time	
2	2	2	*Non oven*	2	1,5	**9,5**
			Oven 40℃	0	2	**7**

Result
Several iterations were carried out to maximize the amount of lignin and cellulose and minimize the water content to optimize the material properties using the binder (see appendix 3 Assessing mixtures). From this, it can be concluded that TU Delft's mixture has already been modified in section 2.2.2 to obtain a printable mix.
In terms of homogeneity, extrudability and adhesion, woodglue is a better binder than methylcellulose, this is also reflected in the scores. It can also be seen that oven curing is faster, but it causes it to become too brittle in the hardened state.
Based on the high scores, it can be concluded that this is a very promising mixture. The downside is that the current mixture consists of 65,4% woodglue. The polyvinyl acetate-based glue is not a sustainable material and this deviates from the principle of bio-based printing. As a result, section 3.3 examines whether the amount of woodglue can be reduced so that the principle of bio-based printing is again satisfied.

3.3 New mixtures
The second phase of material research involves investigating new printable mixtures based on the mixture of woodglue. It looks at reducing the amount of woodglue and an alternative to woodglue.

3.2.1 Reference mix woodglue
Manufacture process
Cellulose was first made small and then mixed with lignin to separate the fibres and improve coverage with the polymer. Instead of water, Valida L.3% with woodglue was added and the mixture was mixed continuously to form a homogeneous and viscous mixture.
From the experiments conducted in this phase, a ratio of 1:2 between lignin and woodglue as well as the ratio of 1:8 between cellulose and lignin proved to be the most promising recipe. See table 22 for the materials in the mix.

Table 22. Reference mix woodglue

Material 1 (Raw material)	Material 2 (Liquid)	Material 3 (Binder)	Material 4 (Filler)
• Cellulose (5g) • Lignin (40g)	• Valida L,3% (60g)	• Woodglue (80g)	• -

Photos of the process are shown in figure 29. The freshly printed material can be seen on the left. The printed material showed excellent adhesion. On the top right, the mixture can be seen after it has been mixed and on the centre right, the material can be seen to turn brown during curing. The picture to the bottom right show however, that this mix turned white after curing.

Figure 29. Pictures reference mix woodglue

Rating

Scores were assigned to the printed material in the fresh state and hardened state. These scores are shown in table 23. The properties of the fresh sate were tested during printing and the properties of the hardened state (one mixture cured with plastic cover, one mixture cured with wooden cover fitted with holes both in the climate room) were tested after 12 days.

Table 23. Material rating reference mix woodglue

Fresh state				Hardened state		Total
Homogeneity	Extrudability	Adhesion		Brittleness	Curing time	
2	2	2	*Wood cover*	2	2	**10**
			Plastic cover	2	1,5	**9,5**

Result
Several iterations were performed to maximize the amount of lignin and cellulose and minimize woodglue to optimize material properties with Valida L,3% (see appendix 3 Assessing mixtures).
On all points, the mixture scores high. Curing with a wooden cover results in slightly better score compared to curing under a plastic cover.
The percentage of woodglue was reduced from 65,4% to 43,3%, ensuring the majority of the mixture consisted of bio-based material. Although the mixture is still not completely 100% bio-based, it is concluded that this is a promising mixture. Hence, this mixture is considered as the first reference mix to be further developed in this study.

The mixture has results similar to the bio-glue mixture, these results are described in section 3.3.3.

3.3.2 Reference mix bio-glue

Manufacture process
Cellulose was first made small and then mixed with lignin to separate the fibres and improve coverage with the polymer. Instead of woodglue, bio-based glue with Valida L.3% was added and the mixture was mixed continuously to form a homogeneous and moderately viscous mix.
From the experiments conducted in this phase, a ratio of 1:1,5 between lignin and bio-based glue as well as the ratio of 1:10 between cellulose and lignin proved to be the most promising recipe. In table 24 the amount of the four materials used in the mix can be seen.

Table 24. Reference mix bio-glue

Material 1 (Raw material)	Material 2 (Liquid)	Material 3 (Binder)	Material 4 (Filler)
• Cellulose (4g) • Lignin (40g)	• Valida L,3% (40g)	• Bio-glue (60g)	• -

Photos of the process are shown in figure 30. The freshly printed material can be seen on the left. The printed material showed excellent adhesion. On the top right, the mixture can be seen after it has been mixed and on the centre right, the material can be seen to turn brown during curing. Bottom right can be seen that material turned white when cured.

Figure 30. Pictures reference mix bio-glue

Rating

Scores were assigned to the printed material in the fresh state and hardened state. These scores are shown in table 25. The properties of the fresh sate were tested during printing and the properties of the hardened state (one mixture cured with plastic cover, one mixture cured with no cover both in the climate room) were tested after 9 days.

Table 25. Material rating reference mix bio-glue

Fresh state				Hardened state		Total
Homogeneity	Extrudability	Adhesion		Brittleness	Curing time	
2	2	2	*Plastic cover*	2	2	**10**
			No cover	2	1	**9**

Result

Several iterations were carried out to optimize the mixture with bio-based glue (see appendix 3 Assessing mixtures). On all points, the mixture scores high. It can be seen that curing under a plastic cover scores slightly better than curing ithout a cover.

By replacing woodglue with bio-based glue, this mixture is 100% bio-based and this fulfills perfectly well the principle of bio-based printing. With a score of 10 and 9 this mixture has results comparable to the woodglue mixture with a score of respectively 10 and 9.5. These results are described in section 3.3.3. Hence, this mixture is considered as the second reference mix to be further developed in this study.

3.3.3 Corresponding results

The printed elements in the hardened state turn white see figure 29 and figure 30 this is not mould. The cause of the whitening is probably due to the use of Valida L,3%. Since without the application of Valida L,3%, the printed elements do not turn white. In consultation with A. Habraken, it was decided not to investigate the exact cause. The whitening has no effect on the structural characteristics, which are being investigated further.

When the mixture is turned in the cartridge, it contains small bubbles as the mixture is not bubble-free. Considered was how to get the mixture bubble-free. The first option that had been looked at was using a vibrating table to vibrate the air bubbles out of the mixture. It was concluded that the air bubbles were not vibrated out with the vibrating table. The second option that had been looked at was by stamping on the mixture to get the air bubbles out. Again, the conclusion was that the air bubbles did not come out. Option three was to knead the air bubbles out. But the mixtures are too liquid to knead. The fourth option was to buy a vacuum plug mill. This device removes the air bubbles from the mixture. However, this device was too expensive to purchase. This led to the conclusion that when the material is turned into the cartridge for printing with the Makita, small air bubbles are always present in the mixture.

In this phase, different curing methods were examined, oven curing, room temperature curing and climate room curing. Different types of covers were also examined. From this, the following can be concluded. Oven curing causes the elements to become too brittle. Curing at room temperature or in the climate room differ little. As a result, it was decided to harden the elements in the climatic room because the temperature here is always the same. The temperature in the climate room is always 20 °C and the average relative humidity (RH) is 60%.
Curing under a glass cover would take too long as the moisture cannot evaporate from the mixture. In contrast, without a cover, the element would cure too quickly. The curing time make use of the plastic cover and perforated wooden cover is about the same. This leads to the conclusion that the printed elements should cure under a plastic film whilst air can reach them from below. This way a combination of the plastic cover and the wooden cover with holes appeared optimal.

Apart from determining the new two reference mixes, this phase also looked at adding fillers to the reference mix of woodglue (see appendix 3 Assessing mixtures). See section 5.4.3 for the description of the effect of the fillers. It can be concluded in this phase that adding sawdust in the reference mix of woodglue causes the material to become too brittle in cured state. Therefore, sawdust is not used as a filler.

At this stage of the study, shrinkage is not included. However, for finding the final mixture for the final element, shrinkage is included. Refer to chapter 5.

4. Printability exploration (material properties)

4.1 Robot set-up

For robotic 3D additive manufacturing, the following four parts are important (see figure 31):

1. ABB Robot;
2. End effector;
3. Makita;
4. Nozzle.

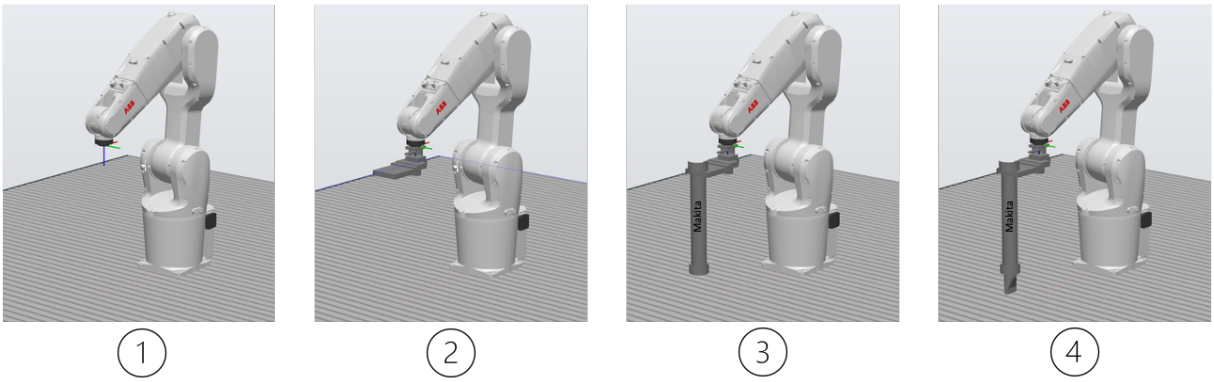

Figure 31. Robot set-up

4.1.1 ABB Robot

The robot used to produce the specimens is an ABB IRB 1200- 5/0.9, see figure 32. This robot is available in TU/e's Structural Engineering and Design lab. The robot can move in six different degrees of freedom (DOF). Each axis needs a rotation value to determine the position of the robot. The rotation value is denoted by the letters A through F followed by a value in degrees. The maximum handling capacity of the robot is a weight of 5 kilograms and a radius of 0.9 meters. The handling capacity of 5 kg will not be reached during production because no material needs to be lifted and the filled cartridge weighs less than 5 kg. More technical information about the ABB IRB 1200-5/0.9 [76] can be found in Appendix 4 Product specifications ABB IRB 1200-5/0.9.

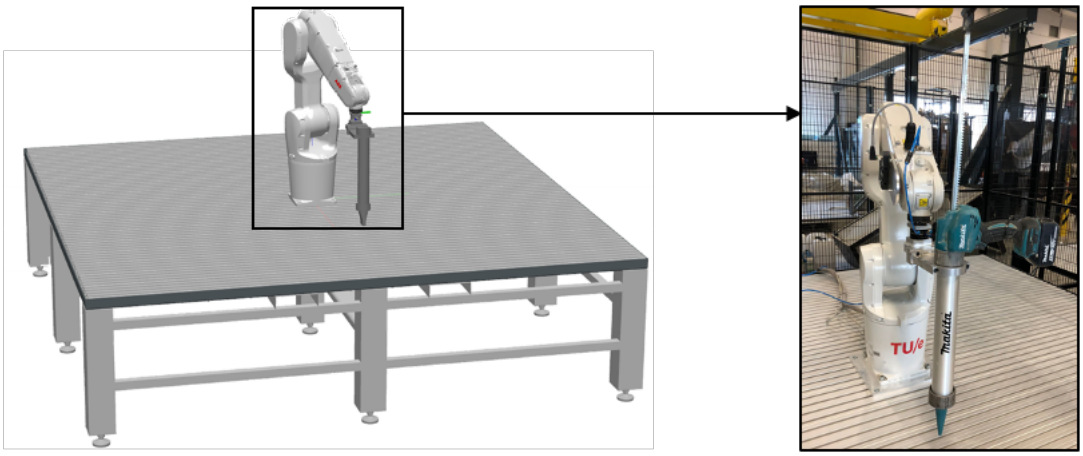

Figure 32. ABB IRB 1200-5/0.9 + Makita

4.1.2 End effector

The robot arm itself can only make movements, but it does not function without an end effector. An end effector is a component that is attached to the end of the robotic arm and determines what properties the robotic arm has. The end effector used was already present in the SED lab. To print the elements for testing, it must be able to direct the Makita extruder to specific points. The end effector consists of a steel plate fitted with a hole (see figure 33). The end of the steel plate (lip) can be unscrewed with two screws (see right figure 33 red circles). Then the cartridge is inserted into the hole

and the lip is screwed back on. As a result, the cartridge is clamped and can be guided to the appropriate points.

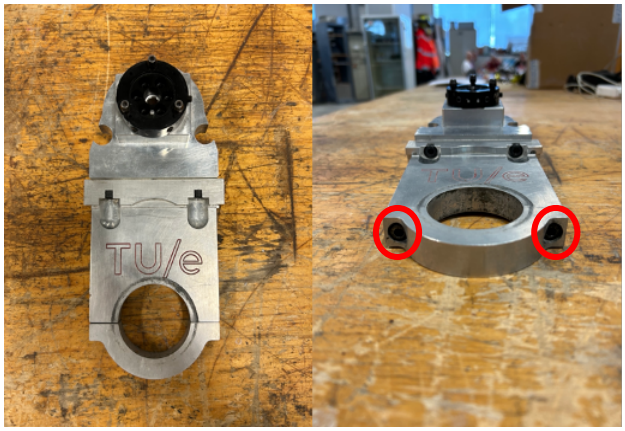

Figure 33. End effector

4.1.3 Makita

With the Makita (see figure 34 [77]), extrusion takes place using a piston. This is the simplest method for extrusion. In piston-based extrusion, a vertical force is applied so that the mixture can be extruded. The Makita is for applying the printable material to the print bed. The amount of material coming out is determined by the on/off switch, speed controller, nozzle and type of material.

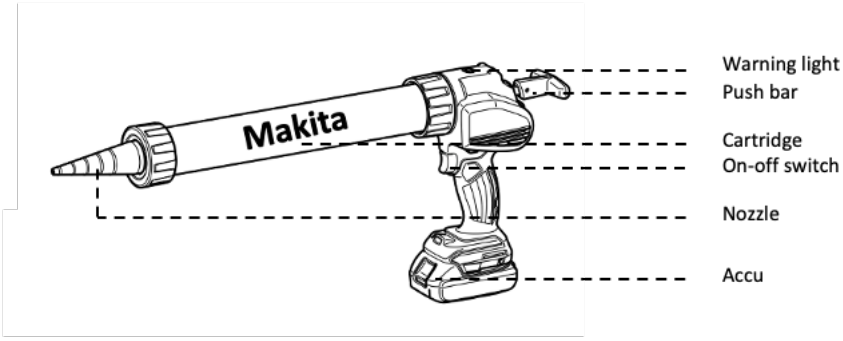

Figure 34. Makita [77]

The two reference mixes chosen for the printability study are woodglue and bio-glue. Additional advantages of the mixes are the easy handling, it does not damage tools or surfaces and no special products are needed to clean it.

The amount of material is matched to the content of the cartridge and should be sufficient to fill it completely. The cartridge has a diameter of 5,2 cm and a length 38,5 cm. An empty cartridge weights 723.5 g and a filled one weights between 1,5 – 2,0 kg, this fulfills the requirement of the handling capacity of the robot of 5kg. The quantities of each material (shown in table 26) is according to the proportions established in Chapter 3.

Table 26. Material quantities – one cartridge

	Reference mix woodglue		Reference mix bio-glue	
	Weight (g)	**Percent (%)**	**Weight (g)**	**Percent (%)**
Cellulose	25	2,71	30	2,78
Lignin	200	21,62	300	27.78
Valida L,3%	300	32,43	300	27,78
Woodglue	400	43,24	-	-
Bio-glue	-	-	450	41,66
Total	925	100	1080	100

Before printing, it is important to fill the cartridge correctly to avoid as many air bubbles as possible and minimize the risk damaging the printed elements. After the mixture is mixed according to the recipe, it is pressed flat on a PVC film or baking paper. It is then pressed on and rotated into the cartridge, see figure 35. This process is repeated until the cartridge is completely filled.

Figure 35. Mixture into the cartridge

4.1.4 Nozzle

The nozzle directly affects the overall resolution of the extrusion result and the level of detail. Also, the nozzle determines the diameter of the minimum layer thickness achievable. The type of nozzle for printing the elements comes from 3D concrete printing. All elements are printed with a rectangular nozzle (see table 27), resulting in layers 40 mm wide and 10 mm high.

Table 27. Rectangular nozzle

Top view	Front view	3D view	Cross-section
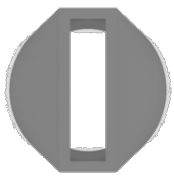		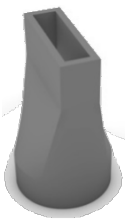	40x10 mm 

4.2 Print parameters

Pressure, print speed and nozzle standoff distance are categorized as print parameters. These factors are thoroughly tested to get the best layer dimension out of the nozzle.

4.2.1 Pressure

The speed at which the push bar pushes the material out of the nozzle can be adjusted by turning the speed controller, see figure 36. If the speed controller is turned in the direction of position 5, the speed at which the push bar pushes the material out of the nozzle increases. If the speed controller is turned in the direction of position 1, the speed at which the push bar pushes the material out of the nozzle becomes lower.

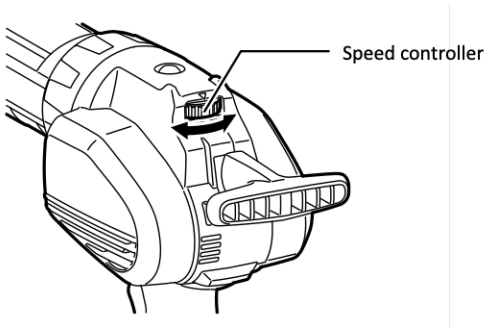

Figure 36. Speed controller Makita [77]

For each different mixture being printed, the speed controller is always set to position 2.
Note. The speed controller is very sensitive to the position. The difference between position 1.9, 2 and 2.1 is immediately visible. Therefore, it is very important to always set it to position 2.

4.2.2 Print speed

Once the processing requirements are met and a layer is successfully printed, the requirements shift to those of the individual layer. To maintain the desired geometry, a sufficiently high yield stress is required to withstand the gravity-induced stresses due to the layer's own weight. Even if the occurring stresses remain below this yield stress, the material must also be sufficiently stiff to limit deformations. Otherwise, layer deformations can accumulate to a significant deviation from the original design.
The following 3 situations can occur during the matching of the material flow from the nozzle and the robot's print speed, see figure 37.

1. If the speed of the robot is higher than the speed at which the material exits the nozzle, cracks form in the layer.
2. For a process performed at proper speed (material flow from the nozzle matched to the speed of the robot), the cross-sectional area of the layer is constant and there are no variations.
3. If the speed of the robot is lower than the speed at which the material exits the nozzle, accumulations occur in the layer.

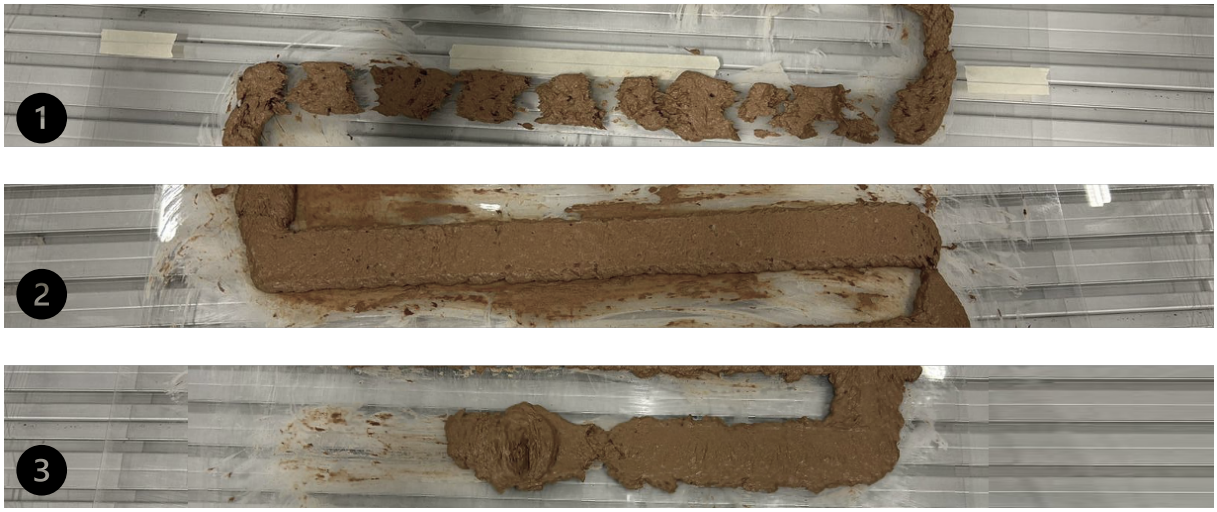

Figure 37. Different print speeds

In order to find the correct print speed of each mix, a pattern is set up in which after each corner the speed at which it is printed decreases (see figure 38).

Figure 38. Test print speed

This test is run as many times until the correct print speed of the particular mix is found, see table 28.

Table 28. Print speed

	Reference mix woodglue	Reference mix bio-based glue
Print speed (v) in mm/s	14,5 – 15,5	16,5

4.2.3 Nozzle standoff distance

The elements printed for determining material properties are 5 layers high. The 5 layers are printed in a continuous process. For the first layer, the nozzle standoff distance is slightly higher than the layers above it, it is 10mm respectively. This is done to create a perfectly leveled surface for the 4 layers to come on top. After the first layer, the nozzle standoff distance for each layer is the same namely 9,5mm. See figure 39 for illustration.

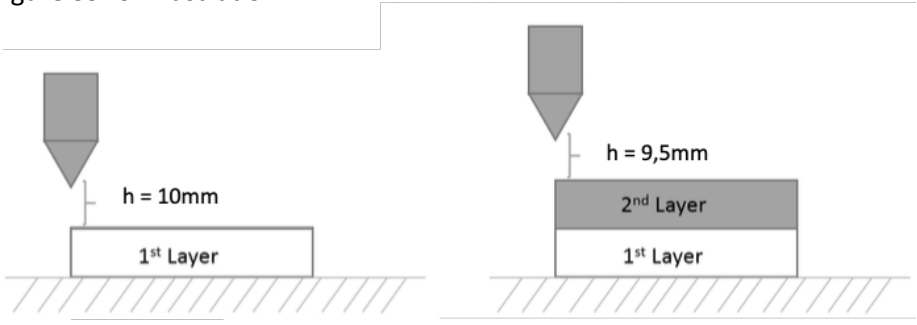

Figure 39. Nozzle standoff distance

4.3 Robotic printing

4.3.1 Robot path

To print the elements (see table 29) of 250mm long, 40mm wide and 5 layers high with the robot, a robot path must be defined to print the element in a continuous session.

Table 29. Element to be printed

Front view	Top view	Side view	3D view
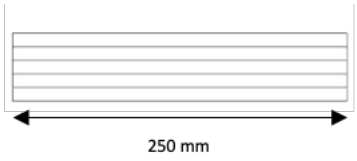		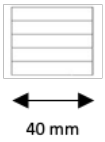	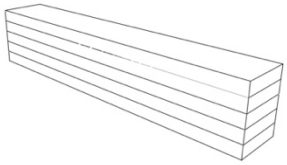

The robot path consists of joint movements and linear movements. The large movements between the starting position and the point of printing and between the end of printing back to the starting position are done with joint movement at a relatively high speed (v = 300 mm/s). When the robot starts printing, it makes linear movements with a lower precision speed. For print speeds, see section 4.2.2. See table 30 and 31 for the properties of the different movements.

Table 30. Different movements

Joint movement	Linear movement
+ Good for posing the robot	+ Maximum precision
- Slightly lower precision	+ Straight / linear movement
Used for moving through workspace ((all less precise movements)	- Can result in singularity
	Used for toolpath operations (all precise movements)

The robot path is visualized in figure 40.

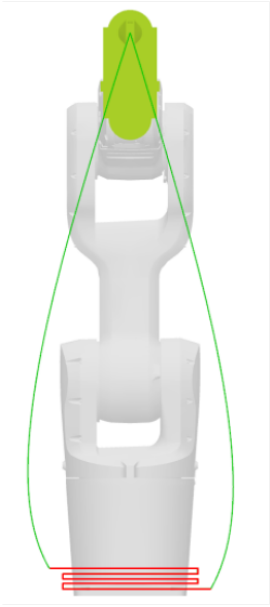

Figure 40. Robot path

Table 31. Movements

Line	Type	Precision	Movement type	Speed
	Free space	Low	Joint movement	High
	Print process	High	Linear movement	low

4.3.2. Robot components

All target points must be placed on the element. Therefore, the plane orientation of the end effector must match the plane orientation of the target points on the element. The plane orientation and the value of the element affect how the robot approaches each point. It is desirable for the robot to move only in horizontal and vertical directions, without moving around the structure. Therefore, the planes of the target points on the element to be printed should be oriented downwards so that it overlaps with the plane orientation of the end effector. Figure 41 visualizes the robot path, and the corresponding plane orientations of the end effector and the target points.
After all the plane orientations are correctly defined, a list of robot targets is created. This list is used to create movements. The movements of the robot are described in Section 4.3.1. The created movements and the defined ABB robot are combined into a list of actions. Using the Robot components plug-in, the RAPID Generator component generates a RAPID script that the robot software understands. The RAPID script consists of a RAPID Program Module (PM) and a RAPID System Module (SM). The PM script (MainModule) defines the robot movements and the SM script (BASE code) determines the orientation of the robot head based on the end-effector tool. See Appendix 5 RAPID script for the RAPID script.

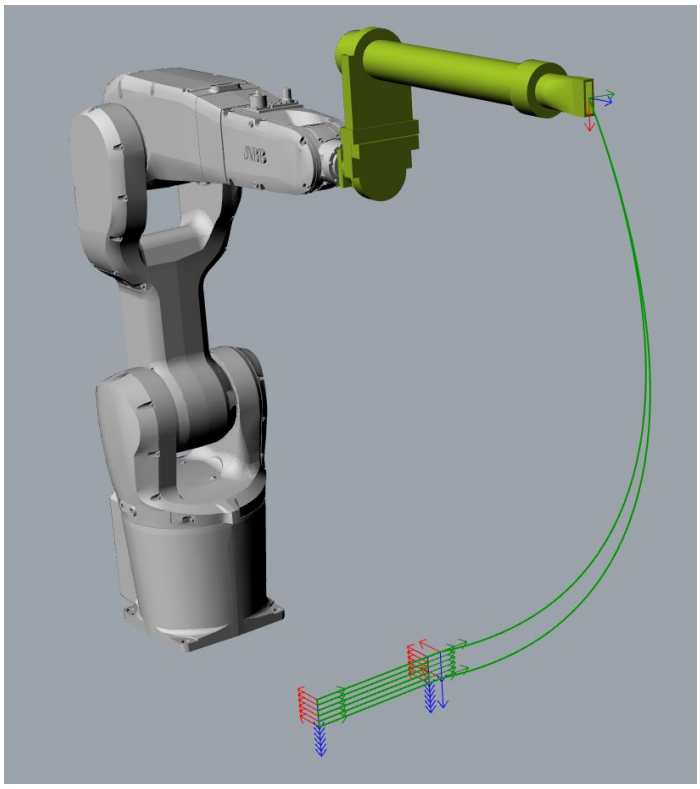

Figure 41. Robot path and plane orientation with Robot components

4.3.3 RobotStudio

The created RAPID program module (PM) and system module (SM) are loaded into Robot Studio to stimulate the full robot path. When the robot cannot reach a certain point due to, for example, robot reach, singularity or joint failure, the program will display an error message. The error message can be fixed by, for example, repositioning the geometry on the robot bed. It is then retested in RobotStudio to see if the new positions are within range, this process is repeated until the entire robot path is executed without an error message. Figure 42 visualizes the final simulated robot path.

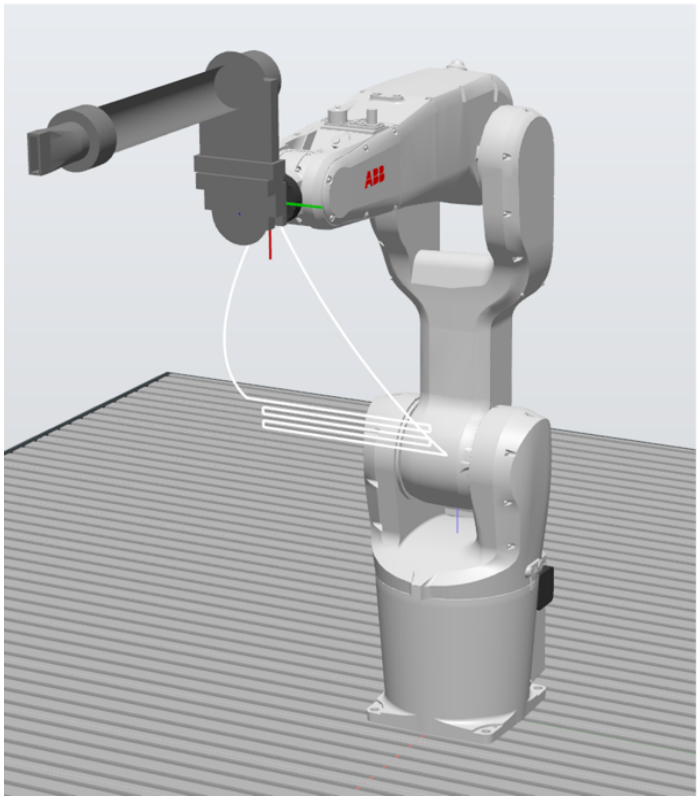

Figure 42. Robot path with RobotStudio

4.3.4 Printing

All prints are made in the Structures Laboratory at Eindhoven University of Technology. In this laboratory the temperature and humidity are regulated and measured. The temperature averages 20.2 – 20.5 °C and the average relative humidity (RH) is 59.7 – 60.3% during the period used. Figure 43 shows the printing process. First, the robot arm moves from its initial position to the starting position for printing (1). Next, the Makita and the motion of the robotic arm are simultaneously turned on and the material is extruded out of the nozzle (2-3). When layer 5 is printed, the Makita and the motion of the robotic arm are turned off and the robotic arm moves back to the initial position (4).

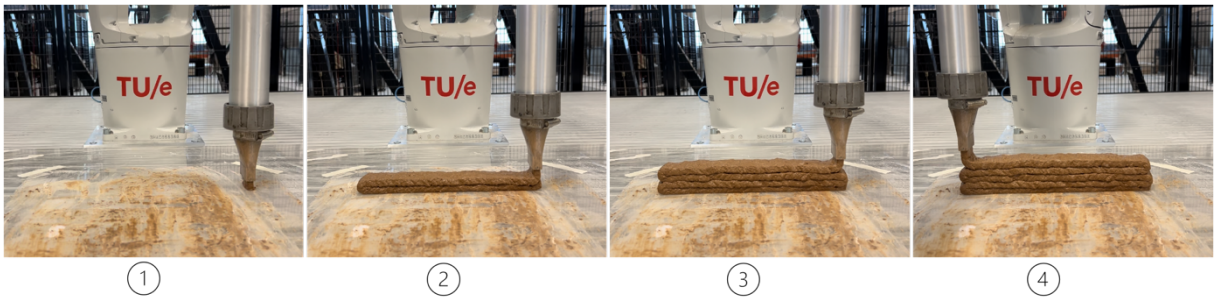

Figure 43. Print process

4.4 Curing time

After printing (1), the elements were kept under a plastic film in the climate room for ±7 days (2). In the climate room it is 20 °C and the average relative humidity (RH) is 60%. After ±7 days, the elements were turned over so that the bottom side could also cure. After turning them over, the elements cure for another ±7 days after which they can be tested (3). Figure 44 shows the process described above. See Appendix 6 Information printed elements for curing time of each element separately.

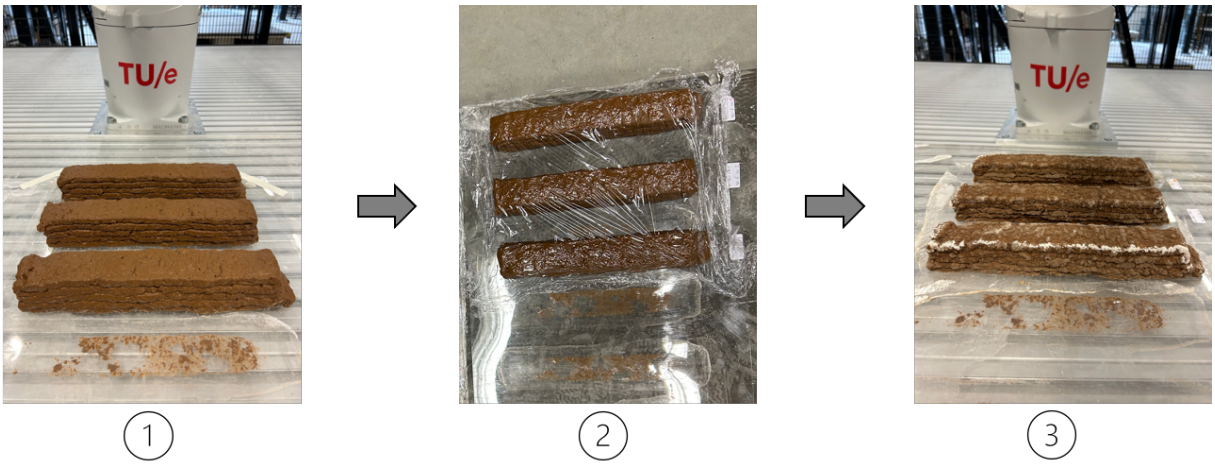

Figure 44. Curing process

4.5 Final elements

In total, there are two types of elements. One type of element is for compression test and the other type of element is for the flexural test.

4.5.1 Elements for the compression test

The elements for the compression test are cut from the main element after the curing period in cubic dimensions of 40 x 40 x 40 mm, see figure 45. Next, the elements were sanded to achieve smooth specimen sides and prevent the occurrence of peak stresses.

Figure 45. Elements for compression test

4.5.2 Element for the flexural test

The element for the flexural test is shown in figure 46. The ends of the element are cut and sanded to create a rectangular element of 250 x 40 x 5 layers.

Figure 46. Element for flexural test

5. Material properties

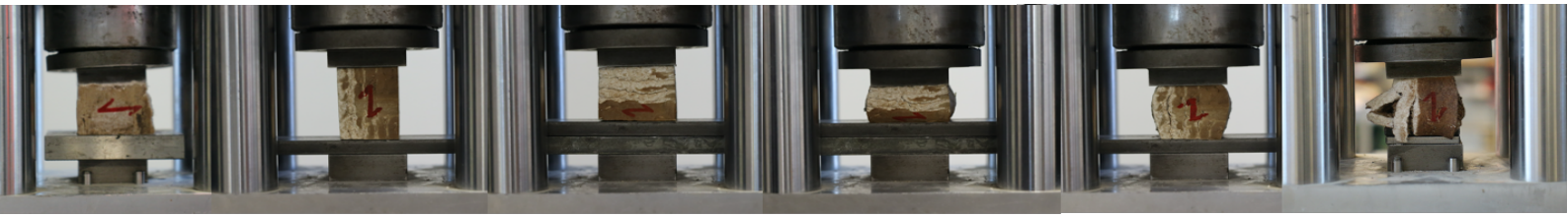

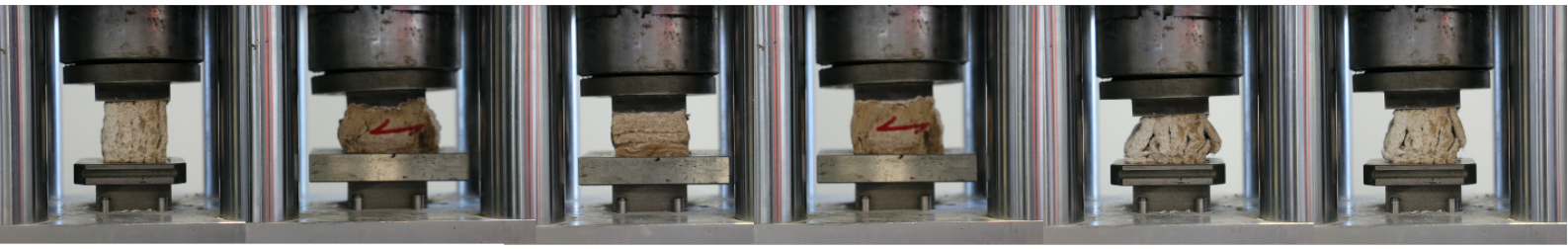

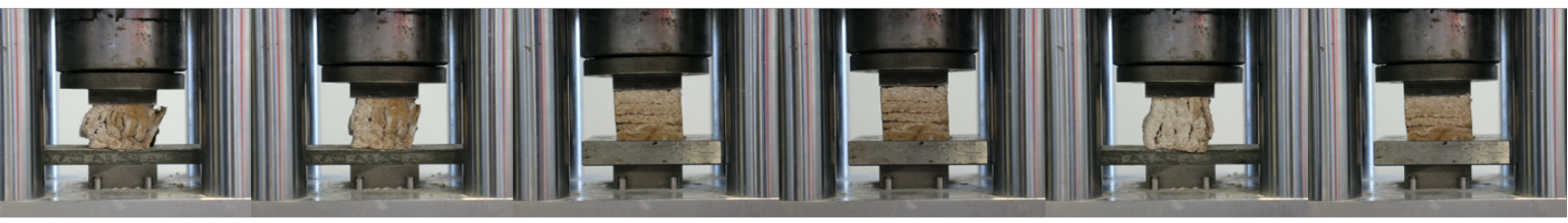
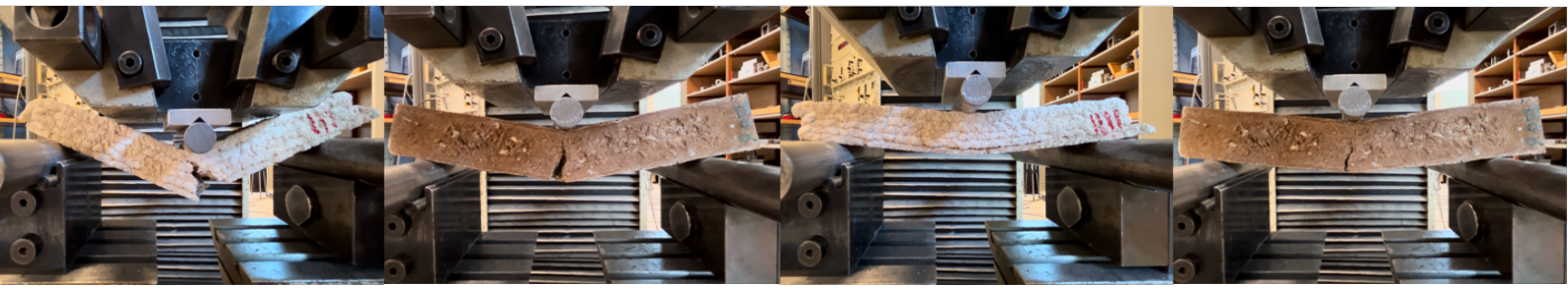
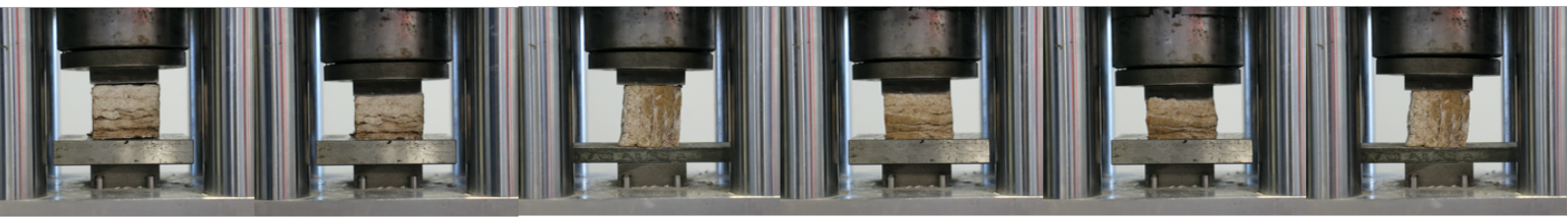


This chapter presents only the results of the tests. For a detailed analysis of the results of the tests, please read Franka Pels Rijcken's research report.
The elements of the two tests performed and the test direction is shown in figure 47. The results of the test data are described in the following paragraphs. The measured parameters vary between the tests. Not only the strength properties are measured and examined, but also some material properties. These material properties are extracted from the results to make it possible to characterize this type of material in a finite element program.

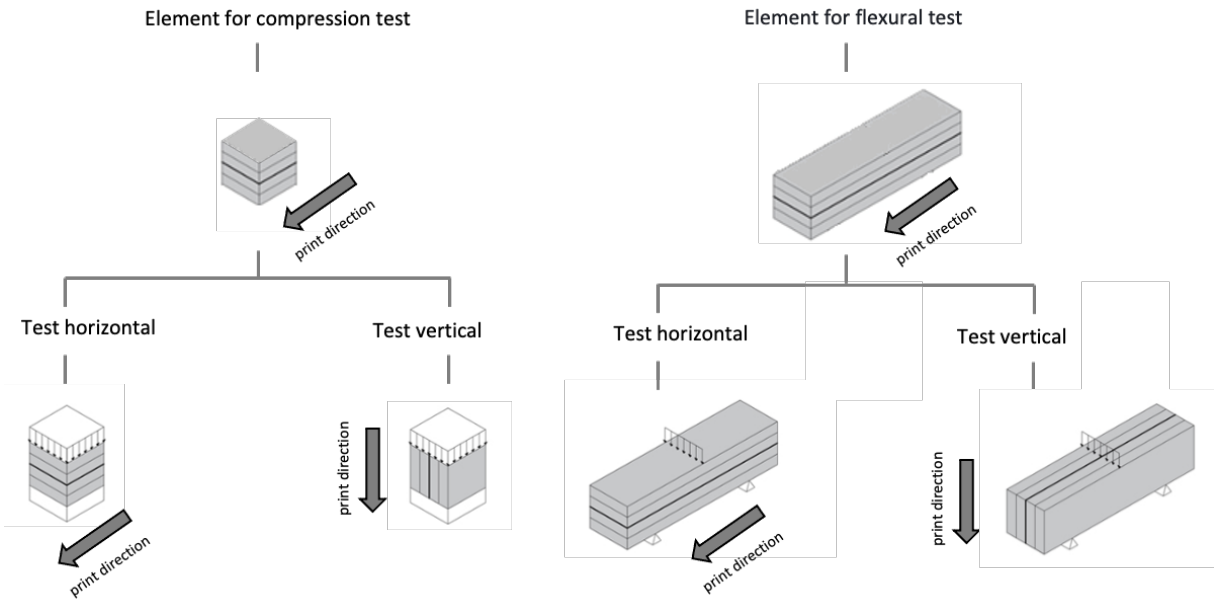

Figure 47. Different tests and print directions

5.1 Reference mixes (with no fillers)

5.1.1 Compressive test

The compression test is based on the standardized mortar pressure test in NEN-EN 196- 1:2005 [78]. The choice to base the compression test on the mortar standard is due to the small particle size in the material. Instead of the standardized load controlled test, this test is deformation controlled at a rate of ± 2 millimeters / minute. This is because of the ability to measure the post-peak effect. This test tests some parameters of the material, namely: compressive stress on the element and Young's modulus.

The test is performed in an available rigid steel frame. Within the range of loads required to collapse the specimens, the rigid frame will not deform. The punch with which force is applied can move a maximum of 15mm. Because of this, we chose to measure three times compressive stresses at displacements of 4mm (cycle 1.1 - 1.3), 8mm (cycle 2.1 - 2.3) and 12mm (cycle 3.1 – 3.3). The measured deformations in the frame are the deformations of the specimens. Figure 48 shows an overview of the compression test set-up. The test was performed in an Schenck Trebel test bench with a 100kN load cell.

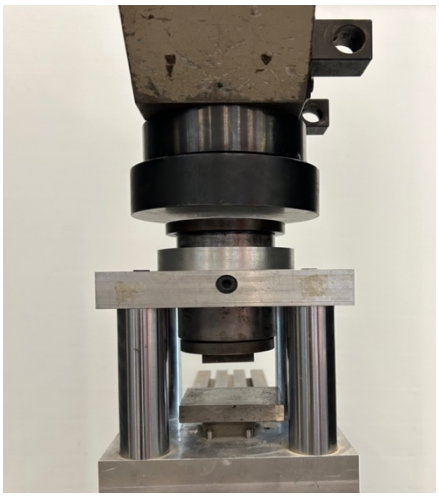

Figure 48. Test set-up

The compression tests were performed on cubic specimens of ± 40 x ± 40 x ± 40 mm in both horizontal and vertical directions, see figure 49.

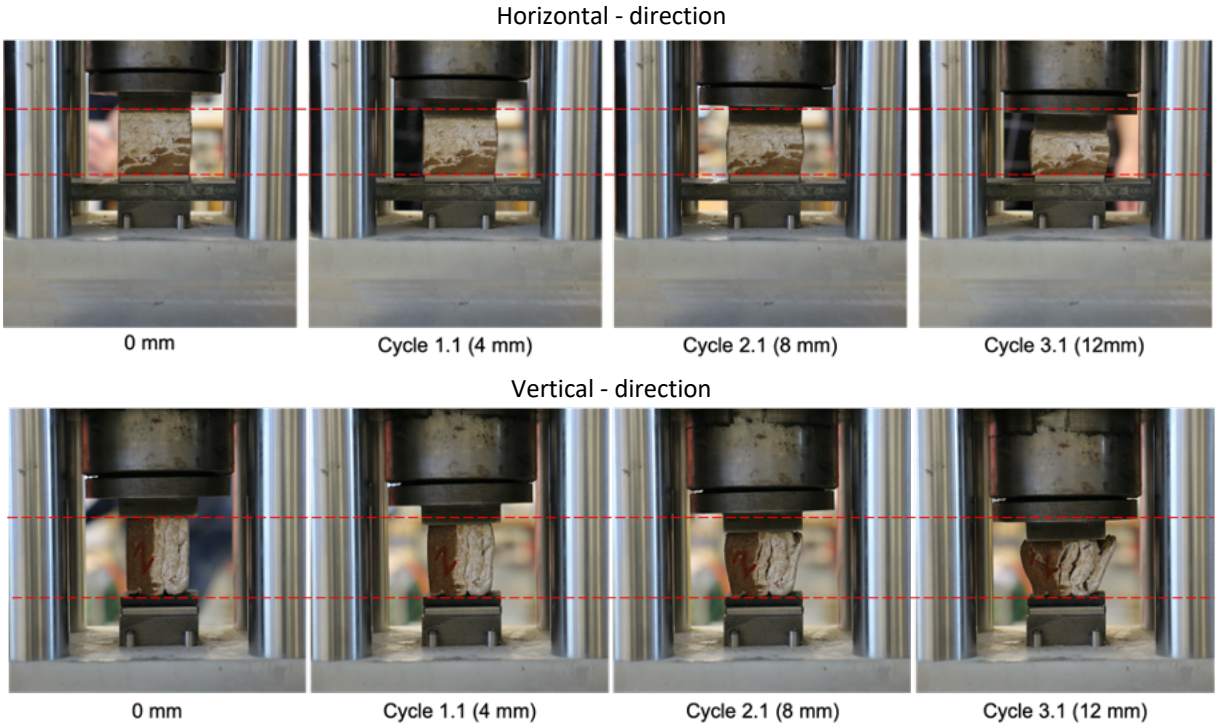

Figure 49. Compression test in horizontal and vertical direction

The crack pattern of the elements are shown in figure 50 for both vertical and horizontal directions. The elements never break completely. In the horizontal direction, the cracks occur at the corners. In the vertical direction, the cracks occur in between the layers.

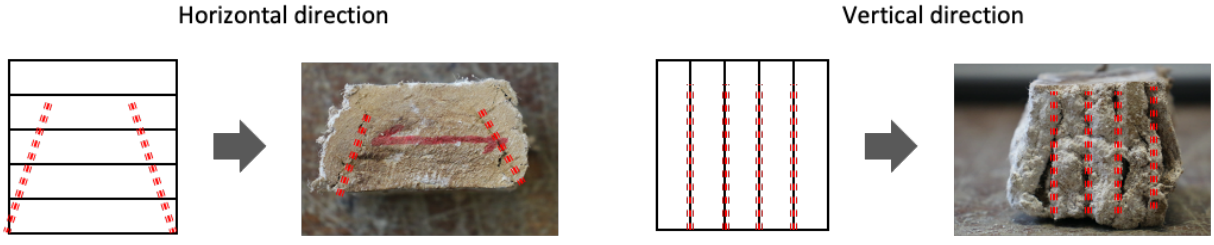

Figure 50. Crack pattern in horizontal and vertical direction

5.1.2 Results compressive strength

Compression strength

Upon 12mm, the load F_b was recorded and used to calculate the compression strength f_b of the specimen as follows:

$$f_b = \frac{F_b}{A_b} \quad (5.1)$$

Where:

- f_b is the compression strength (MPa)
- F_b is the recorded load (N)
- A_b is the cross-sectional area of the specimen (mm^2)

The results of the compression tests of cycle 1.1, 2.1 and 3.1 are shown in a box-and-whisker graph in figure 51, for the horizontal and vertical directions. A box-and-whisker graph shows how data are distributed across quartiles, highlighting the mean and outliers. Vertical lines ("whiskers") can be drawn from the boxes to indicate variability outside the upper and lower quartiles. Any point outside these lines is considered an outlier or outlier [79]. Each test is worked out individually in Appendix 7 Compression tests.

Reference woodglue

There were 3 specimens tested in horizontal direction and 3 specimens tested in vertical direction. However, test 3 in horizontal direction and test 1 in vertical direction showed different values, therefore they were not included in the comparison. This results in two tests horizontally and two tests vertically.

Horizontal

figure 51 shows that the compressive strength increases significantly with each cycle. The compressive strength of the woodglue mixture is between 4,62 – 5,21 MPa for cycle 1.1. For cycle 2.1, the compressive strength is between 8,42 – 9,59 MPa and for cycle 3.1 between 16,55 – 17,44 MPa.

Vertical

Figure 51 shows that the compressive strength in the vertical direction is a lot lower than for the horizontal direction. Also, the value of compressive strength per cycle increases a lot less. The compressive strength of the woodglue mixture is between 2,40 – 2,96 MPa for cycle 1.1. For cycle 2.1 the compressive strength is between 3,45 – 4,24 MPa and for cycle 3.1 between 4,65 – 5,57 MPa.

Reference bio-glue

There were 3 specimens tested in horizontal direction and 3 specimens tested in vertical direction. However, test 3 in horizontal direction and test 3 in vertical direction showed different values, therefore they were not included in the comparison. This results in two tests horizontally and two tests vertically.

Horizontal

Figure 51 shows that the compressive strength increases with each cycle, but less than woodglue. The compressive strength of the bio-glue mixture is between 1,62 – 1,68 MPa for cycle 1.1. For cycle 2.1 the compressive strength is between 2,94 – 3,12 MPa and for cycle 3.1 between 4,81 – 5,51 MPa.

Vertical

Figure 51 shows that the compressive strength in the vertical direction increases slightly between cycle 1.1 and 2.1. Between cycle 2.1 and 3.1, the compressive strength decreases. The compressive strength of the bio-glue mixture is between 2,21 – 2,89 MPa for cycle 1.1. For cycle 2.1 the compressive strength is between 2,23 – 2,98 MPa and for cycle 3.1 between 1,81 – 2,86 MPa.

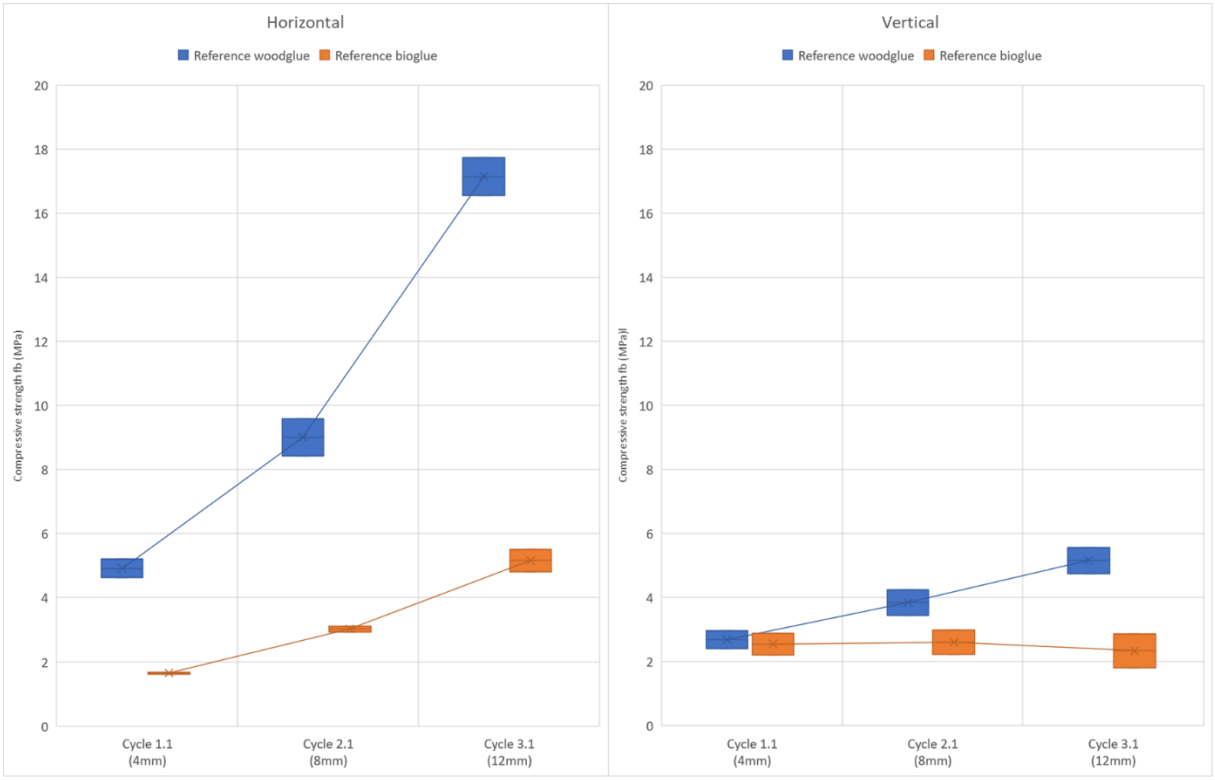

Figure 51. Results of the compressive strength of the mix with woodglue and bio-glue in horizontal and vertical direction

Young's modulus (compressive strength)

The Young's modulus (E-modulus) is extracted out of the stress-strain diagram of all single tests. It is common to use the stress-strain diagram in compression to calculate this property. The stress was calculated using the formula for the compression strength. The strain was calculated using Hooke's law with the following formula:

$$\varepsilon = \frac{\Delta L}{L} \quad (5.2)$$

Where:

- ε is the strain (-)
- ΔL is the amount of deformation (the change in length) produced by the force F_b (mm)
- L is the length of the specimen (mm^2)

If the stress-strain diagram is known, the slope of the line in the linear part of cycle 1.1 is the Young's modulus, see figure 52. The parts of cycle 2.1 and 3.1 were not considered because in reality a structural element doesn't deflect that far.

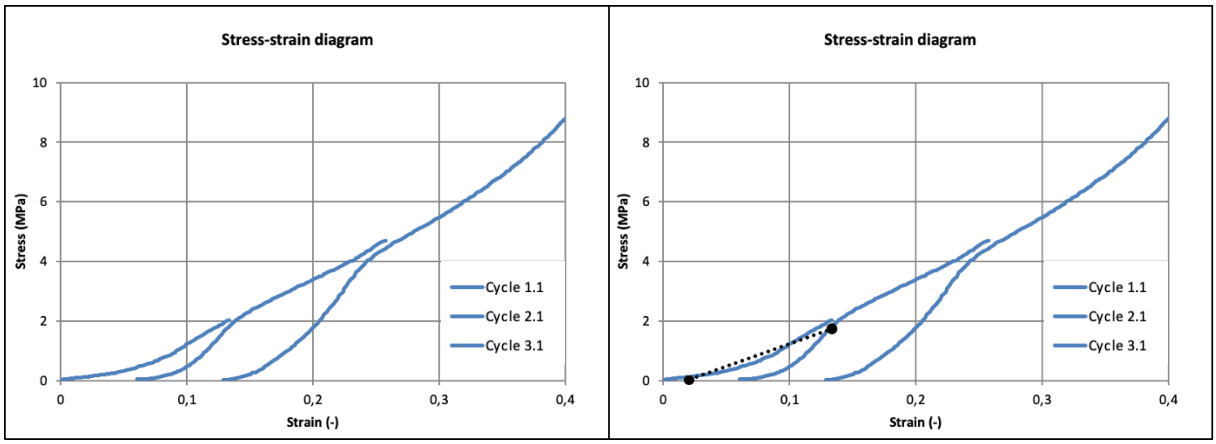

Figure 52. Determination Young's modulus of cycle 1.1

The elaboration of the E-modulus results of cycle 1.1 are shown in a box-and-whisker graph in figure 53, for the horizontal and vertical directions.

Reference woodglue

Horizontal

The E-modulus of the woodglue mixture is between 43,01 – 46,07 MPa for cycle 1.1.

Vertical

Figure 53 shows that the E-modulus in vertical direction is lower than for the horizontal direction. The E-modulus of the woodglue mixture is between 24,83 – 29,95 MPa for cycle 1.1.

Reference bio-glue

Horizontal

The E-modulus of the bio-glue mixture is a lot lower than the woodglue mixture. The E-modulus is between 14,12 – 14,13 MPa for cycle 1.1.

Vertical

Figure 53 shows that the E-modulus in the vertical direction is higher than for the horizontal direction. The E-modulus of the bio-glue mixture is between 19,46 – 21,40 MPa for cycle 1.1.

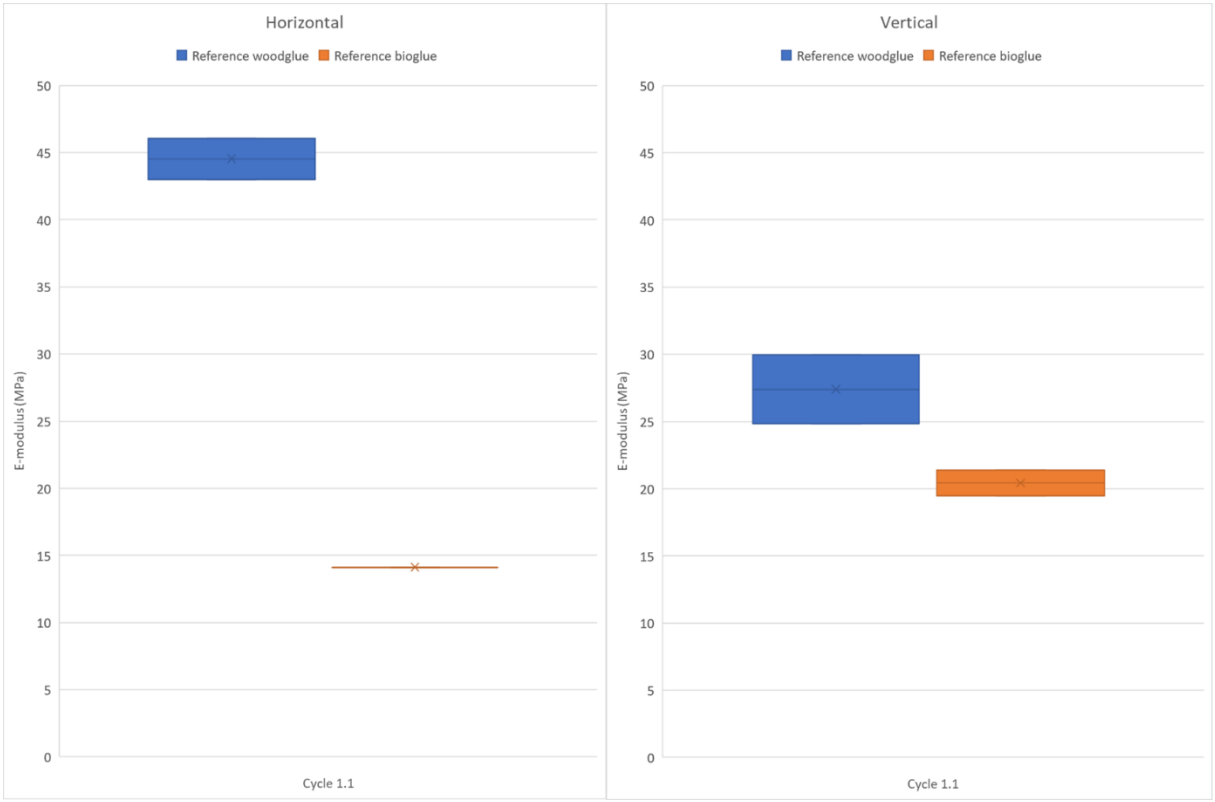

Figure 53. Results of the E-modulus of the mix with woodglue and bio-glue in horizontal and vertical direction

5.1.3 Flexural test

Flexural strength was determined by performing three-point bending tests on prismatic specimens, according to NEN-EN 196-1 [78]. Figure 54 shows an overview of the flexural test set-up. The test was performed in an Schenck Trebel test bench with a 100kN load cell.

Figure 54. Test set-up

The printed specimens has the dimensions of ± 40 × ± 40 × ± 250 mm, and the deformation is controlled at a rate of ± 3 millimeters / minute. This test tests some parameters of the material, namely: flexural stress on the element and Young's modulus. The load is applied at the center of the specimen and the flexural tests were performed on prismatic specimens in both horizontal and vertical directions, see figure 55.

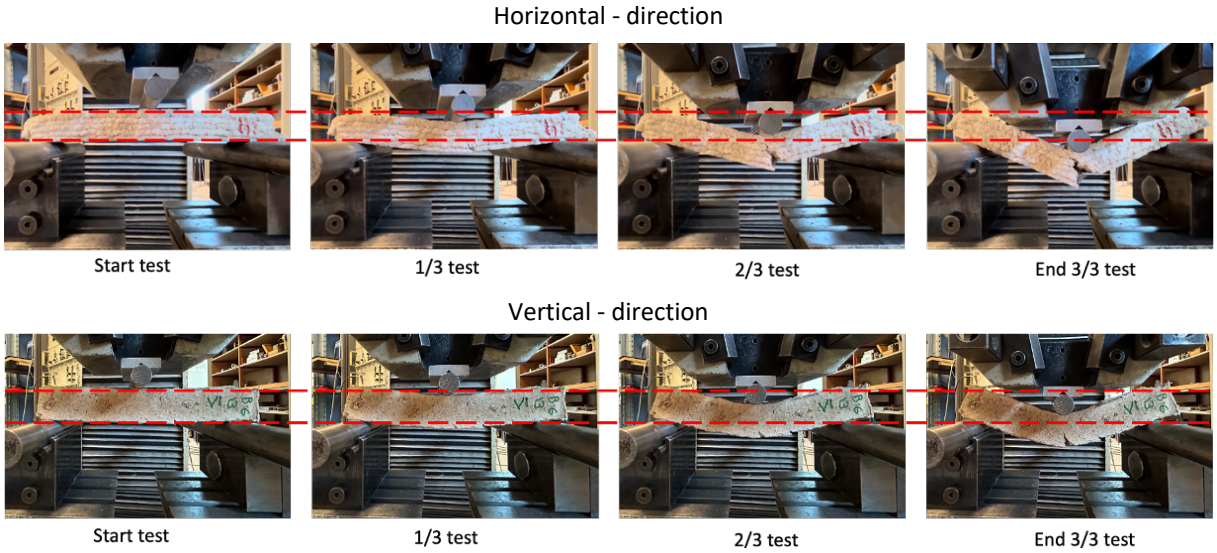

Figure 55. Flexural test in horizontal and vertical direction

The crack pattern of the elements is shown in figure 56 for both vertical and horizontal directions. The elements never break completely. In both horizontal and vertical directions, the crack occurs in the bottom center of the element.

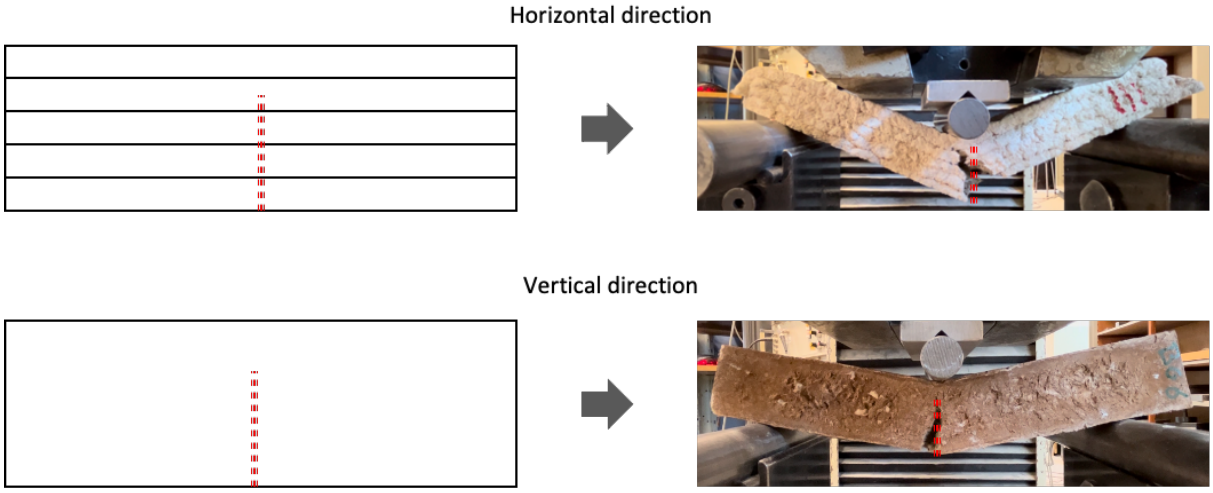

Figure 56. Crack pattern in horizontal and vertical direction

5.1.4 Results flexural strength

Flexural strength

Upon failure, the load F_f is recorded and used to calculate the flexural strength f_f of the specimen as follows:

$$f_f = \frac{3F_f \cdot l}{2 \cdot b \cdot d^2} \quad (5.3)$$

Where:

- f_f is the flexural strength (MPa)
- F_f is the recorded load (N)
- l is the distance between supports (mm)
- b is the side of the specimen (mm)
- d is the depth of the specimen (mm^2)

Or

$$f_f = \frac{M \cdot z}{I} \quad (5.4)$$

Where:

- f_f is the flexural strength (MPa)
- M is the moment (Nmm)
- z is distance to extreme fiber (mm)
- I is the moment of inertia (mm^4)

The results of the flexural strength are shown in a box-and-whisker graph in figure 57, for the horizontal and vertical directions. Each test is worked out individually in Appendix 8 Flexural tests.

<u>Reference woodglue</u>

There were 6 specimens tested in horizontal direction and 5 specimens tested in vertical direction. However, no crack was visible in tests 1 to 5 in horizontal direction and in tests 1 and 2 in vertical direction (see pictures in Appendix 8 Flexural tests for the respective tests). Because no crack was visible, these tests have different values and are not included in the comparison. This results in one test horizontally and three tests vertically.

Horizontal
The flexural strength of the woodglue mixture is 3,91 MPa.

Vertical
Figure 57 shows that the flexural strength in the vertical direction is higher than for the horizontal direction. The flexural strength of the woodglue mixture is between 4,19 – 4,70 MPa.

<u>Reference bio-glue</u>
There were 7 specimens tested in horizontal direction and 6 specimens tested in vertical direction. However, no crack was visible in tests 6 and 7 in horizontal direction and in tests 4 to 6 in vertical direction (see pictures in Appendix 8 Flexural tests for the respective tests). Because no crack was visible, these tests have different values and are not included in the comparison. This results in five tests horizontally and three tests vertically.

Horizontal
The flexural strength of the bio-glue mixture is between 3,39 – 4,78 MPa.

Vertical
Figure 57 shows that the flexural strength in the vertical direction is higher than for the horizontal direction. The flexural strength of the bio-glue mixture is between 3,66 – 4,93 MPa.

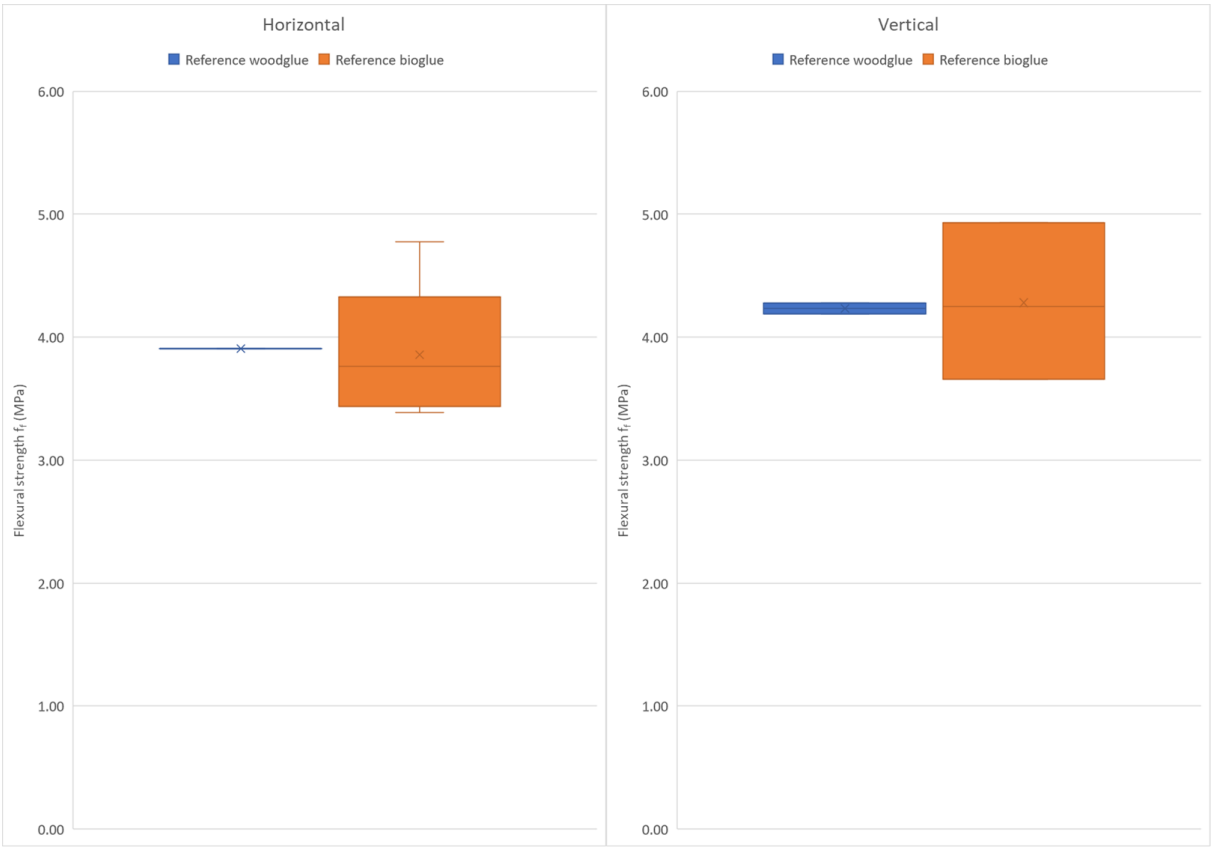

Figure 57. Results of the flexural strength of the mix with woodglue and bio-glue in horizontal and vertical direction

Flexural modulus

The flexural modulus is extracted out of the stress-strain diagram of all single tests. It is common to use the stress-strain diagram in flexural to calculate this property. The stress was calculated using the formula for the flexural strength. The strain was calculated with the following formula:

$$\varepsilon = \frac{6D \cdot d}{L^2} \quad (5.5)$$

Where:

- ε is the strain (-)
- D is the amount of deformation produced by the force F_f (mm)
- d is the depth of the specimen(mm)
- L is the length of the specimen (mm^2)

If the stress-strain diagram is known, the slope of the line until 2 MPa is the Young's modulus see figure 58. The last part of the graph after the peak is not considered, because this part is not linear.

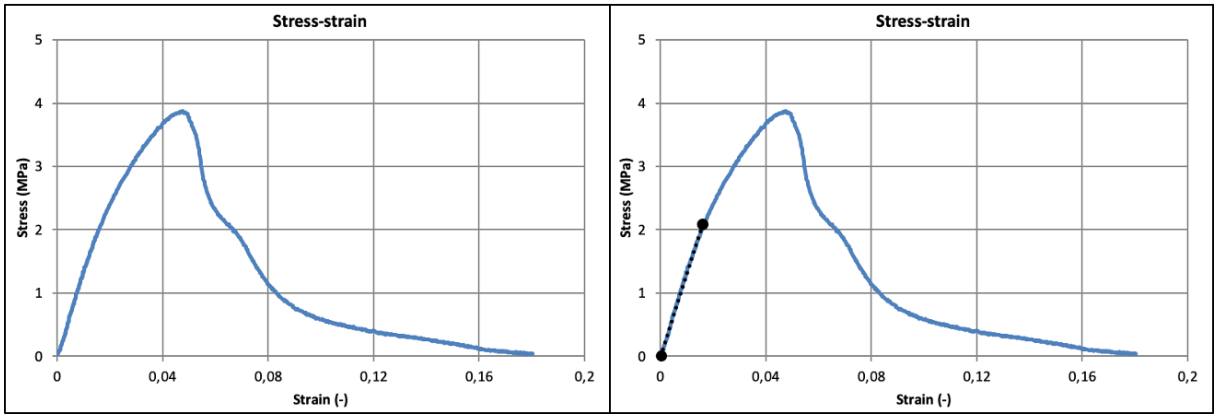

Figure 58. Determination Young's modulus

The elaboration of the flexural modulus results are shown in a box-and-whisker graph in figure 59, for the horizontal and vertical directions.

<u>Reference woodglue</u>

Horizontal

The flexural modulus of the woodglue mixture is 149,29 MPa.

Vertical

Figure 59 shows that the flexural modulus in vertical direction is higher than for the horizontal direction. The flexural modulus of the woodglue mixture is between 159,15 – 212,6 MPa.

<u>Reference bio-glue</u>

Horizontal

The flexural modulus of the bio-glue mixture is a little bit lower than the woodglue mixture. The flexural modulus is between 113,73 – 129,88 MPa.

Vertical

Figure 59 shows that the flexural modulus in the vertical direction is higher than for the horizontal direction. The flexural modulus of the bio-glue mixture is between 158,7 – 181,58 MPa.

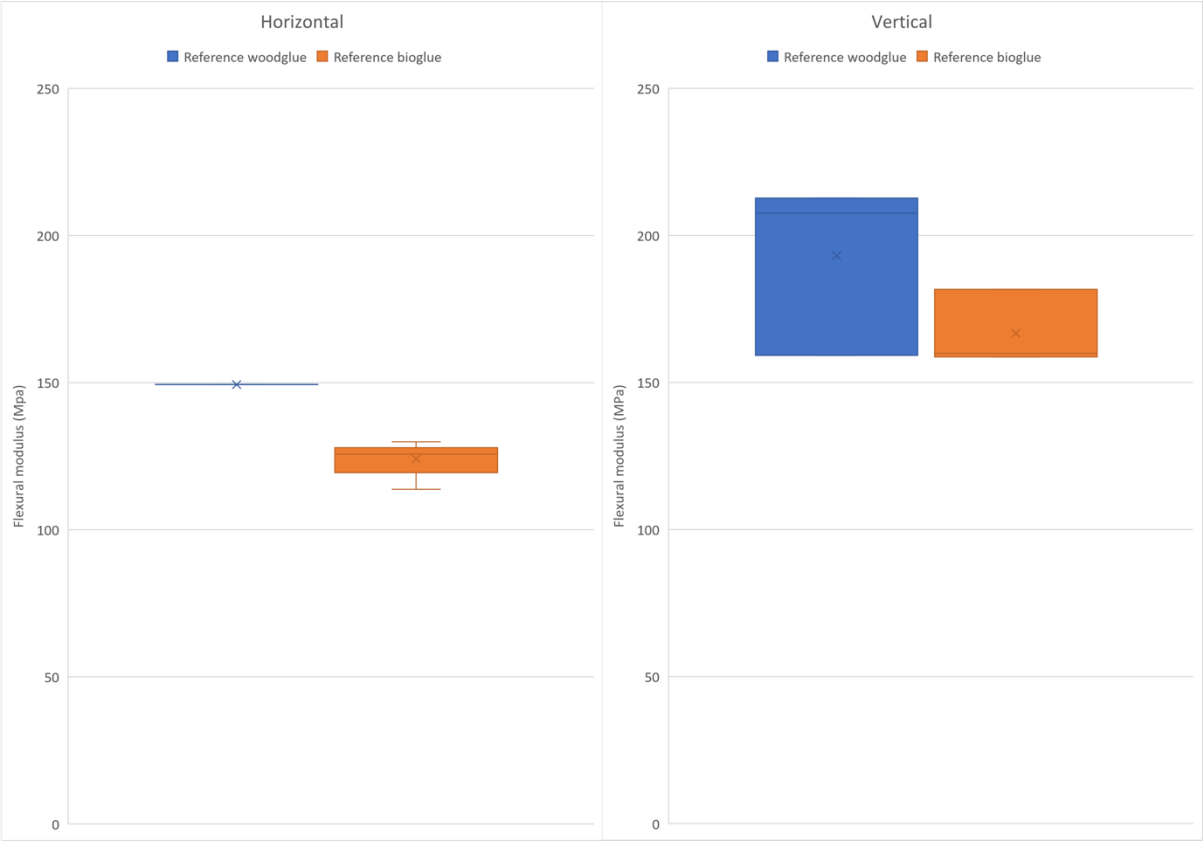

Figure 59. Results of the flexural modulus of the mix with woodglue and bio-glue in horizontal and vertical direction

5.1.5. Conclusion: reference woodglue vs reference bio-glue

Compression test:

- The compressive strength of the mixture with woodglue is higher in both vertical and horizontal directions than the mixture with bio-glue.
- The compressive strength for both mixtures is stronger in the horizontal direction than in the vertical direction.
- The flexural modulus of the mixture with woodglue is higher than the mixture with bio-glue in both vertical and horizontal directions.
- The flexural modulus is higher for woodglue in the horizontal direction than in the vertical direction and vice versa for the bio-glue.

Flexural test:

- The flexural strength of the mixture with bio-glue shows a greater variation and therefore has values where it is stronger than woodglue, but it also gives values where it is weaker than woodglue.
- The flexural strength is almost the same for both mixtures in both horizontal direction and vertical direction.
- The flexural modulus of the mixture with woodglue is higher in the horizontal direction than the mixture with bio-glue. In the vertical direction, the values are more similar with the mixture with woodglue having a higher maximum value than the mixture with bio-glue.
- The flexural modulus is stronger for both mixtures in the vertical direction than in the horizontal direction.

It can be concluded on the points mentioned above that the compressive strength of the mixtures with woodglue is higher than the mixture with bio-glue. The flexural strength is almost the same for the two mixtures. Based on the research question (see introduction), it was chosen to continue with the mixture with bio-glue in the remaining part of the research, since this mixture is more bio-based than the mixture with woodglue.

5.2 Reference mix + filler

By adding a filler, the aim is to see if the material properties of the bio-glue mixture can be improved. It was decided to look at up to 3 new bio-glue mixtures. In the first new bio-glue mixture, the addition of bentonite is being considered. Bentonite will make the mixture denser and stronger, also increasing its stiffness. The second new bio-glue mixture involves the addition of flax. This natural fiber reinforcement with long threads (length more than 10mm) should increase the material properties in tensile. The last new bio-adhesive mixture consists of a combination of both fillers.

5.2.1 Reference mix + bentonite

For the first batch, 10g of bentonite (see table 32) was added to the dry materials celullose and lignin. Next, this was mixed with the wet materials Valida L,3% and bio-glue to form a homogeneous mass. The result was a denser and too dry mix where the adhesion of the mix was not optimal. Despite the mix not having the right consistence for extrusion, elements were still printed to see what 10g changes to the material properties.

In the second batch, 5g (see table 32) of bentonite was added. It was mixed into a homogeneous paste. The result was a denser and drier paste where the adhesion of the mix is optimal. The mix has the right homogeneity, appearance and consistency optimal for extrusion.

The addition of bentonite also made it easier to turn the mix into the cartridge because of the increased stiffness of the mix. The printed elements were found to be more resistant to contact pressure compared to the original bio-glue mixture. The only small disadvantage of this mix is that the printed elements showed a high moisture content. Over time, all this moisture sank to the bottom layer making this layer watery.

The shrinkage of the cured elements is appeared to be between 10-18%. See Appendix 6 Information printed elements for a detailed analysis of the shrinkage.

Table 32. Reference mix bio-glue + bentonite

Material 1 (Raw material)	Material 2 (Liquid)	Material 3 (Binder)	Material 4 (Filler)
• Cellulose (4g) • Lignin (40g)	• Valida L,3% (40g)	• Bio-glue (60g)	• Bentonite (5 – 10g)

5.2.2 Reference mix + flax

For this new batch, 1,5g of flax (see table 33) was added to the dry materials cellulose and lignin. The fibers were cut to a length of about 10mm before combining with cellulose and lignin. This separated the threads and prevented clusters and clumps. Next, this was mixed with the wet materials Valida L,3% and bio-glue. Despite being more difficult to mix as bentonite powder, the result was also a homogeneous mix. This mix has the right homogeneity, appearance and consistency optimal for extrusion.

Fiber reinforcement (although in small amounts) was clearly observed with the formation of long chains of threads completely covered by the material mix. The long chain of threads made filling the cartridge less easy than with the bio-glue mixture with bentonite. The printed elements were found to have a lower moisture content than with the bio-glue mixture with bentonite, so the bottom layer did not become watery.

The shrinkage of the cured elements is appeared to be between 7-24%. See Appendix 6 Information printed elements for a detailed analysis of the shrinkage.

Table 33. Reference mix bio-glue + flax

Material 1 (Raw material)	Material 2 (Liquid)	Material 3 (Binder)	Material 4 (Filler)
• Cellulose (4g) • Lignin (40g)	• Valida L,3% (40g)	• Bio-glue (60g)	• Flax (1,5g)

5.2.3 Reference mix + bentonite + flax

The latest new batch consists of adding both 5g bentonite and 1,5g flax, see table 34. Bentonite clay powder and flax were added to the dry materials cellulose and lignin. Next, this was mixed with the wet materials Valida L,3% and bio-glue until homogeneous. The mix has the correct homogeneity, appearance and consistency optimal for extrusion.

The addition of bentonite and flax made it easy to rotate the mix in the cartridge because the stiffness of the mix increased and flax increased adhesion. The moisture content was not too high so the bottom layer did not become too watery.

The shrinkage of the cured elements is appeared to be between 8-24%. See Appendix 6 Information printed elements for a detailed analysis of the shrinkage.

Table 34. Reference mix bio-glue + bentonite + flax

Material 1 (Raw material)	Material 2 (Liquid)	Material 3 (Binder)	Material 4 (Filler)
• Cellulose (4g) • Lignin (40g)	• Valida L,3% (40g)	• Bio-glue (60g)	• Bentonite (5g) • Flax (1,5g)

For a detailed overview of the mixing process of the above 3 new bio-glue mixtures see Appendix 2 Mix process

5.2.4 Results compressive strength

In order to speed up the test, it was chosen to measure the value at cycle 1.1, 1.2 and 1.3 only once for the mixtures with the fillers instead of 3 times (as was done for the reference mixtures of woodglue and bio-glue).

Compressive strength

The compressive strength was tested and calculated in the same manner as in section 5.1.2. The results of the compressive strength of the bio-glue mixture with the fillers is shown in a box-and-whisker graph in figure 60, for the horizontal and vertical directions. Each test is worked out individually in Appendix 7 Compression tests.

Bio-glue + 5g bentonite
2 specimens were tested in horizontal direction and one specimen tested in vertical direction.

Horizontal
Figure 60 shows that the compressive strength increases with each cycle. The compressive strength of the bio-glue mixture + 5g bentonite is between 2,66 – 2,72 MPa for cycle 1.1. For cycle 2.1, the compressive strength is between 6,33 – 6,80 MPa and for cycle 3.1 between 10,89 – 11,58 MPa.

Vertical
Figure 60 shows that the compressive strength for cycle 1.1 is higher than in the horizontal direction. Cycle 2.1 and 3.1 are lower than in the horizontal direction. Also, the value of compressive strength per cycle increases less than in the horizontal direction. The compressive strength of the bio-glue mixture + 5g bentonite is 5,13 MPa for cycle 1.1. For cycle 2.1, the compressive strength is 6,49 MPa and for cycle 3.1, the value is 6,80 MPa.

Bio-glue + 10g bentonite
2 specimens were tested in horizontal direction and 2 specimens were tested in vertical direction.

Horizontal
Figure 60 shows that the compressive strength increases with each cycle. The compressive strength of the bio-glue mixture + 10g bentonite is between 5,40 – 6,52 MPa for cycle 1.1. For cycle 2.1 the compressive strength is between 9,48 – 12,29 MPa and for cycle 3.1 between 13,31 – 17,77 MPa.

Vertical
Figure 60 shows that the compressive strength for cycle 1.1 is about the same as in the horizontal direction. Cycle 2.1 and 3.1 are lower than in the horizontal direction. Also, the value of compressive strength per cycle increases less than in the horizontal direction. The compressive strength of the bio-glue mixture + 10g bentonite is between 5,61 – 6,40 MPa for cycle 1.1. For cycle 2.1 the compressive strength is between 6,72 – 7,89 MPa and for cycle 3.1 between 6,34 – 8,08 MPa.

Bio-glue + flax
3 specimens were tested in horizontal direction and 3 specimens were tested in vertical direction.

Horizontal
Figure 60 shows that the compressive strength increases with each cycle. The compressive strength of the bio-glue mixture + flax is between 2,03 – 2,24 MPa for cycle 1.1. For cycle 2.1 the compressive strength is between 4,59 – 4,97 MPa and for cycle 3.1 between 8,84 – 9,82 MPa.

Vertical
Figure 60 shows that the compressive strength for cycle 1.1 and 2.1 are higher than in the horizontal direction. Cycle 3.1 is lower than in the horizontal direction. Also, the value of compressive strength per cycle increases less than in the horizontal direction. The compressive strength of the bio-glue mixture + flax is between 4,24 – 5,07 MPa for cycle 1.1. For cycle 2.1 the compressive strength is between 5,48 – 5,86 MPa and for cycle 3.1 between 5,83 – 6,31 MPa.

Bio-glue + bentonite + flax
4 specimens were tested in horizontal direction and 3 specimens were tested in vertical direction.

Horizontal
Figure 60 shows that the compressive strength increases with each cycle. The compressive strength of the bio-glue mixture + bentonite + flax is between 2,31 – 2,77 MPa for cycle 1.1. For cycle 2.1 the compressive strength is between 4,51 – 5,23 MPa and for cycle 3.1 between 7,91 – 9,47 MPa.

Vertical

Figure 60 shows that the compressive strength for cycle 1.1 is higher than in the horizontal direction. Cycle 2.1 and 3.1 are lower than in the horizontal direction. Also, the value of compressive strength per cycle increases less than in the horizontal direction. The compressive strength of the bio-glue mixture + bentonite + flax is between 4,20 – 4,40 MPa for cycle 1.1. For cycle 2.1 the compressive strength is between 4,30 – 4,93 MPa and for cycle 3.1 between 4,04 – 5,24 MPa.

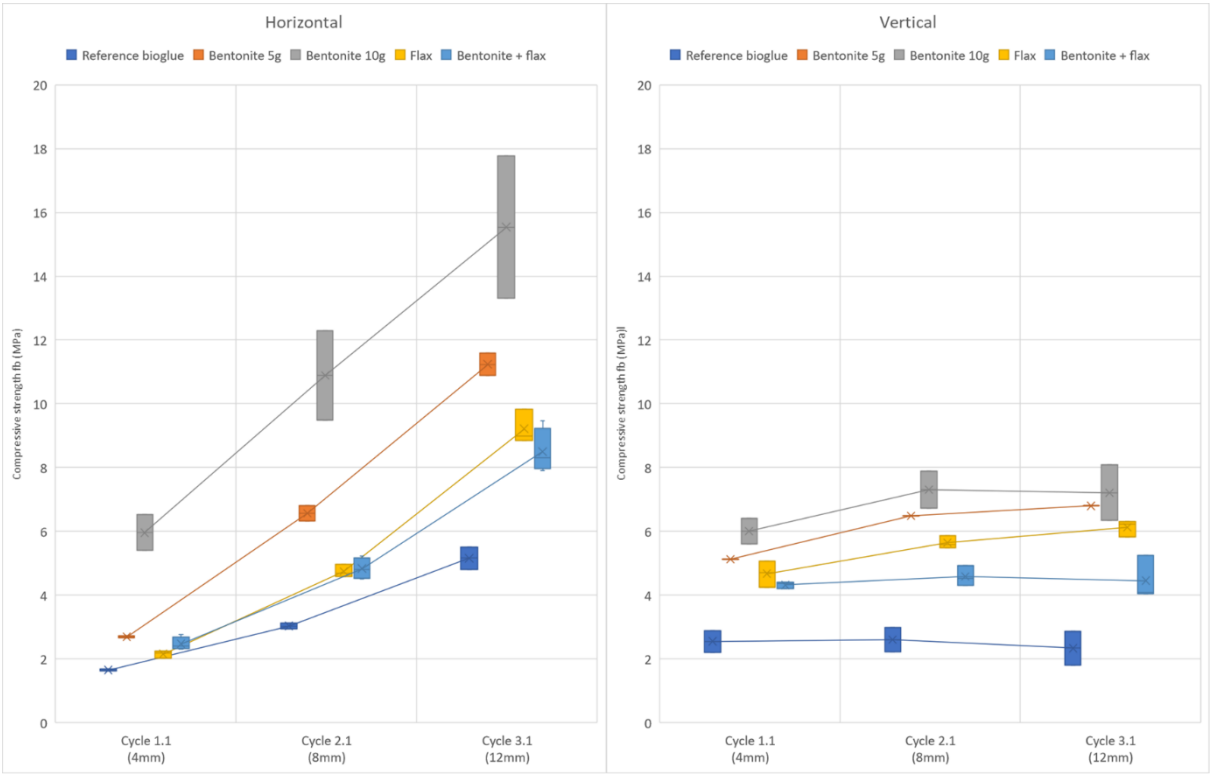

Figure 60. Results of the compressive strength of the mix with bio-glue + fillers in horizontal and vertical direction

Young's modulus (compressive strength)

The E-modulus was calculated in the same manner as in section 5.1.2. The results of the E-modulus of the bio-glue mixture with the fillers is shown in a box-and-whisker graph figure 61, for the horizontal and vertical directions.

<u>Bio-glue + 5g bentonite</u>

Horizontal

The E-modulus of the bio-glue mixture + 5g bentonite is between 19,34 – 20,07 MPa for cycle 1.1.

Vertical

Figure 61 shows that the E-modulus in vertical direction is higher than for the horizontal direction. The E-modulus of the bio-glue mixture + 5g bentonite is 49.49 MPa for cycle 1.1.

<u>Bio-glue + 10g bentonite</u>

Horizontal

The E-modulus of the bio-glue mixture + 10g bentonite is the highest of all fillers. The E-modulus is between 44,88 – 57,09 MPa for cycle 1.1.

Vertical
The E-modulus of the bio-glue mixture + 10g bentonite in vertical direction is between 54,97 – 58,30 MPa for cycle 1.1.

Bio-glue + flax
Horizontal
The E-modulus of the bio-glue mixture + flax is between 15,11 – 16,82 MPa for cycle 1.1.

Vertical
Figure 61 shows that the E-modulus in vertical direction is higher than for the horizontal direction. The E-modulus of the bio-glue mixture + flax is between 44,83 – 48,74 MPa for cycle 1.1.

Bio-glue + bentonite + flax
Horizontal
The E-modulus of the bio-glue mixture + bentonite + flax is between 19,12 – 22,97 MPa for cycle 1.1.

Vertical
Figure 61 shows that the E-modulus in vertical direction is higher than for the horizontal direction. The E-modulus of the bio-glue mixture + bentonite + flax is between 43,68 – 50,04 MPa for cycle 1.1.

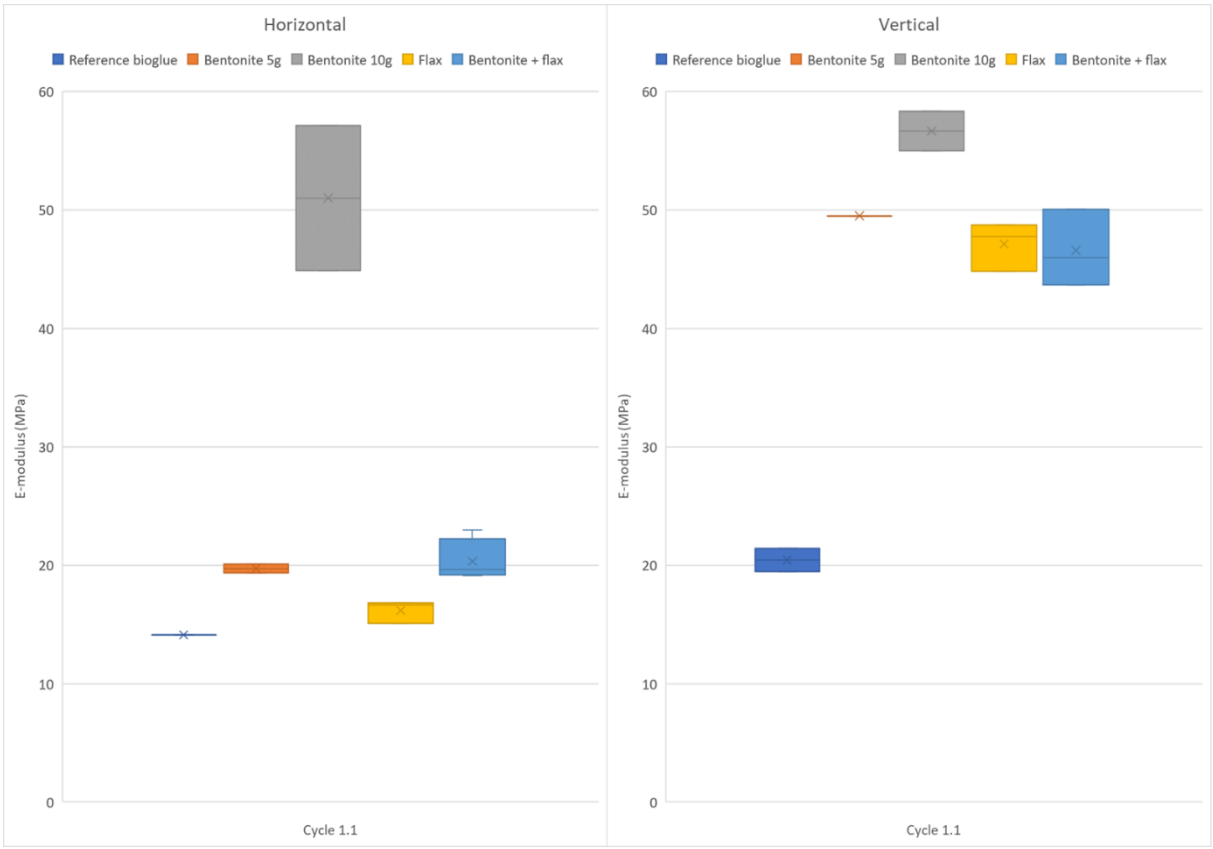

Figure 61. Results of the E-modulus of the mix with bio-glue + fillers in horizontal and vertical direction

5.2.5 Results flexural strength

Flexural strength

The flexural strength was tested and calculated in the same manner as in section 5.1.4. The results of the flexural strength of the bio-glue mixture with the fillers is shown in a box-and-whisker graph in figure 62, for the horizontal and vertical directions. Each test is worked out individually in Appendix 8 Flexural tests

Bio-glue + 5g bentonite

2 specimens were tested in horizontal direction and 2 specimens were tested in vertical direction.

Horizontal

The flexural strength of the bio-glue mixture + 5g bentonite is between 4,00 – 4,74 MPa.

Vertical

Figure 62 shows that the flexural strength in vertical direction is higher than for the horizontal direction. The flexural strength of the bio-glue mixture + 5g bentonite is 6,34 – 6,46 MPa.

Bio-glue + 10g bentonite

One specimen was tested in horizontal direction and 2 specimens were tested in vertical direction.

Horizontal

The flexural strength of the bio-glue mixture + 10g bentonite is 4,74 MPa.

Vertical

Figure 62 shows that the flexural strength in vertical direction is higher than for the horizontal direction. The flexural strength of the bio-glue mixture + 10g bentonite is between 5,07 – 5,30 MPa.

Bio-glue + flax

3 specimens were tested in horizontal direction and 3 specimens were tested in vertical direction.

Horizontal

The flexural strength of the bio-glue mixture + flax is between 4,55 – 5,37 MPa.

Vertical

Figure 62 shows that the flexural strength in vertical direction is higher than for the horizontal direction. The flexural strength of the bio-glue mixture + flax is between 6,25 – 6,94 MPa.

Bio-glue + bentonite + flax

3 specimens were tested in horizontal direction and 3 specimens were tested in vertical direction.

Horizontal

The flexural strength of the bio-glue mixture + bentonite + flax is the highest of all fillers and is between 3,74 – 5,05 MPa.

Vertical

Figure 62 shows that flexural strength varies in the vertical direction, with values higher and lower than in the horizontal direction. The flexural strength of the bio-glue mixture + bentonite + flax is between 3,49 – 6,84 MPa.

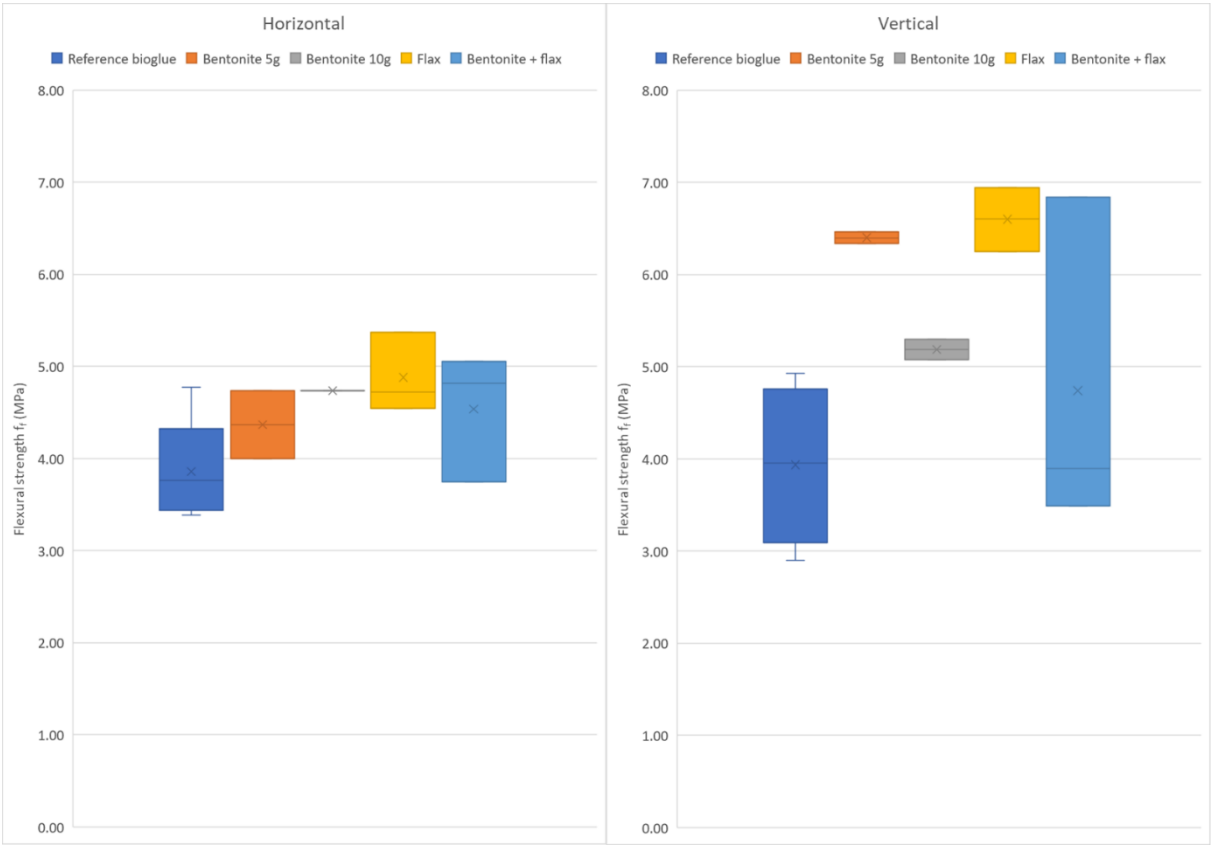

Figure 62. Results of the flexural strength of the mix with bio-glue + fillers in horizontal and vertical direction

Flexural modulus

The flexural modulus was calculated in the same manner as in section 5.1.4. The results of the flexural modulus of the bio-glue mixture with the fillers is shown in a box-and-whisker graph in Figure 63, for the horizontal and vertical directions.

<u>Bio-glue + 5g bentonite</u>

Horizontal

The flexural modulus of the bio-glue mixture + 5g bentonite is between 116,99 – 120,89 MPa.

Vertical

Figure 63 shows that the flexural modulus varies in the vertical direction, with values higher and lower than in the horizontal direction. The flexural modulus of the bio-glue mixture + 5g bentonite is between 78,36 – 155,85 MPa.

<u>Bio-glue + 10g bentonite</u>

Horizontal

The flexural modulus of the bio-glue mixture + 10g bentonite is 194,61 MPa.

Vertical

Figure 63 shows that the flexural modulus in vertical direction is lower than for the horizontal direction. The flexural modulus of the bio-glue mixture + 10g bentonite is between 127,67 – 153,01 MPa.

<u>Bio-glue + flax</u>

Horizontal

The flexural modulus of the bio-glue mixture + flax is between 110,10 – 151,48 MPa.

Vertical
Figure 63 shows that the flexural modulus in vertical direction is lower than for the horizontal direction. The flexural modulus of the bio-glue mixture + flax is between 83,10 – 118,88 MPa.

Bio-glue + bentonite + flax
Horizontal
The flexural modulus of the bio-glue mixture + bentonite + flax is between 99,28 – 147,58 MPa.

Vertical
Figure 63 shows that the flexural modulus in vertical direction is lower than for the horizontal direction. The flexural modulus of the bio-glue mixture + bentonite + flax is between 77,53 – 113,94 MPa.

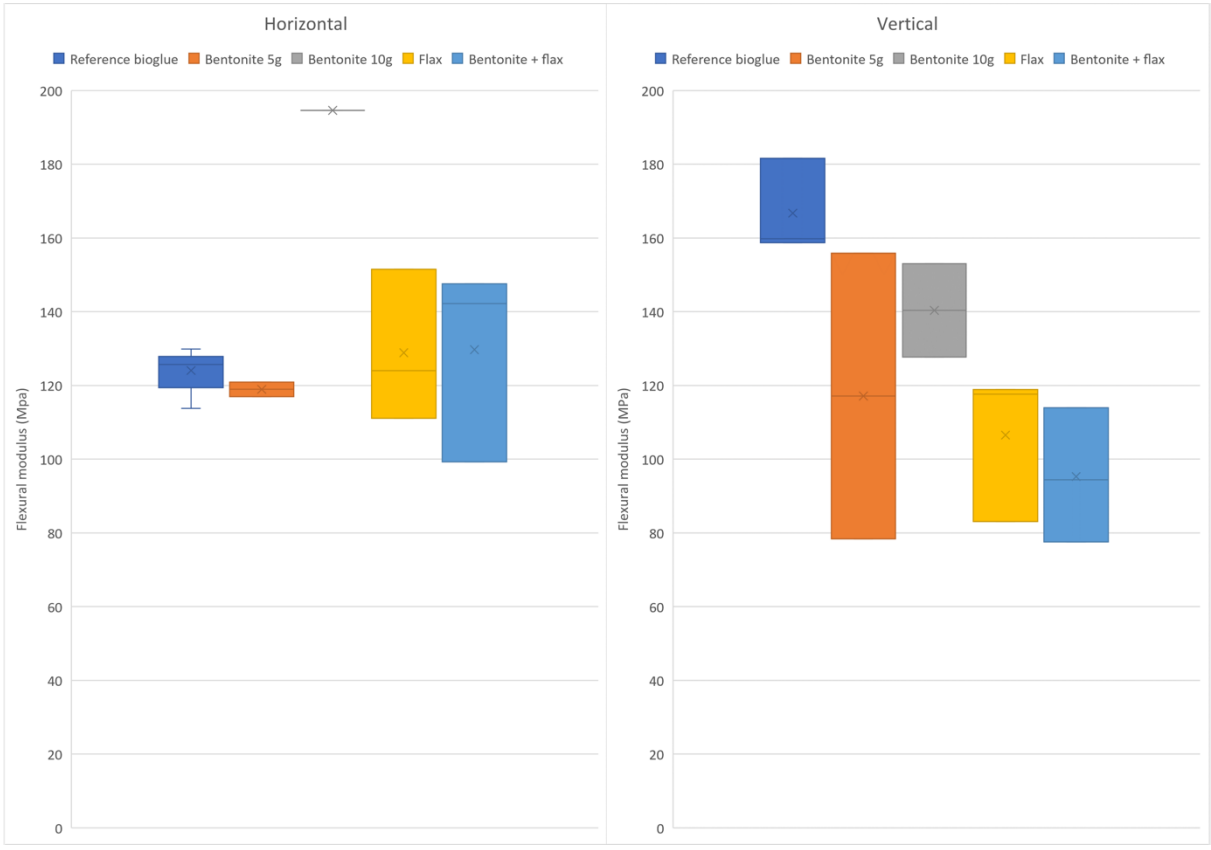

Figure 63. Results of the flexural modulus of the mix with bio-glue + fillers in horizontal and vertical direction

5.2.5. Conclusion: reference bio-glue vs reference bio-glue + fillers

Compression test:

- The fillers have a positive effect on strength, with the bio-glue mixture + 10g bentonite being the strongest. As previously described, the mixture did not comply with the printing process. Hence it is concluded that the bio-glue mixture + 5g bentonite is the preferred mixture.
- The horizontal direction is stronger than the vertical direction.

Flexural test:

- The fillers have a strengthening effect on the strength, with the bio-glue mixture + flax being the strongest.
- The vertical direction is stronger than the horizontal direction.

The structural element consists of a column loaded in axial compression. It can be concluded that mixture used to print the final element consists of the bio-glue mixture + 5g bentonite. It can also be concluded that the layers of the final element should be printed in horizontal direction.

5.3 Classification material

Figure 64 shows the classification of engineering materials. The y-axis shows the Young's modulus which ranges from 0.0001 to almost 1000 GPa. The x-axis shows the density of the material, which ranges from 0.01 to 20 Mg/m^3. Ceramics and metal families have a high Young's modulus (greater than 10 GPa) and density (greater than 1.7 Mg/M^3). By contrast, polymers all have a Young's modulus of less than 10 GPa and a density (usually around 1 Mg/m^3) that is lower den ceramics and metals. Elastomers have about the same density as polymers, but the Young's modulus is lower by a factor of 100 or more. Materials with lower density than polymers are porous (foams and natural cellular structures such as wood and cork) [80].

The cured bio-based material (mix bio-glue + 5g bentonite) has a Young's modulus of a 0.1971 GPa, see figure 61 (E-modulus 19,71 MPa). The density of the material is 1.0 Mg/m^3 (for the calculation see Appendix 6 Information printed elements). This places the material under natural materials with an overlap with polymers. It can also be seen that the bio-based material is still far from being as strong as structural building materials such as wood, steel and concrete.

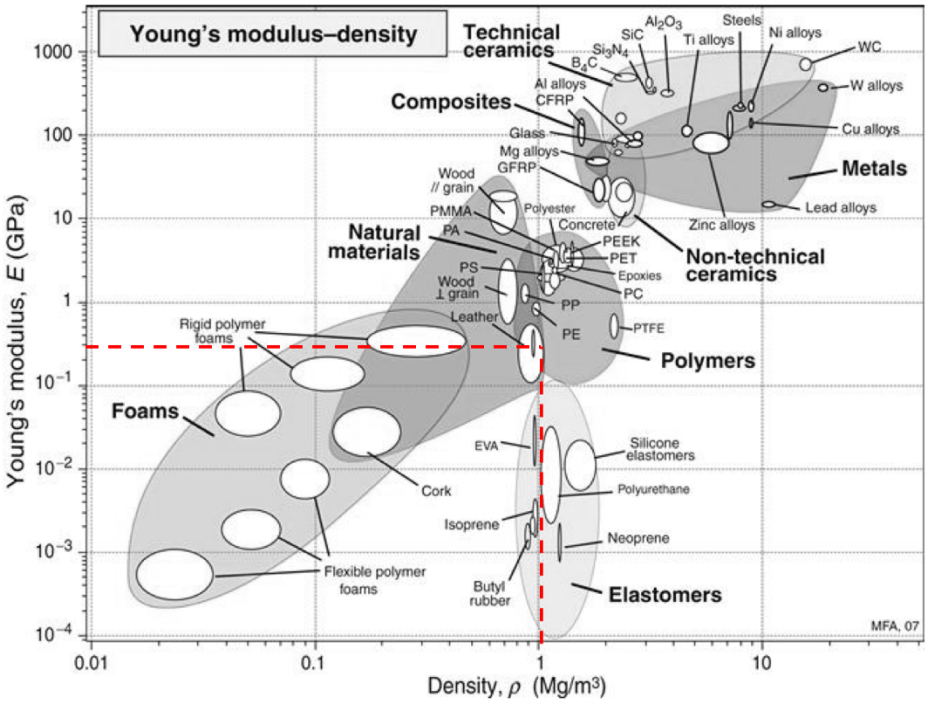

Figure 64. Classification material [80]

6. Numerical model

6.1 Design

The design of the final element consists of a simple supported one meter bio-based column and is robotically fabricated by 3D additive manufacturing. The structural column is optimized for the cross-section based on axial compression (cross-section remains the same over the full height). Figure 65 shows a schematized representation of the column, with the dotted line representing the optimized cross section of the printed structure.

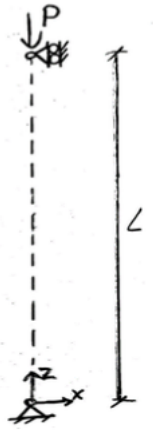

Figure 65. Schematization column

Buckling is a sudden and severe deformation of a column, exposing the component to a small increase in the existing load. Buckling analysis is important for axially loaded components because the compressive stress at the point of failure is less than the maximum compressive stress in the material [81]. The German-Swiss mathematician Euler analyzed buckling in the 18th century and established several Eulerian conditions for predicting critical loads. See the formula below to predict the critical load (F_{crit}) of a column loaded in axial compression [82].

$$F_{crit} = \frac{\pi^2 \cdot E \cdot I}{(K \cdot L)^2} \quad (6.1)$$

Where:

- E is the elasticity modulus (E-modulus)
  The E-modulus is a measure of the stiffness of the material. A stiff material is sensitive for high resistance to buckling. See section 5.2.4 for E-modulus.
- I is the moment of inertia.
  The moment of inertia indicates the resistance to deflection that results from the shape of the cross-section of the column. Increased moment of inertia results in an increase in critical load.
- L is the buckling length.
  The buckling length is the length of the column, in this case it is 1m.
- K is the effective length factor.
  The effective length factor depends on the method of attachment of the nodes, in this case K=1 see figure 66 [83].

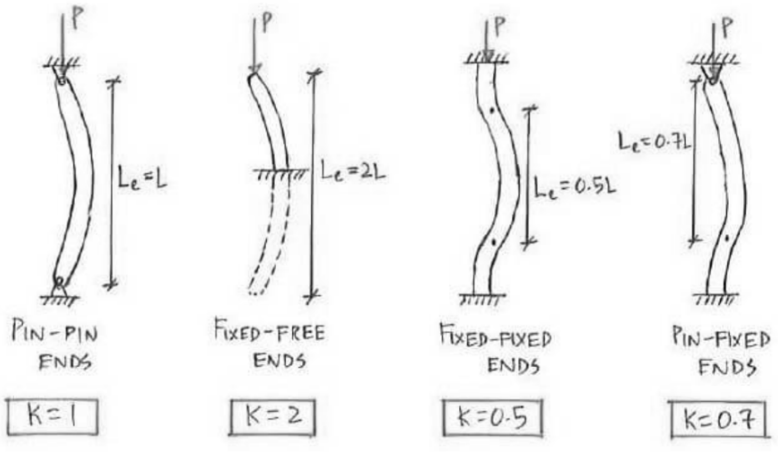

Figure 66. The different buckling modes with the effective length factor [83]

6.2 Process model

Figure 67 shows the process model of numerical optimization in Rhino (1) through a script written in the visual programming plug-in Grasshopper (1). First, the basic Grasshopper components and several plug-ins are used to generate the geometry. After the basic geometry is defined, a structural analysis is performed using the Karamba3D (2) plug-in. Karamba3D is a plug-in that uses the Finite Element

Method (FEM) to make calculations of parametrized geometric models in the environment of Grasshopper [84]. The results of the first Karamba3D structural calculation are used for geometric optimization in Galapagos (3). While changing the geometric parameters, Galapagos searches for an optimized structure that maximizes resistance to buckling. Then, with the plug-in Geometry gym (4), the component ggKarambaToGSA is used to create a gwa-file that can be imported into GSA (5) to verify the structural calculation of Karamaba 3D. If the Karamba3D and GSA results match, the print path is determined from the final geometry with the plug-in Salad Slicer (6). Salad Slicer is an open-source Rhinoceros Grasshopper plugin developed for slicing objects for 3D concrete printing, however, the plugin is also suitable for slicing objects to print other materials such as biomaterials [85]. The resulting point sequence is used as input to the Robot Components (7) plug-in. The RAPID code created by this plug-in can finally be loaded into Robot Studio (8) to simulate the print path and print the structure.

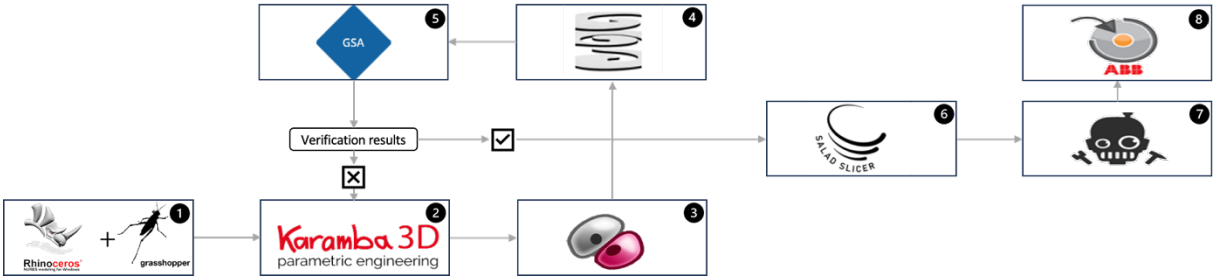

Figure 67. Process model numerical optimization

6.3 Parameters cross-section

The numerical optimization is performed in the parametric modelling software Rhinoceros, through a script written in the visual programming plug-in Grasshopper. The first part of the Grasshopper script defines the geometry of the structural column, which can be influenced by four different parameters:

1. Radius of the cross section, see black arrow figure 68.
2. Number of corners, see red crosses figure 68.
3. Rounding of corners, see light green lines figure 68.
4. Depth of corners, see orange arrow figure 68.

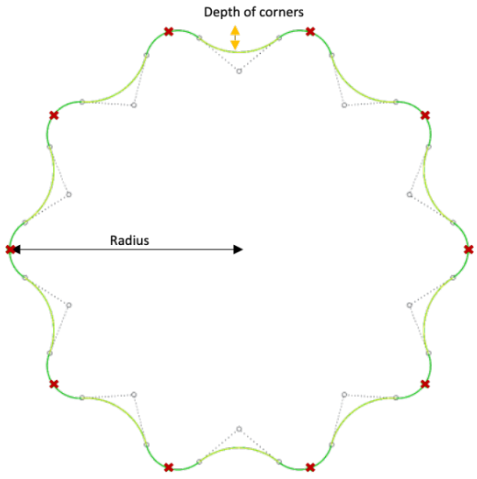

Figure 68. Parameters cross-section

6.3.1 Radius

This parameter determines the size of the geometric shape. The larger the cross-sectional area of the geometric shape the greater the buckling force, hence the parameter is subject to a maximum of 125mm. A small maximum radius was chosen so that the column collapses on global buckling and not on local buckling.

6.3.2 Number of corners
This parameter determines the number of corners of the geometric shape. The minimum value is 3 corners so that a basic geometric shape can always be created (triangle). In addition, the maximum number of corners is set to 10 (circle) to avoid an overcomplicated print path.

6.3.3 Rounding of corners
This parameter determines how sharp the angle is of each corner. A sharp corner (angle between 0° and 90°) is more difficult to print with the robot than corner that overlaps smoothly (angle between 90° and 180°).

6.3.4 Depth of corners
This parameter determines how far the angle is placed inward with respect to the outer edge. If the angle is not placed inward, the minimum value of this parameter is reached and the geometric shape is a circle. If the angle is placed inward, a new geometric shape is created.

These four parameters are used to determine the geometric shape of the column, where the thickness of the cross-section is always 15mm. Figure 69 shows different geometries that the script can generate.

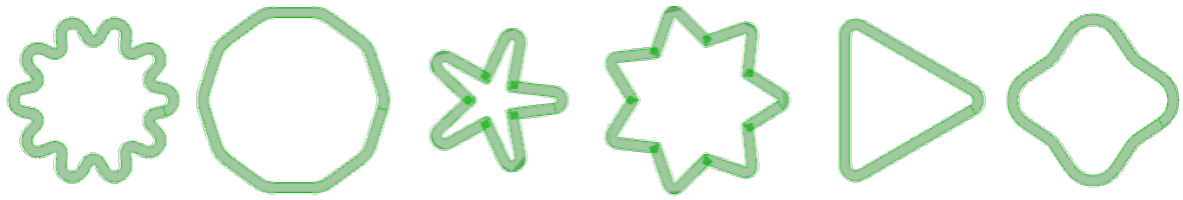

Figure 69. Different shapes that can be generated by the Grasshopper script

6.4 Structural analysis
The structural calculation is performed using the parametric, structural tool Karamba3D. First, the 'MeshToShell' component (1) is used to convert the triangular mesh into a group of shell elements with a given cross-section. To define the cross-section, the 'Material Properties' component (4) is used. The properties of the bio-based material (E = 19,71 MPa) are described in section 5.2.4 and entered manually because this material is unknown within the Karamba3D material library. Rigid elements are added to the top and bottom of the column. These elements represent the end node of the column. The rigid elements consist of a spider web of lines (see green lines figure 70). The 'LineToBeam' component (5) is used to convert all line segments into beam elements with a circular cross section. To define the cross section, again the 'Material Properties' component (7) is used. The properties of the rigid element are entered manually so that lines of the spider web behave like a rigid element.

Next, the boundary conditions are defined. The 'Beam-Joint' (6) component is used to define the connection between the rigid elements and the printed column. This component ensures that rotation is allowed and translation is limited. The supports (2) are added to the center of the rigid elements. The lower support prevents translation in X, Y and Z directions and allows rotation. The upper support also prevents translation in X and Y directions but allows translation in the Z direction. Rotation in the Z direction is also restricted at the upper support to prevent torsional movement. The column is axially loaded with a point load of 5 kN (3). The rigid elements transfer this force to the printed column. Figure 70 shows the column visualizing the supports, mesh, rigid elements and applied point load.

All defined elements, supports, connections and loads are the input for the 'Assemble' component (8). This component creates a structural model from the collected data. Next, the 'Analyze' component (9)

is used for a first-order structural analysis to determine the internal elastic energy. For the second-order buckling analysis of the column, the component 'AnalyzeThII' (10) is used. During the second-order analysis, the deformation of the column due to the applied point load is taken into account. The results of the column can be visualized with the components 'ModelView' (11) and 'ShellView' (12). The output of the structural calculation includes the maximum displacement, stresses and buckling load factor. The buckling load factor is used for numerical optimization.

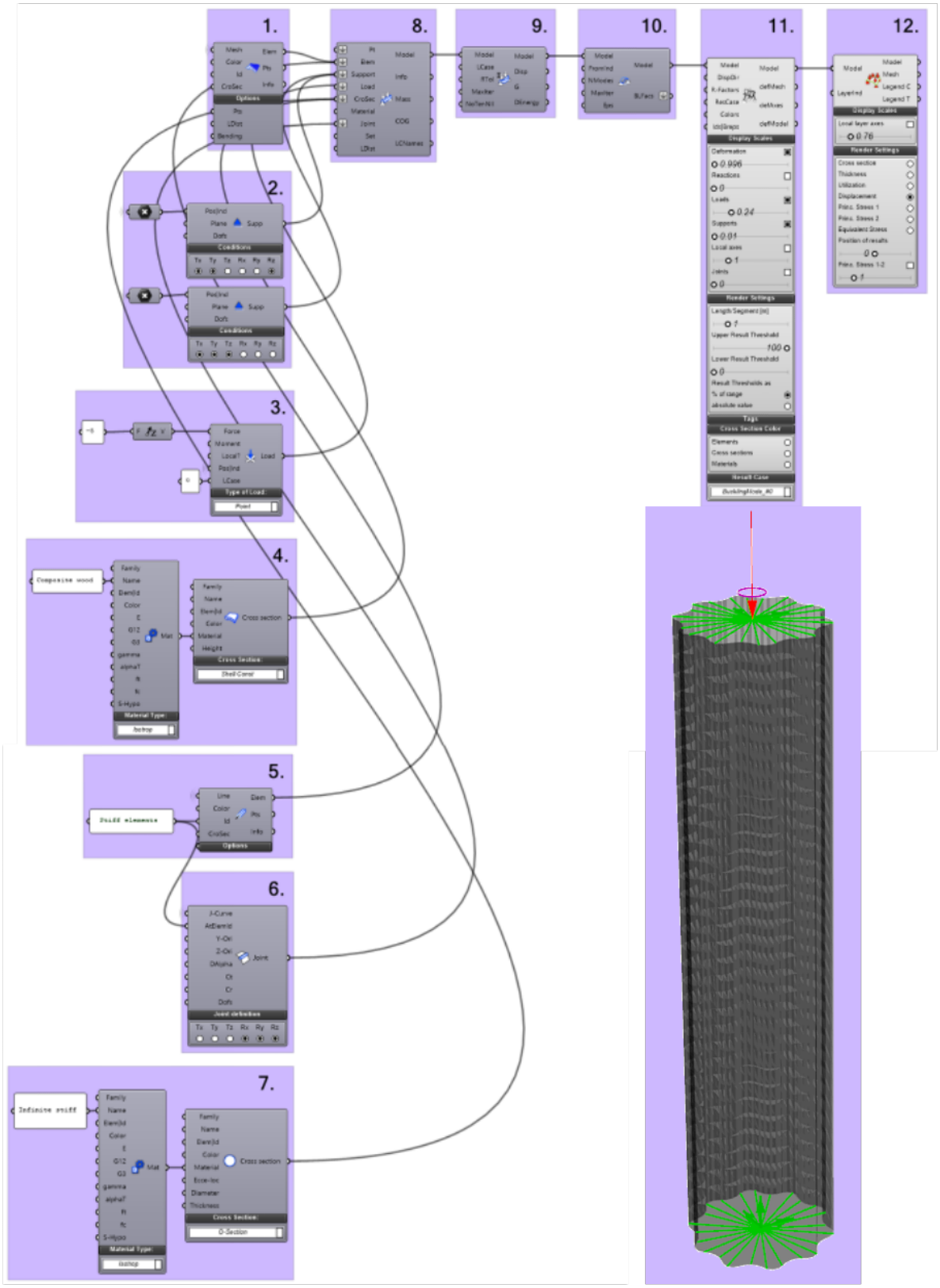

Figure 70. Set-up Karamba3D model

6.5 Cross-section optimization

Cross-sectional optimization is performed using Galapagos see figure 71. See appendix 9 Overview Grasshopper scripts for the script of the numerical optimization. Galapagos is a component in grasshopper that can optimize a shape so that it best achieves a user-defined goal. The component is based on a genome input and a fitness input. The genomes (parameters) are numeric values within a certain range (sliders with minimum and maximum values) that Galapagos can try out in different combinations. The genomes are described in section 6.3. Each combination, or genome, produces a unique object. The second input requires the fitness, which is the variable to be maximized or minimized. In this study, it is the Karamba3D resulting value for the buckling load factor that is maximized.

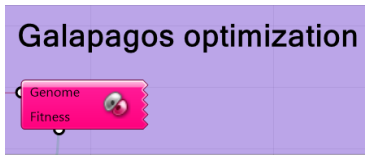

Figure 71. Galapagos

The optimization was performed using the Galapagos evolutionary solver. This solver is based on the idea of genetic algorithm, which is based on natural selection theory [86]. The first step of the solver is to fill the model space with random genomes after which the fitness of each genome is determined, resulting in a distribution can be seen in the lower left of the Galapagos editor. While working, the lower right box of the Galapagos editor shows the best solution so far. The first iteration with random values for the genomes is not a good solution because they are random generation 0 choices. After this iteration, the solution will produce a new generation (generation 1), so to speak, which will give better results. This can be seen on the horizontal axis on the Galapagos editor window. At this point the randomness has faded and genome selection has become rational, instead of the random values of generation 0. If no better generation can be found, the solver stops. The graphical interface of the evolutionary solver is shown in figure 72.

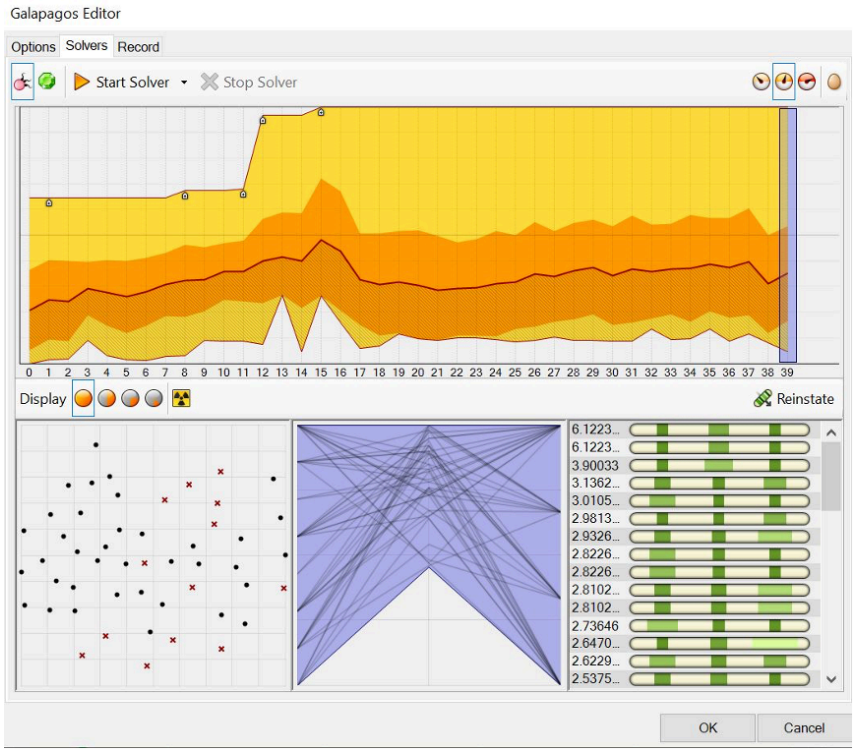

Figure 72. Optimization process in Galapagos

6.5.1 Final design

The Galapagos optimization results in a single solution where the buckling load factor is as high as possible. The geometry of the final design is shown in table 35.

Table 35. Final design

Front view	Top view	3D view
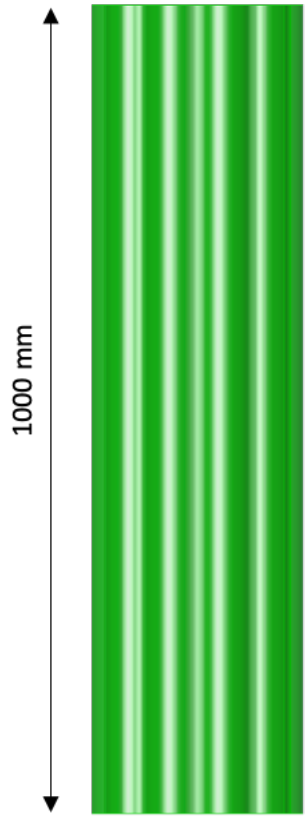	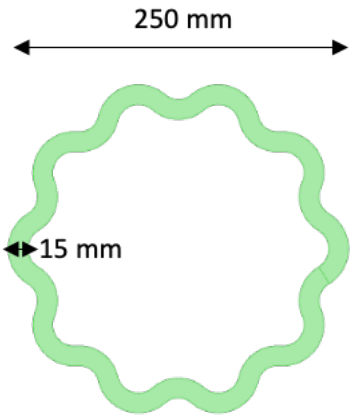	

The column is 1000mm high. A gear-like cross section can be seen with a width of 250mm and a thickness of 15mm. The number of corners is 10 and the corners flow nicely into each other.

6.5.2 Structural analysis

For this study, the Karamba3D structural calculation results are verified in GSA. This is done because the results of Karamba3D will be compared with the test results at a later stage. The Geometry gym plug-in is installed and with the component ggKarambaToGSA the structural model is exported from Grasshopper to GSA. This is done by creating a dwg-file. The file is imported into GSA and the model is calculated. The results of the structural calculation are shown in table 36. In figure 73 the first buckling modes are compared.

Table 36. Verification of Karamba3D structural analysis in GSA

	Reaction force (kN)	Buckling load factor (-)
Karamba3D (A)	5	6,12
GSA (B)	5	5,59

Table 36 shows that the resulting value for the reaction force exactly match. However, there is a slight difference in the buckling load factor. Figure 73 shows that the first buckling mode for both analyses results in global buckling. The differences between the structural analyses are negligible (< 10%). Therefore, it can be concluded that GSA verifies the structural calculation of Karamba3D.

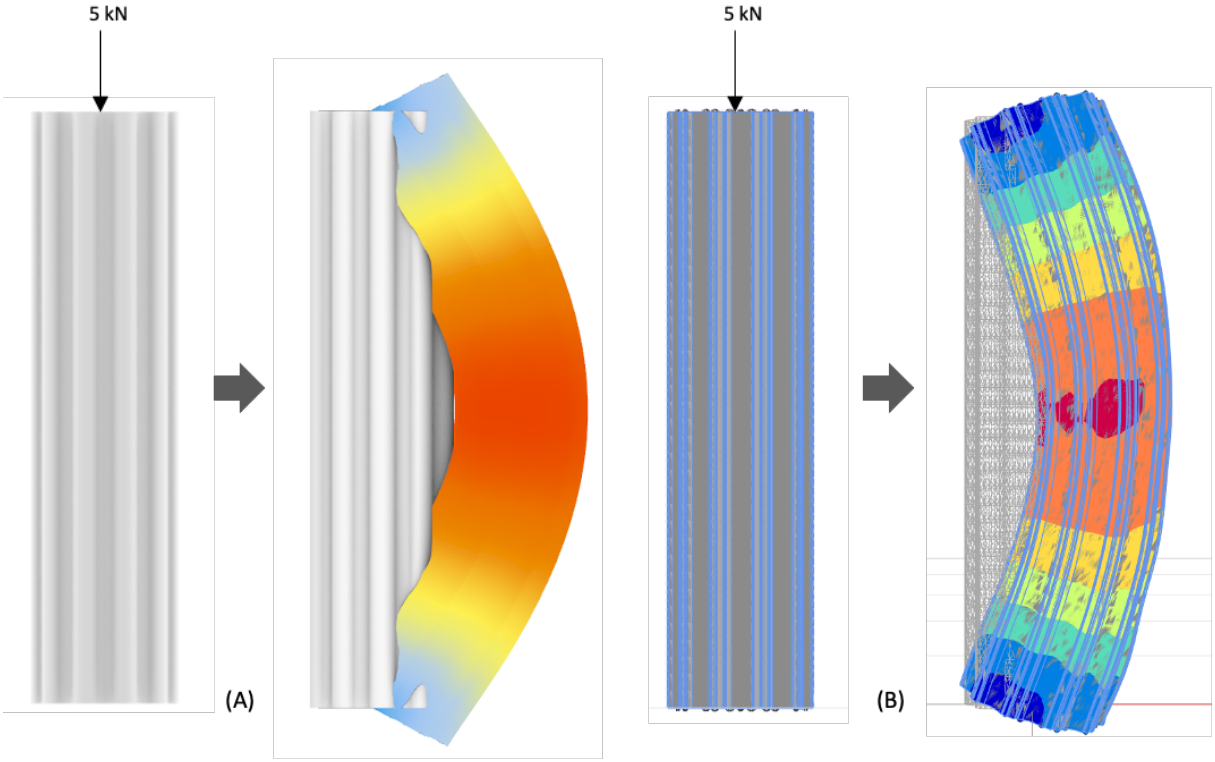

Figure 73. First buckling modes Karamba3D (A) and GSA (B)

7. Printability exploration (final element)

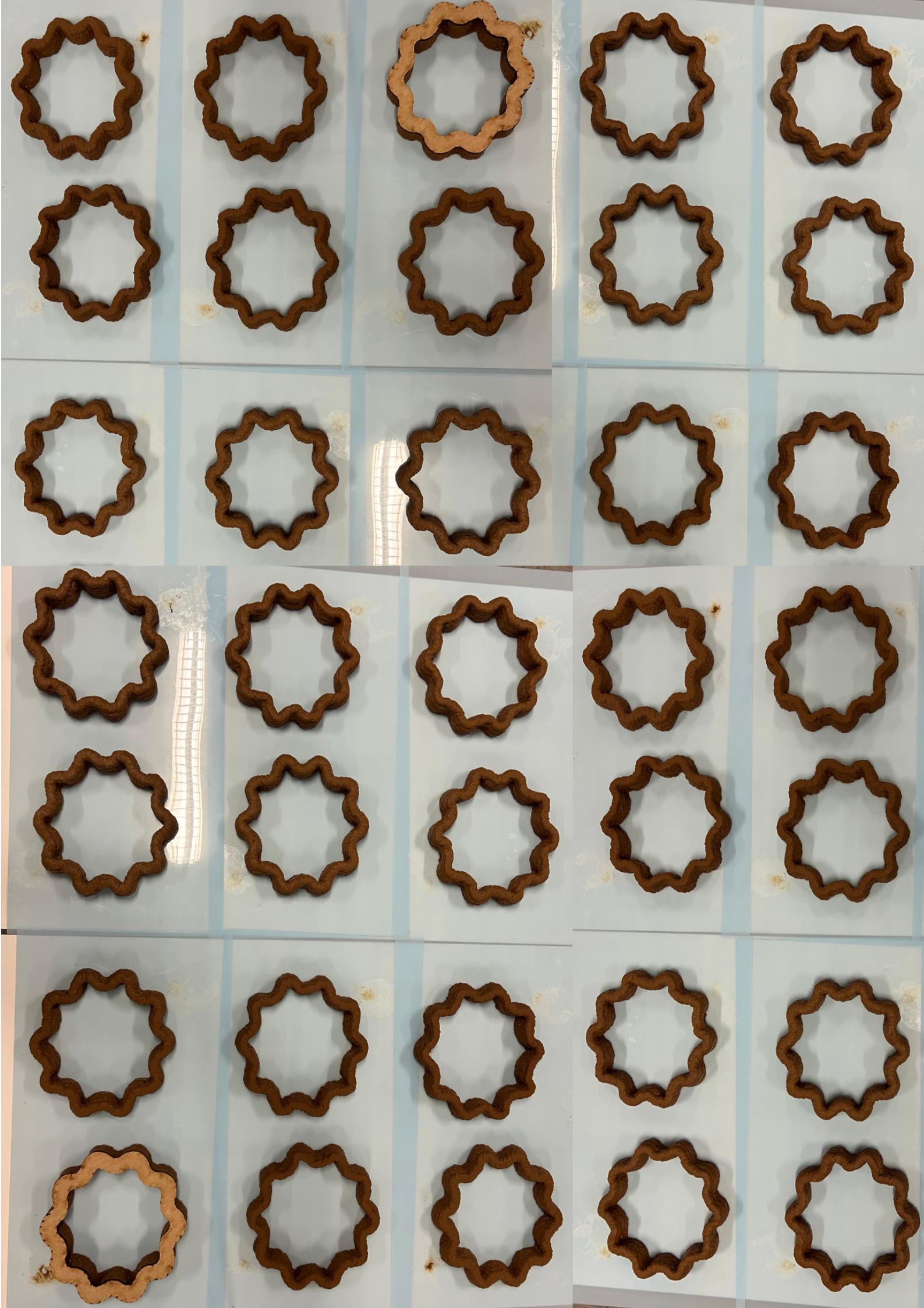

7.1 Robot set-up

For robotic 3D additive manufacturing, the following four parts are important (see figure 74):

1. ABB Robot;
2. End effector;
3. Makita;
4. Nozzle.

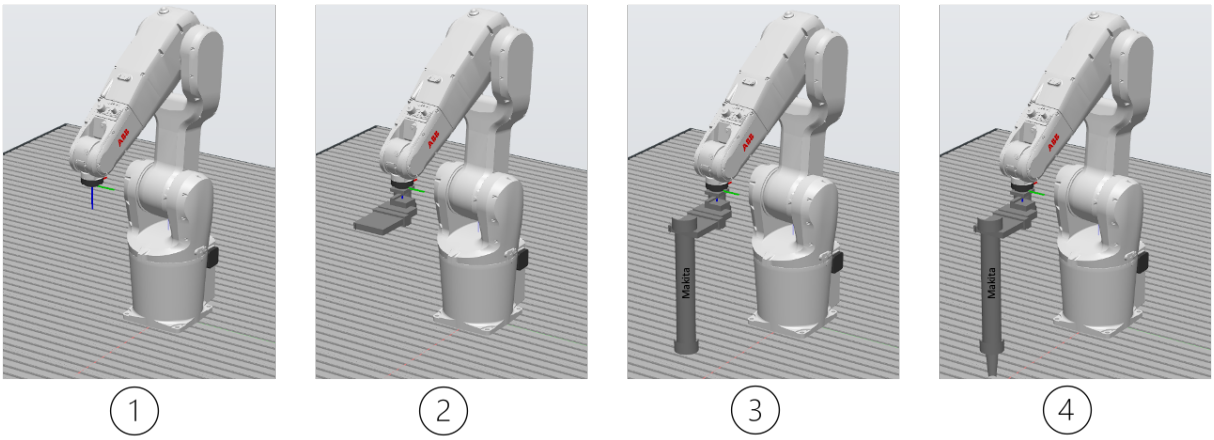

Figure 74. Robot set-up

The ABB Robot and the end effector are exactly the same as described in Chapter 4. Only the mixture going into the cartridge and nozzle are different.

7.1.1 Makita

The Makita is exactly the same as described in section 4.1.3. Only the mixture going into the cartridge was changed one last time. From the reference mix bio-based + 5g bentonite came the following: after the element was printed all the moisture dropped to the bottom layer, making this bottom layer too watery. To prevent the bottom layer from becoming too watery, the mixture was adjusted one more time. The ratio of cellulose to bentonite was 0.8:1. The new ratio of cellulose to bentonite is 1:1. Increasing the cellulose by 1g (from 4g to 5g) remedied some over-watering of the bottom layer.

The amount of material is matched to the contents of the cartridge and is sufficient to fill it completely. The amounts of each material are shown in the table 37.

Table 37. Material quantities final mix

	Final mix. Bio-based glue + bentonite	
	Weight (g)	**Percent (%)**
Cellulose	37,5	3,33
Lignin	300	26,67
Valida L,3%	300	26,67
Bio-based glue	450	40,0
Bentonite	37,5	3,33
Total	1125	100

7.1.2 Nozzle

Printing the end element is not possible with a rectangular nozzle. In the case of a the cross-section of the end element, position F axis 6 (see Appendix 4 Product specifications ABB IRB 1200-5/0.9) of the robot will always have to rotate with it to ensure that the rectangular nozzle is rotated to the correct position. This means that position F axis 6 must continue to rotate infinitely around its own axis, but

continuing to rotate infinitely around position F axis 6 is not possible because this is a turnmotion. Therefore, printing with a round nozzle was chosen, because in this case position F axis 6 does not need to rotate (because the cross-sectional area of the nozzle is the same at each point). As a result, a round nozzle has greater design freedom with which all shapes can be printed. All elements are printed with the nozzle shown in table 38. With the layer is 15mm wide and 5mm high.

Table 38. Round nozzle

Top view	Front view	3D view	Cross-section
			Ø 10 mm 

7.2 Print parameters

Pressure, print speed and nozzle standoff distance are categorized as print parameters. These factors are thoroughly tested to get the best layer dimension out of the nozzle.

7.2.1 Pressure

For the description of this parameter see section 4.2.1. The cross-section of the final element contains 10 vertices. Because of these many curves, very precise printing is required and therefore it was chosen to set the speed controller, see figure 36, to 1. This means that the push bar slowly pushes the material out of the nozzle, allowing very accurate printing.

7.2.2 Print speed

For the description of this parameter see section 4.2.2. To find the correct print speed in cooperation with the speed controller, a pattern was set up in which the print speed keeps decreasing, see figure 75. In right picture of figure 75, it can be seen that the layer width increases as the print speed decreases. In terms of bond strength, the effect did not appear to be much different for the three different speeds.

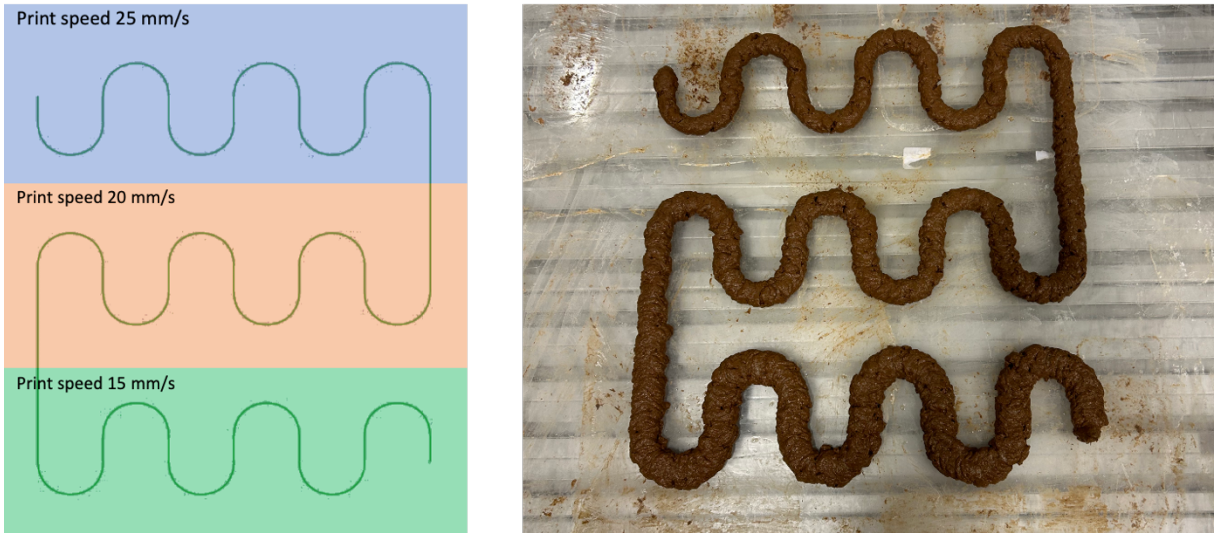

Figure 75. Test print speed

The test was run so many times until the correct print speed was found with the speed controller set to 1 and the layer width 15mm. See table 39 for the print speed of the final mix.

Table 39. Print speed

	Final mix mix bio-based glue + bentonite
Print speed (v) in mm/s	20

7.2.3 Nozzle standoff distance

For both the first layer and all layers above it, the nozzle standoff distance is 5mm. See figure 76 for illustration. This was chosen because with a nozzle standoff distance of 5mm, the layer width is 15mm.

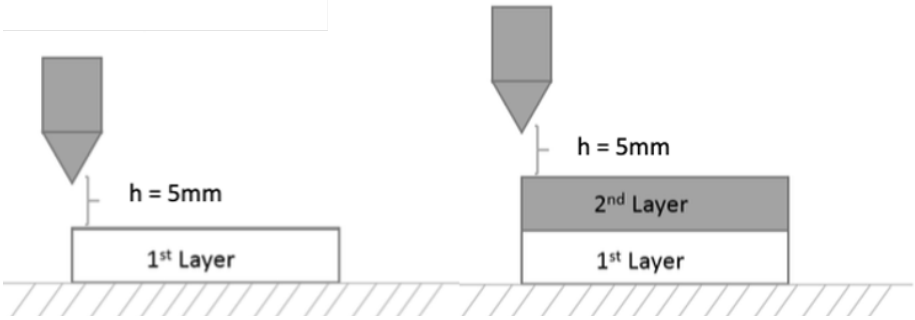

Figure 76. Nozzle standoff distance

7.3 Robotic printing

7.3.1 printing the number of layers

The question is how many layers can be printed on top of each other, using the cross section of the final element. The final element is 1m high, this consists of +/- 200 printed layers. A maximum of 6 layers can be printed with a full cartridge. After filling a new cartridge and again applying 6 layers to the first 6 layers, the element starts at the 8th layer with plastic collapse see left photo figure 77. From this it is concluded that 6 layers can be printed, since these also come from one cartridge. 7 layers could also have been chosen but having to fill a cartridge to print 1 layer takes too much time.

Next, printing of 6 layers with curing time of 24 hours was considered. After 24 hours of curing time, the first 6 layers were sufficiently cured for printing 6 new layers (see middle picture figure 77). Note to this photo. 2x6 layers were printed within 24 hours. However after printing the first 6 layers the robot was used by another student so the element was moved aside, after 24 hours the new 6 layers could be printed. As can be seen these new 6 layers were not printed exactly above the first 6 layers because there is a small inaccuracy in moving the element back). In one week a maximum of 30 layers can then be printed, this means that the final element consists of 7 elements of 29 layers. The robot must then be reserved for a full week as no shifting of the elements is allowed otherwise the next 6 new layers will not be printed exactly on the bottom layers. However, it is impossible within the faculty to reserve the robot for five days in a row since several students and PHDs are doing research using the robot. Hence, this option is eliminated.

In the end, the decision was made to print 36 elements of 6 layers (see right-hand photo figure 77). This eliminates the need to take into account other students needing to use the robot and the elements don't have to be moved.

Figure 77. Printing number of layers

7.3.2 Robot path

To print the end elements (see Table 40) with a radius of 250mm long, 15mm wide and 6 layers high with the robot, a robot path must be defined to print the element in a continuous session.

Table 40. Final element to be printed

Front view	Side view
	
Top view	**3D view**
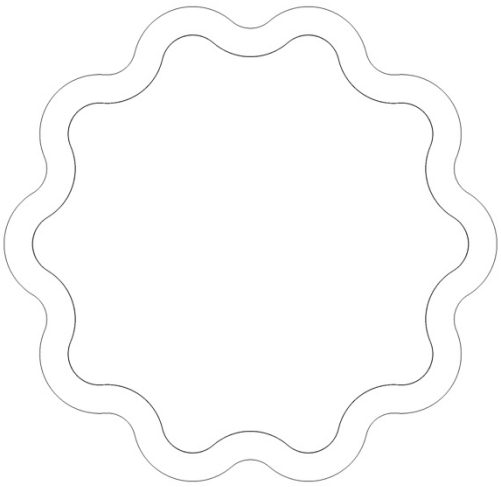	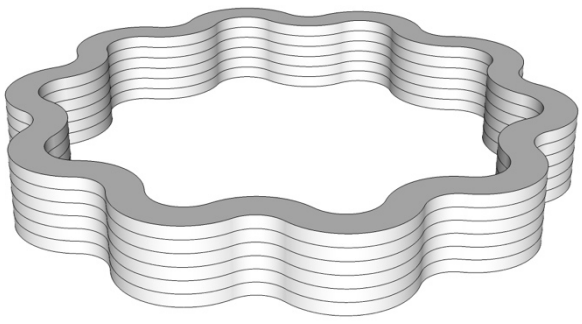

The robot path is visualized in figure 78 and the movements in table 41.

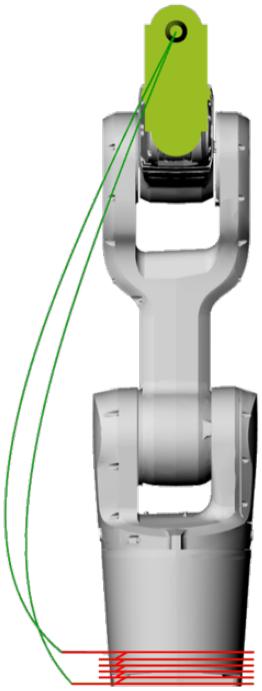

Figure 78. Robot path

Table 41. Movements

Line	Type	Precision	Movement type	Speed
	Free space	Low	Joint movement	High
	Print process	High	Linear movement	low

7.3.3. Robot components and RobotStudio

Robot components and RobutStudio is applied in the same way as in sections 4.4.2 and 4.4.3. The left image in figure 79 visualizes in Robot components the robot path and the corresponding plane orientations of the end-effector and target points. The right image in figure 79 visualizes in RobotStudio the final simulated robot path. See appendix 9 Overview Grasshopper scripts for the script of the Robot components.

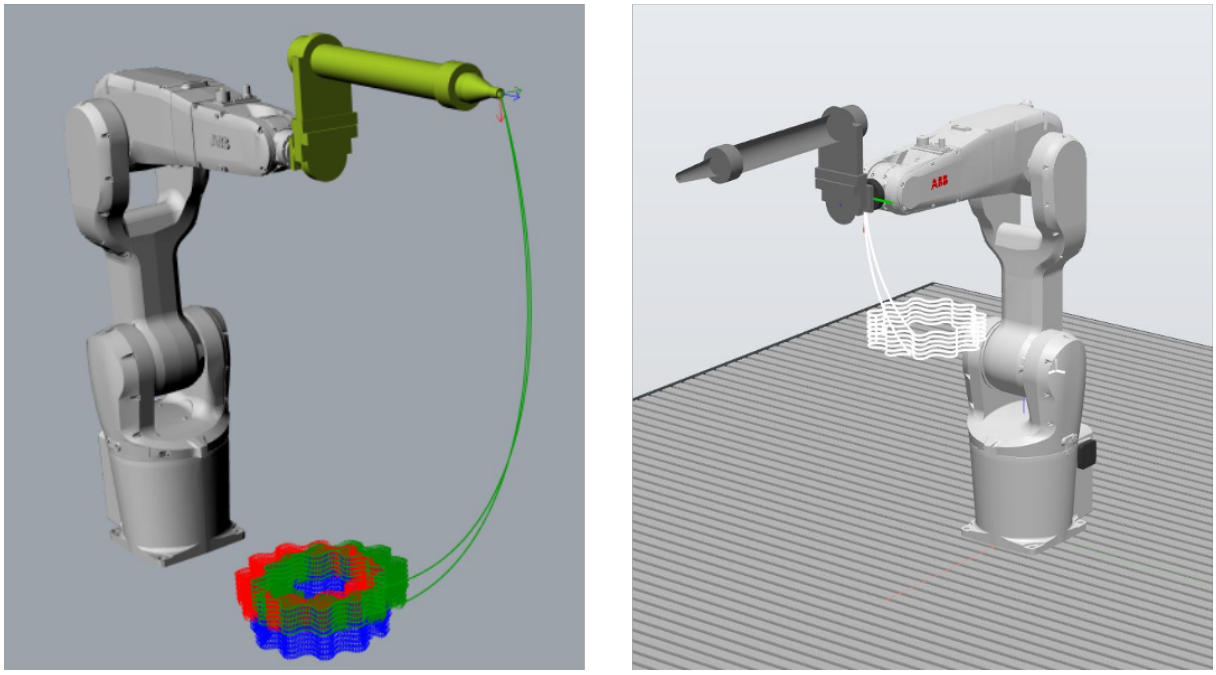

Figure 79. Left robot path with plane orientations in Robot components and right final robot path in RobotStudio

7.3.4 Printing

Figure 80 shows the printing process of the final element. First, the robot arm moves from its initial position to the starting position for printing (1). Next, the Makita and the motion of the robotic arm are simultaneously turned on and the material is extruded out of the nozzle (2-3). When layer 6 is printed, the Makita and the motion of the robotic arm are turned off and the robotic arm moves back to the initial position (4). After the element is printed, the element is leveled. This is done by placing a wooden square on the element. After which the wooden element is pushed until it is levelled. Leveling of each element is done so that after curing it does not have to undergo any operation of sawing and sanding. This allows faster construction of the final element.

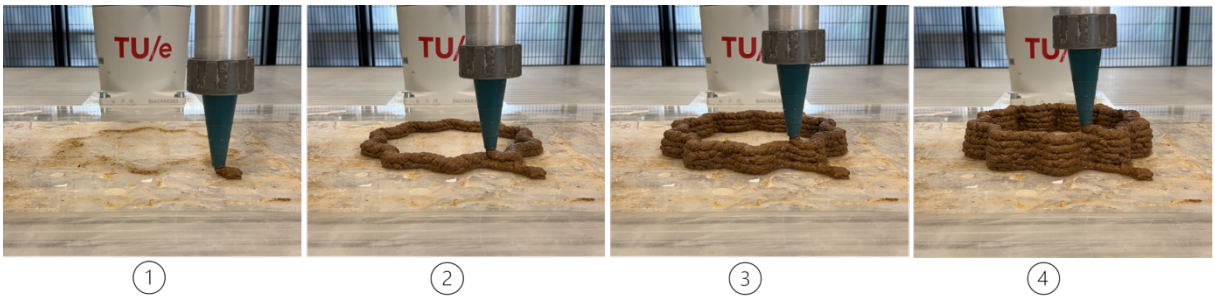

Figure 80. Print process

After the element is printed, the element is leveled. This is done by placing a wooden square on the element. After which the wooden element is pushed until it is levelled, see figure 81. The leveling of each element is done so that after curing it doesn't have to undergo any operation of sawing and sanding. This allows faster construction of the final element. Several pictures of the printing process are shown in figure 81.

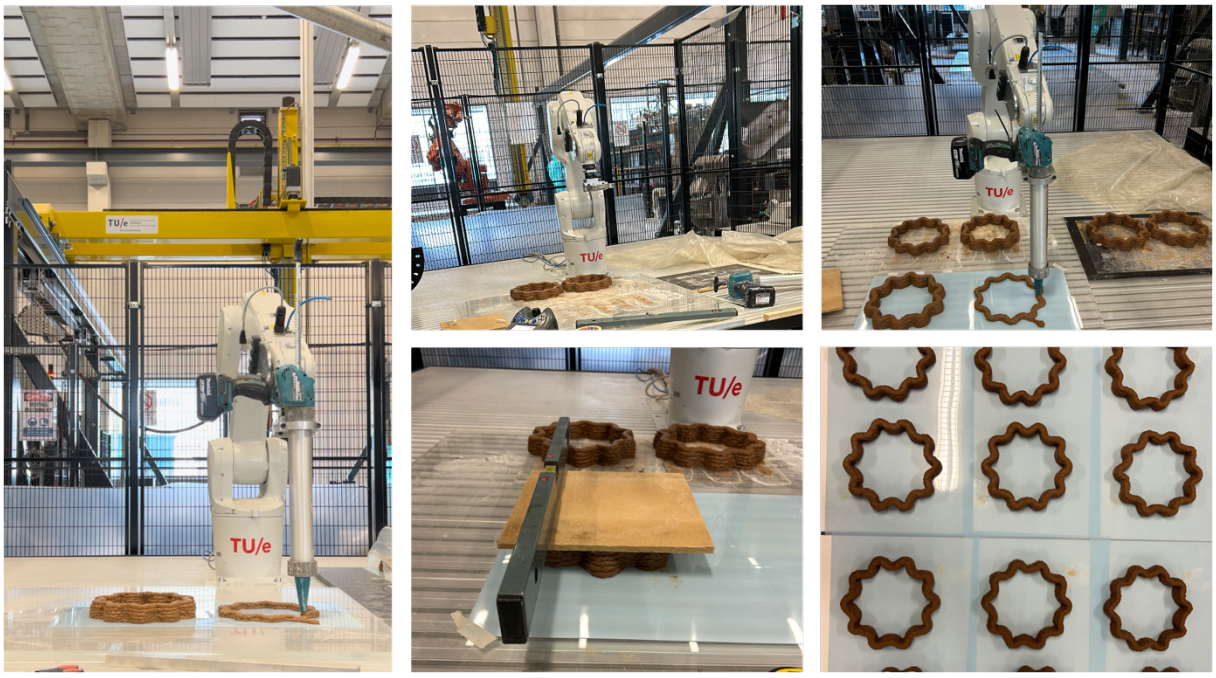

Figure 81. Photos during the printing process

7.3.5 Points of attention during printing

During the printing of the elements, there are a number of concerns that need to be identified. The first concern is blending the cellulose. If this is not done accurately, cellulose lumps will form in the mixture. Since the round nozzle has a small diameter, these cellulose clumps can cause a blockage in the nozzle. Next, the blockage prevents material from being pushed out of the nozzle. This disrupts the printing pattern and requires the element to be reprinted. The second concern is the roughness of the inner wall of the cartridges. Three different cartridges were used during the printing of all the elements. One of the three cartridges could hold more material than the other because the roughness of the inner wall was different. Because more material in the cartridge allowed more than 6 layers to be printed, this required manually turning off the Makita early. Also, in this cartridge, more material stuck to the inner wall. The third point of concern was adjusting the speed to the mixture made. During the printing of the elements, the mixture was mixed simultaneously. As a result, it could happen that the mixture was ready for some time before it could be printed. During this phase, the properties of the mixture changed and the printing speed had to be adjusted to achieve 6 layers. The fourth and final point of interest is that dimensions of the grasshopper model are not exactly the same as the printed elements. For instance, the thickness of the cross-section in grasshopper is 15mm and in the printed element it is 18mm, this is due to the standoff distance of the nozzle. The width and height are not exactly the same as in the grasshopper model because printed elements are shrunk.

7.4 Curing time

After printing (1), the elements were kept under a plastic film in the climate room for 7 days (2). In the climate room it is 20 °C and the average relative humidity (RH) is 60%. is. After 7 days, the elements were turned over so that the bottom side could also cure. After turning them over, the elements cure for another ±7 days after which they can be tested (3). Figure 82 shows the process described above.

7.4.1 Shrinkage

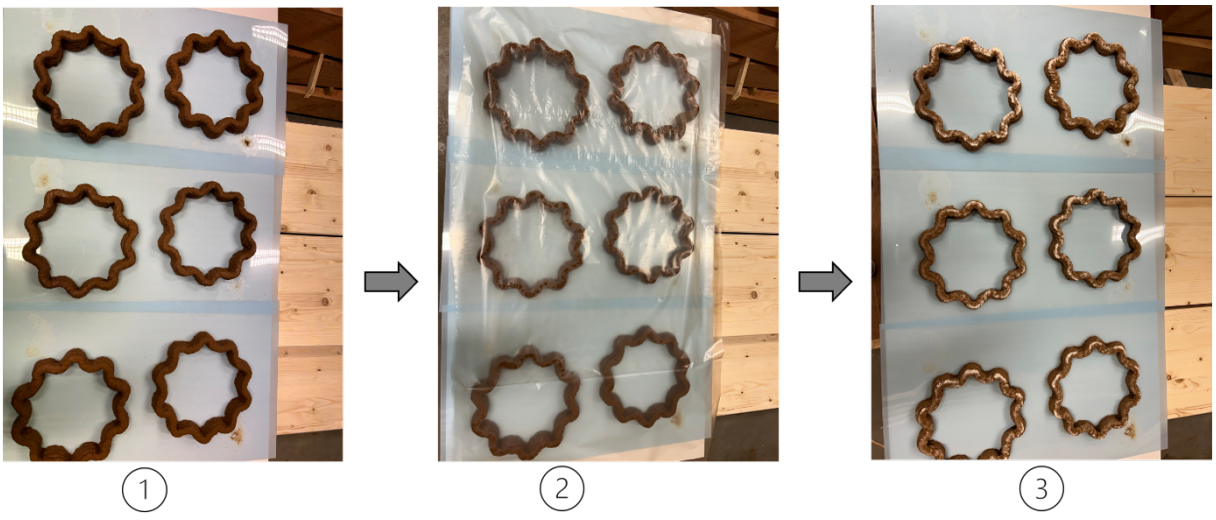

Figure 82. Curing process

In the fresh state, the height of an element composed of 6 layers is 35mm high and 250mm wide. In the hardened state, the height of the element is 30mm and the width is 210mm. This means that all elements shrink 14-16% in height and width during the curing process.

7.5 Final element

The final element consists of 36 elements that are stacked one by one. Figure 83 shows the assembly of the final element. How the elements are connected is described in Chapter 8. Photo 1 shows the first element. Photo 2 shows elements 1 to 12. Photo 3 contains elements 1 to 24, and photo 4 shows all the elements stacked on top of each other. Finally, the top and bottom of the final element are provided with a square wooden plate. The center of the of both wooden plates is provided with a spherical hinge, this allows the column to be placed centrally in the compression testing machine. The wooden plate also ensures that the point load is transferred optimally to the column.

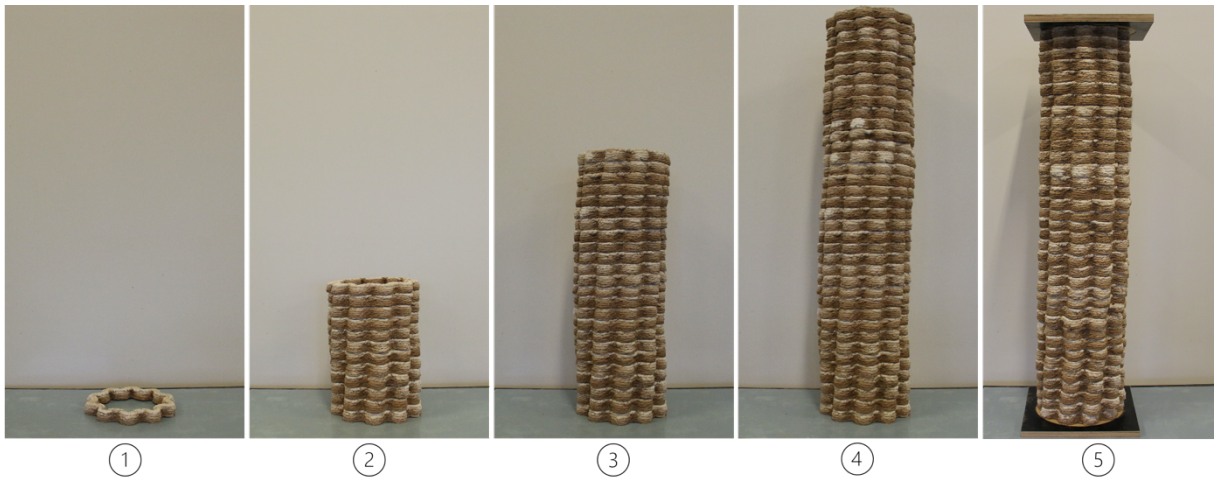

Figure 83. Construction of final element (column)

8. Final element

8.1 Construction final element

The assembly of the final element is shown in figure 84. Glue is used to join the printed wood elements together. Gluing elements is less common than screws or nails but is still used in wood construction [87]. The joint is quite simple and can achieve good strength.

Figure 84. Assembly final element (column)

1. Stacking elements

The bottom and top of the final element are glued to a square wooden plate. In between, 36 elements are glued together one by one.

2. Gluing elements

The glue used for gluing the elements is Bison PU Bruislijm. For the technical data of the glue see Appendix 10 Technical data sheet PU Bruislijm.
The glue is applied to the top of the element. The surface of the top must be clean and free of dust.

3. Spread glue over the element

The glue is spread with a brush over the cross section of the element. For optimal glue bonding between the elements, the underside of the new element to be placed on top was moistened with a damp cloth.

4. Centering elements

After two elements were glued together, the position of the final element was centered. Figure 84.3 shows that above the column, a wooden plate was fitted with a blue square of styrofoam. This styrofoam has at the bottom the cross section of the element to be glued. Figure 84.4 shows the styrofoam fits exactly over the cross section. This means that the column is straight. If the cross-section of the element does not fall under the styrofoam, then the column is not straight. By stacking 36 elements, the column will never be 100% completely straight, this creates a small imperfection. Process 1 to 4 was repeated until the length of 1m was reached.

5. Curing time glue

The technical specification of the glue states that all glue joints must be bonded within 30 minutes, because after 30 minutes the glue begins to fizz. After all elements are glued, the final element should be provided with a pressing pressure of 2-5 kg/cm^2 for 4 hours. In this study, a press pressure of 2 kg/cm^2 was chosen because the behavior of the material was not known. The cross section of the final element is rounded up to 150 cm^2 (since the thickness of the cross-section is 18mm), this means that the pressing force should be 3 kN. Figure 85 shows that the final element is provided 4 hours with a pressing force of 3 kN. The final strength of the adhesive is reached after 24 hours at 20°C.

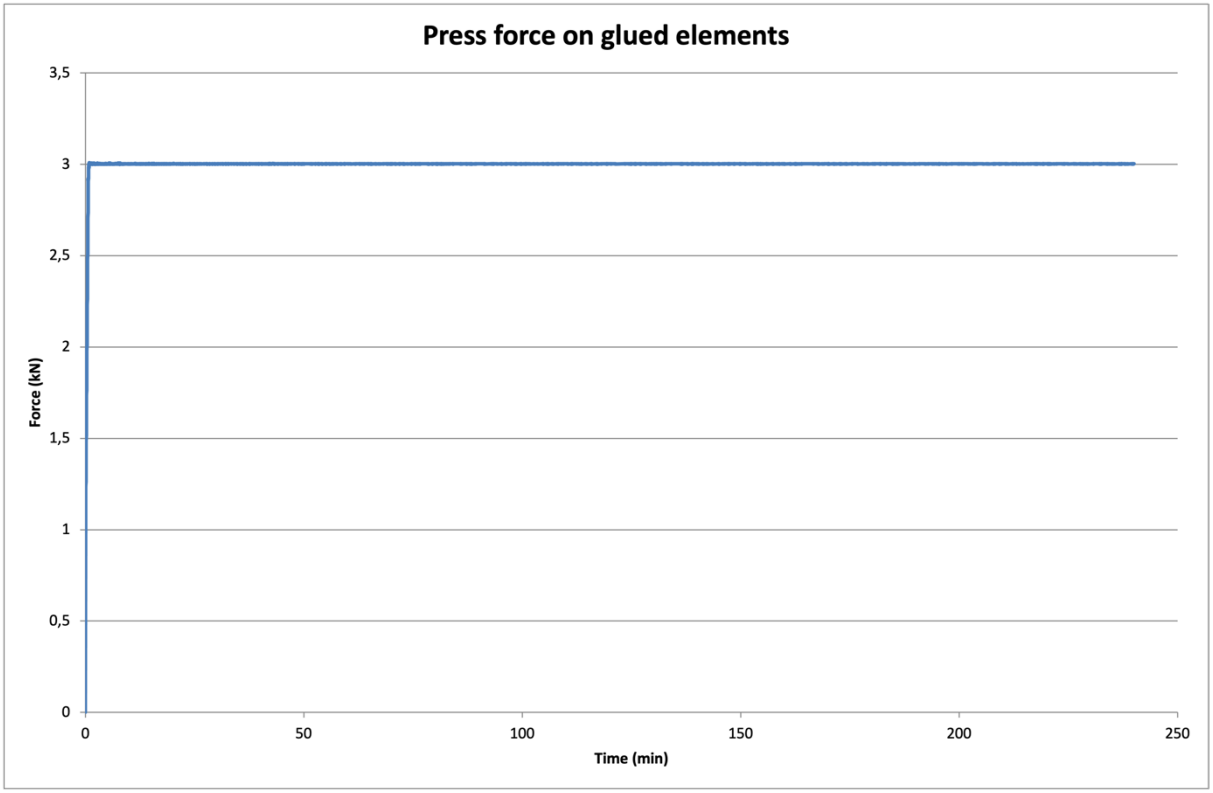

Figure 85. Press force on glued elements

8.2 Structural test

8.2.1 Test set-up

The 3D printed bio-based column was tested in axial compression in the compression testing machine in TU/e's SED lab. The column must be easily supported. Therefore, the final element at the column supports must be free to rotate but fixed to move. Figure 86 shows the experimental set-up for the buckling test of the column. The bottom is fitted with a spherical hinge with a steel plate. The wooden plate of the column fits exactly on this steel plate. The top is also provided with a spherical hinge. Attached to this hinge is a steel plate that fits exactly on the wooden plate and covers the column. The axial pressure point load is transferred through the steel plate to the wooden plate which distributes the load to the column.

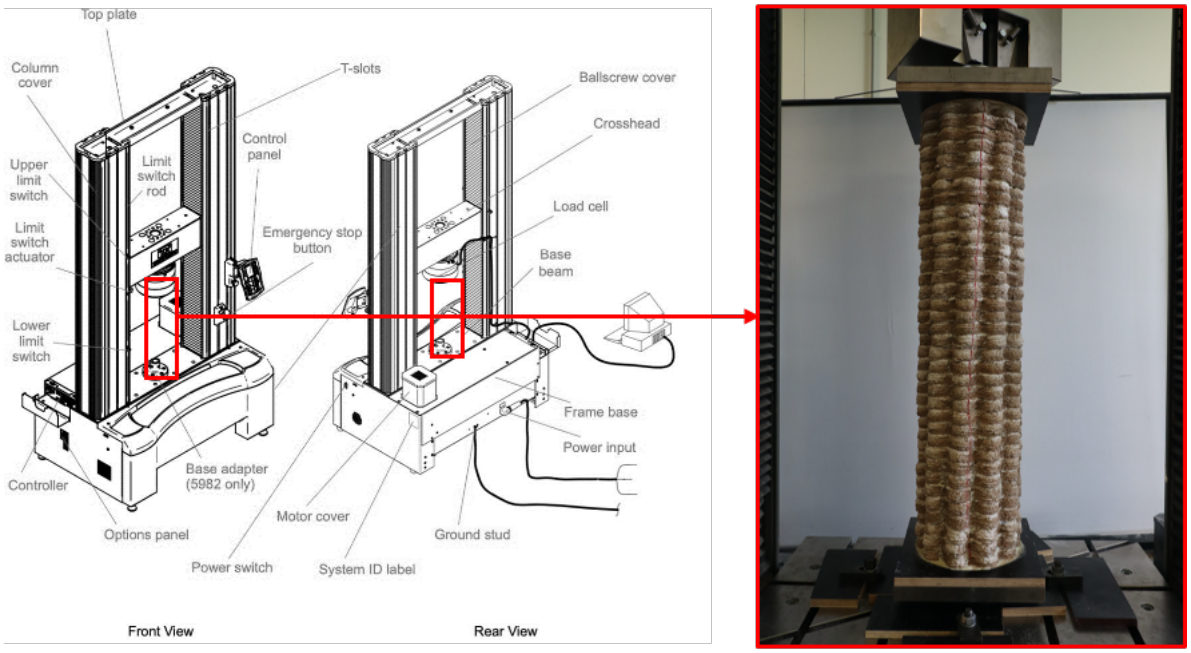

Figure 86. Test set-up buckling test

8.2.2 Buckling test

Figure 87 shows the results of the axial compression test (buckling test) of the column in a force-displacement diagram.

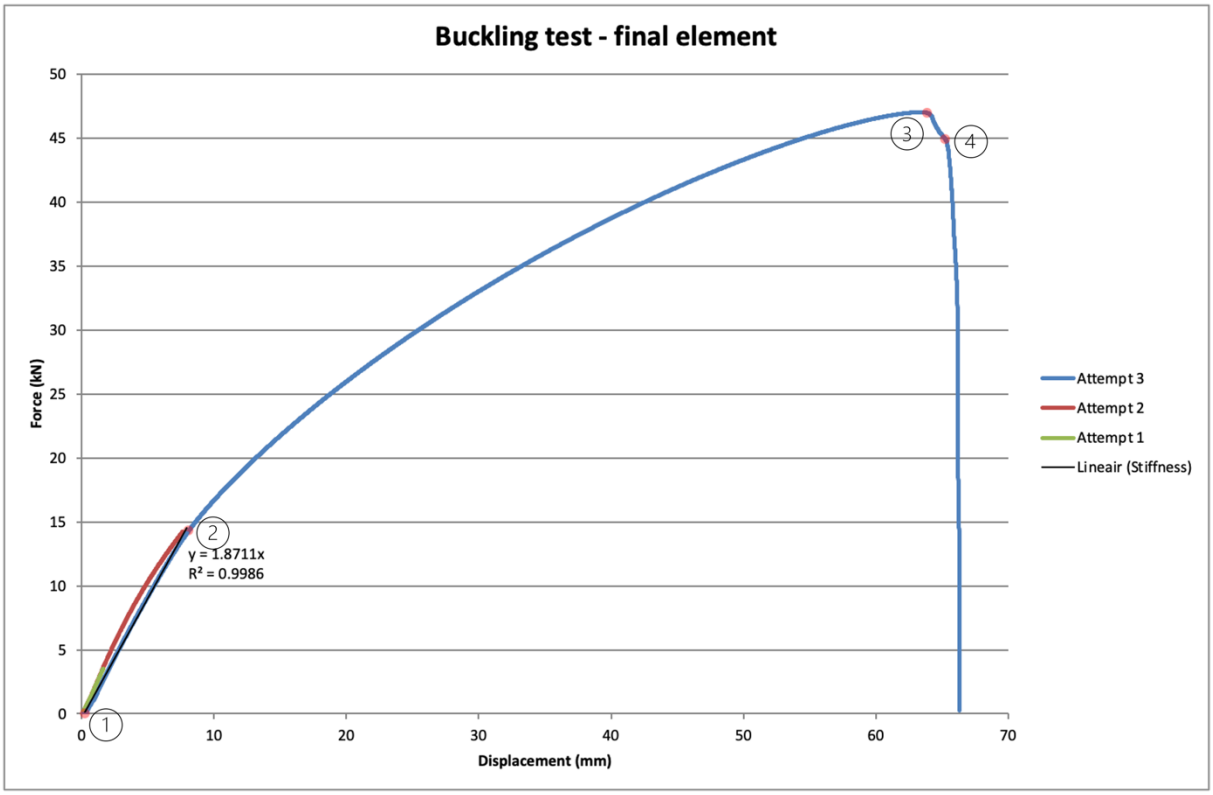

Figure 87. Force displacement diagram buckling test - column

Figure 88 shows the test situation at points 1,2,3 and 4 indicated in the graph. The column was placed in the compression testing machine between two spherical hinges, see figure 88.1. Between points 1 and 2 up to 15 kN, a stiff behavior (stiffness is 1,87 kN/mm) can be observed and the force increases rectilinearly with the deformation. The linear part between point 1 and 2 was caused by the failure of attempts 1 and 2 of the buckling test. In attempts 1 and 2, the photo camera did not work and this caused them to stop early. When starting attempt 3, this created a linear part first. Between figure 88.1. and figure 88.2 it can be seen that the vertical displacement of 10 mm caused by the compression testing machine does not represent horizontal deformation of the column yet. Between points 2 and 3, the displacement increases more than the force increases, creating a decreasing rise. The peak load is reached in point 3 at 46,82 kN and the stress is 312,2 MPa. Figure 88.3 (photo was taken from different angle to clearly show the horizontal displacement) shows that column collapses on global buckling due to the horizontal deformation. After the peak load is reached, the displacement increases and the force decreases. As the displacement continues to increase, pressure in the upper right side of the column (see figure 88.4) becomes so great that a vertical crack is created through the printed layers. Then, on the other side of the column (see upper left figure 88.4), the glue seam between the elements lets go and the column collapses on local buckling. After the column collapsed, the measurements of force and displacement stopped.
A video of the full test is attached to Appendix 11 Videos buckling test.

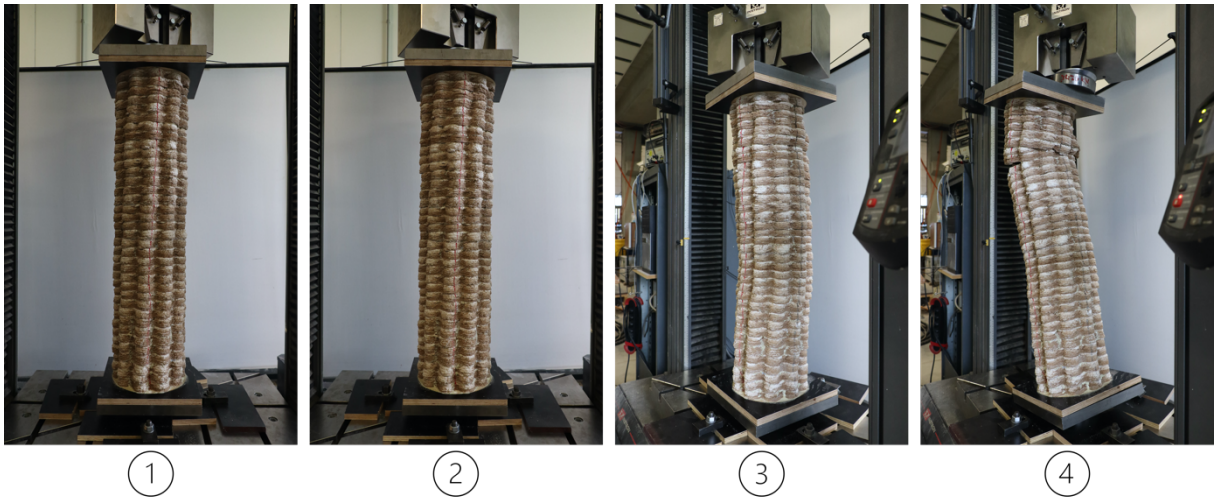

Figure 88. Pictures buckling test

Table 42 summarizes the results of the buckling test, showing the maximum compressive force achieved and the maximum force according to the numerical model.

Table 42. Test result of buckling test

Sample name	Buckling length (mm)	Expected compressive force (kN)	Tested compressive force (kN)	Factor difference
Buckling test	960	41,84	46,82	1,12

9. Conclusion

The aim of this research project was to design and assess the structural performance of an optimized three-dimensional parametric structural element (column) consisting of bio-based material. This one-meter-high column was made by additive manufacturing.

The final mixture used to print the column consists of the materials cellulose, lignin, valida L,3%, bio-glue and bentonite. It is a 100% bio-based material, combined with nice homogeneity, high viscosity and good adhesion, which were successfully demonstrated in the printability tests, shows the potential of this material as a raw material for additive manufacturing.
Also, in horizontal print direction with a value of 11,58 MPa and in vertical print direction with a value of 6,80 MPa, this mixture showed the highest values for compression strength compared to the other bio-based mixtures.

The focus of the column was on stacking the elements to arrive at one meter, where the resistance to buckling should be as high as possible until it collapses globally. Parameters and the optimization target were used to set up the numerical model in the parametric modelling software Rhino, via a script written in grasshopper. While changing the geometric parameters, the script searches for an optimized structure to accommodate an axial compression force. This resulted in a final design where the buckling resistance is as high as possible.
Printing the column is possible, but with limitations regarding to the total height. As a result, the column consists of 36 elements of six layers glued together after curing. If the column needs to be printed in one go in the future, more research needs to be done on material optimization.

The cured bio-based column was tested for buckling in the compression testing machine as this is the main failure mechanism for a slender structure loaded in axial compression. At a force of 46,82 kN, the column failed. The main failure mechanism of the axial compression test was global buckling. The calculated force in the numerical model was 41,81 kN, after which an average factor difference of 1,12 was found between the test and numerical results for the axial force. The cured bio-based material has a Young's modulus of 19,71 MPa. The density of the material is 1.0 Mg/m^3. This places the material under natural materials with an overlap with polymers. It can also be concluded that the bio-based material is still far from being as strong as structural building materials such as wood, steel and concrete.
After this, it can be concluded that it is feasible to create a bio-based optimized column design through additive manufacturing. It has good potential in the construction industry, but further research and refinement of the properties is needed for large-scale structural applications.

The research project was able to smartly evaluate the various components (design, print parameters and mechanical properties) involved in 3D bio-based printing. The components have been designed in such a way that they can be easily modified or replaced with new data, as much more (experimental) research will be done on 3D bio-based printing in the coming years, specifically at Eindhoven University of Technology. Therefore, in the next and final section of this thesis, some recommendations are made based on the findings of this thesis project.

10. Recommendations

This research is a continuation of the thesis project by C. Bierach and A. Coelho started in 2022 using woodglue and methylcellulose as a binder. Significant progress has been made in improving the mixture with woodglue, although much more research needs to be done before it can be used in structures.

TU Delft mix methylcellulose getting mould-free
Mix methylcellulose starts to mould a few days after it is cured. In the case of the two former Delft students, the cured mix also started to mould. The cause of the moulding is probably due to the methylcellulose, since if it is not applied the moulding does not occur. Our study did not address this further because the focus immediately turned to the mixture with woodglue. An investigation can be conducted into how the mould occurs and how it can be prevented.

Mixture with bio-glue turns white
Before printing, the bio-glue mixture has a brown colour. On top of the brown printed layers, a kind of white powder appears during curing, which causes the printed element to turn white. The whitening is not mould, but it does stain clothes, for example. The cause of the whitening is probably due to the addition of Valida L,3%, since if it is not applied the non-mixture does not whiten. In the continuation of the study, no further research was done on whitening as it had no effects on the printing process and mechanical properties. An investigation can be conducted into how the white powder occurs and how it can be prevented.

Getting printed mixture bubble-free
When the mixture is rotated in the cartridge, the mixture contains small air bubbles, these small air bubbles are reflected in the printed elements. The options of vibrating, stamping and kneading were described in the report. From this, it was concluded that these methods did not get the mixture bubble-free. One option that does get the air bubbles out of the mixture is through a vacuum plug mill, but this device is too expensive to buy. Another option not considered in this study is printing with a pump instead of a Makita cartridge. Within the 3D concrete printing department within TU/e, MAI 2 pump pictor is extensively used. This pump ensures that no air bubbles are present when it is printed. In this study, this pump was not applied because only a maximum of 6 layers could be printed and a lot of material was left behind in the connected hose from the robot to the mixing bowl.

Interval time between printed layers
This study did not look at the interval time between the printed layers. An interval time between the printed layers of 15s, 1h, 4h, 7h and 24h was examined by R. Wolfs at TU/e in 3D concrete printing. From this, it was concluded that the higher the interval time between the printed layers, the more the flexural tensile and tensile splitting strength decreases. This study can also be performed on the mixture bio-glue + bentonite. As already shown in this study, 6 new layers could be printed on the first 6 layers after 24 hours.

Material properties
More research into the material properties of the mixture is needed to be fully integrated as a structural building material. The material properties elasticity, tensile strength, brittleness, toughness, creep, hardness, resistance to oxidation and application in aggressive environments still need to be investigated. The tests for compressive strength and flexural strength will have to be carried out several more times to increase reliability. The stiffness of the printed material needs to be increased to come close to the stiffness of wood. Also, the shrinkage is on the high side at 14-16%, this can be reduced by reducing Valida L.3%. Other fibers can be tested as reinforcement. Besides mechanical properties, chemical properties such as moisture resistance, fire safety, corrosion resistance etc. should also be investigated. In short, the structural properties of the mixture need to be improved before it can be used constructively.

Using prestressing to join the printed elements
In the final element (column), all 36 elements are glued together. In 3D concrete printing, it is common for elements to be joined together using internal prestressing. A new study could look into joining elements using internal prestressing..

Time between mix process and print process
The time between the mix process and the print process should be optimized so that the behaviour of the mixture is always the same. In this study, the time between mixing the mix and printing the mix was not always the same. From this, it was concluded that the material changes the print behaviour during this phase. As a result, the printing speed of the robot was adjusted according to the mix to be printed. A study should be conducted on what is the optimal time between the mixing and printing process so that the behaviour of the mix is always the same.

Freshly printed bio-based material
This study did not investigate the printed properties of the mixture in the fresh state. Once the fresh state properties are known, a structural analysis of the printed object can be made. In R. Wolfs' research, five time-dependent material properties were obtained from experimental tests to analyse the behaviour of the print object. These five properties are poisson's ratio, Young's modulus, cohesion between particles, angle of internal fraction and angle of dilatancy. These five material properties in the fresh state can also be investigated for this mixture to analyse the print object.

Curing time material
In this study, it was chosen to cure the elements in the following way: 7 days under plastic foil, then 7 days without plastic foil and after it, turn the elements over and let them cure for another 7 days. Research can be done on the optimal curing time of the elements observing the shrinkage of the elements.

Bibliography

[1] Abergel T, Dean B, Dulac J. Towards a zero-emission, efficient, and resilient buildings and construction sector. 2017.
[2] Cabeza LF, Rincón L, Vilariño V, Pérez G, Castell A. Life cycle assessment (LCA) and life cycle energy analysis (LCEA) of buildings and the building sector: A review. Renewable and Sustainable Energy Reviews 2014;29:394–416. https://doi.org/10.1016/j.rser.2013.08.037.
[3] Huang L, Krigsvoll G, Johansen F, Liu Y, Zhang X. Carbon emission of global construction sector. Renewable and Sustainable Energy Reviews 2018;81:1906–16. https://doi.org/10.1016/j.rser.2017.06.001.
[4] Ministry of Infrastructure and Water Management. Circular Dutch economy by 2050 2021. https://www.government.nl/topics/circular-economy/circular-dutch-economy-by-2050 (accessed January 2, 2023).
[5] Sartori I, Hestnes AG. Energy use in the life cycle of conventional and low-energy buildings: A review article. Energy Build 2007;39:249–57. https://doi.org/10.1016/j.enbuild.2006.07.001.
[6] Sustainability of biobased materials in a circular economy n.d. https://www.maastrichtuniversity.nl/research/sustainability-of-biobased-materials-circular-economy (accessed January 2, 2023).
[7] King M. How Industry 4.0 and BIM are Shaping the Future of the Construction Environment. GIM International 2017.
[8] Camacho DD, Clayton P, O'Brien W, Ferron R, Juenger M, Salamone S, et al. Applications of additive manufacturing in the construction industry - A prospective review. ISARC 2017 - Proceedings of the 34th International Symposium on Automation and Robotics in Construction, International Association for Automation and Robotics in Construction I.A.A.R.C); 2017, p. 246–53. https://doi.org/10.22260/isarc2017/0033.
[9] Gibson I, Rosen DW, Stucker B. Additive manufacturing technologies: Rapid prototyping to direct digital manufacturing. Springer US; 2010. https://doi.org/10.1007/978-1-4419-1120-9.
[10] Gauss C, Pickering KL, Muthe LP. The use of cellulose in bio-derived formulations for 3D/4D printing: A review. vol. 4. Elsevier B.V.; 2021. https://doi.org/10.1016/j.jcomc.2021.100113.
[11] Pessoa S, Guimarães AS, Lucas SS, Simões N. 3D printing in the construction industry - A systematic review of the thermal performance in buildings. Renewable and Sustainable Energy Reviews 2021;141. https://doi.org/10.1016/j.rser.2021.110794.
[12] Guvendiren M, Molde J, Soares RMD, Kohn J. Designing Biomaterials for 3D Printing. ACS Biomater Sci Eng, vol. 2, American Chemical Society; 2016, p. 1679–93. https://doi.org/10.1021/acsbiomaterials.6b00121.
[13] Kruth JP, Mercelis P, Van Vaerenbergh J, Froyen L, Rombouts M. Binding mechanisms in selective laser sintering and selective laser melting. vol. 11. 2005. https://doi.org/10.1108/13552540510573365.
[14] Liebrand T. 3D printed fiber reinforced lignin. Building Technology. Tu Delft, 2018.
[15] Hubs n.d.
[16] Mantrala MK, Suresh G, Narayana KL, Mallik MK. A Review on Development of Medical Implants by Rapid Prototyping Technology Article in. International Journal of Pure and Applied Mathematics 2017;117:257–76.
[17] Materiom n.d.
[18] Ford S, Despeisse M. Additive manufacturing and sustainability: an exploratory study of the advantages and challenges. J Clean Prod 2016;137:1573–87. https://doi.org/10.1016/j.jclepro.2016.04.150.
[19] Dr-Ing Michael Rosenthal A, Henneberger C, Gutkes A, Claus-Thomas Bues habil. Liquid Deposition Modeling-a promising approach for 3D printing of wood. European Journal of Wood and Wood Products 2018. https://doi.org/10.1007/s00107.

[20] Kariz M, Sernek M, Kuzman MK. Use of wood powder and adhesive as a mixture for 3D printing. European Journal of Wood and Wood Products 2016;74:123–6. https://doi.org/10.1007/s00107-015-0987-9.
[21] Omlab n.d.
[22] Zarna C, Opedal MT, Echtermeyer AT, Chinga-Carrasco G. Reinforcement ability of lignocellulosic components in biocomposites and their 3D printed applications – A review. Composites Part C: Open Access 2021;6. https://doi.org/10.1016/j.jcomc.2021.100171.
[23] Liebrand T. 3D printed fiber reinforced lignin. Building Technology. Tu Delft, 2018.
[24] Bierach C. WOOD-BASED 3D PRINTING. Architecture. TU Delft, 2022.
[25] Alberts Coelho A. CELLULOSE & LIGNIN IN ADDITIVE MANUFACTURING. Architecture. TU Delft, 2022.
[26] Garnousset P, Detoeuf M, de Pingon P. Blast-studio 2018. https://www.blast-studio.com (accessed January 23, 2023).
[27] Mitra S. 3D-PRINTED LIVING SOIL WALLS BY UNIVERSITY OF VIRGINIA CAN GROW PLANTS. YANKO DESIGN 2022.
[28] Aouf RS. University of Virginia 3D-prints living soil walls that sprout greenery. Dezeen 2022.
[29] Parkes J. Tecla house 3D-printed from locally sourced clay. Dezeen 2021.
[30] Eco-sustainable 3D printed house - Tecla. WASP 2019. https://www.3dwasp.com/en/3d-printed-house-tecla/ (accessed February 1, 2023).
[31] Chiusoli A. The 3d printed house Gaia. WASP 2018. https://www.3dwasp.com/en/3d-printed-house-gaia (accessed January 26, 2023).
[32] Marani M. The Gaia House is a 3D-printed prototype made of biodegradable materials. The Architect's Newspaper 2019.
[33] Jordahn S. 3D-printed Gaia house is made from biodegradable materials. Dezeen 2019.
[34] Sjöström E. Wood Chemistry (Second Edition) 1993:1–20. https://www.sciencedirect.com/science/article/abs/pii/B978008092589950005X?via%3Dihub (accessed March 7, 2023).
[35] Forest Service U, Products Laboratory F. Wood Handbook, Wood as an Engineering Material. 2010.
[36] Zarna C, Opedal MT, Echtermeyer AT, Chinga-Carrasco G. Reinforcement ability of lignocellulosic components in biocomposites and their 3D printed applications – A review. Composites Part C: Open Access 2021;6. https://doi.org/10.1016/j.jcomc.2021.100171.
[37] Chiujdea RS, Nicholas P. Design and 3D Printing Methodologies for Cellulose-based Composite Materials. n.d.
[38] Vijay Y, Sanandiya ND, Dritsas S, Fernandez JG. Control of process settings for large-scale additive manufacturing with sustainable natural composites. Journal of Mechanical Design 2019;141. https://doi.org/10.1115/1.4042624.
[39] Firmanda A, Syamsu K, Sari YW, Cabral J, Pletzer D, Mahadik B, et al. 3D printed cellulose based product applications. Mater Chem Front 2022;6:254–79. https://doi.org/10.1039/d1qm00390a.
[40] Gunasekera DHAT, Kuek S, Hasanaj D, He Y, Tuck C, Croft AK, et al. Three dimensional ink-jet printing of biomaterials using ionic liquids and co-solvents. Faraday Discuss 2016;190:509–23. https://doi.org/10.1039/c5fd00219b.
[41] Yang J, An X, Liu L, Tang S, Cao H, Xu Q, et al. Cellulose, hemicellulose, lignin, and their derivatives as multi-components of bio-based feedstocks for 3D printing. Carbohydr Polym 2020;250. https://doi.org/10.1016/j.carbpol.2020.116881.
[42] Mastrolitti S, Borsella E, Giuliano A, Petrone M, De Bari I, Gosselink R, et al. Sustainable lignin valorization Technical lignin, processes and market development With inputs from: H. 2021.

[43] Giachini PAGS, Gupta SS, Wang W, Wood D, Yunusa M, Baharlou E, et al. A P P L I E D S C I E N C E S A N D E N G I N E E R I N G Additive manufacturing of cellulose-based materials with continuous, multidirectional stiffness gradients. vol. 6. 2020.
[44] Rajesh Banu J, Kavitha S, Yukesh Kannah R, Poornima Devi T, Gunasekaran M, Kim SH, et al. A review on biopolymer production via lignin valorization. Bioresour Technol 2019;290. https://doi.org/10.1016/j.biortech.2019.121790.
[45] Chung H, Washburn NR. Extraction and Types of Lignin. Lignin in Polymer Composites, Elsevier Inc.; 2016, p. 13–25. https://doi.org/10.1016/B978-0-323-35565-0.00002-3.
[46] Kurlansky M. Paper : paging through history. WW Norton & Company 2016. https://archive.org/details/paperpagingthrou0000kurl (accessed February 8, 2023).
[47] Mili M, Hashmi SAR, Ather M, Hada V, Markandeya N, Kamble S, et al. Novel lignin as natural-biodegradable binder for various sectors—A review. J Appl Polym Sci 2022;139. https://doi.org/10.1002/app.51951.
[48] Ebers LS, Arya A, Bowland CC, Glasser WG, Chmely SC, Naskar AK, et al. 3D printing of lignin: Challenges, opportunities and roads onward. Biopolymers 2021;112. https://doi.org/10.1002/bip.23431.
[49] Tanase-Opedal M, Espinosa E, Rodríguez A, Chinga-Carrasco G. Lignin: A biopolymer from forestry biomass for biocomposites and 3D printing. Materials 2019;12. https://doi.org/10.3390/ma12183006.
[50] Suntornnond R, An J, Chua CK. Roles of support materials in 3d bioprinting - Present and future. Int J Bioprint 2017;3:83–6. https://doi.org/10.18063/IJB.2017.01.006.
[51] De Carvalho Oliveira G, Filho GR, Vieira JG, De Assunção RMN, Da Silva Meireles C, Cerqueira DA, et al. Synthesis and application of methylcellulose extracted from waste newspaper in CPV-ARI Portland cement mortars. J Appl Polym Sci 2010;118:1380–5. https://doi.org/10.1002/app.32477.
[52] Li H, Tan YJ, Leong KF, Li L. 3D Bioprinting of Highly Thixotropic Alginate/Methylcellulose Hydrogel with Strong Interface Bonding. ACS Appl Mater Interfaces 2017;9:20086–97. https://doi.org/10.1021/acsami.7b04216.
[53] De Carvalho Oliveira G, Filho GR, Vieira JG, De Assunção RMN, Da Silva Meireles C, Cerqueira DA, et al. Synthesis and application of methylcellulose extracted from waste newspaper in CPV-ARI Portland cement mortars. J Appl Polym Sci 2010;118:1380–5. https://doi.org/10.1002/app.32477.
[54] Norström E, Demircan D, Fogelström L, Khabbaz F, Malmström E. Green Binders for Wood Adhesives. Applied Adhesive Bonding in Science and Technology, InTech; 2018. https://doi.org/10.5772/intechopen.72072.
[55] Das AK, Agar DA, Rudolfsson M, Larsson SH. A review on wood powders in 3D printing: processes, properties and potential applications. Journal of Materials Research and Technology 2021;15:241–55. https://doi.org/10.1016/j.jmrt.2021.07.110.
[56] Barakat A, de Vries H, Rouau X. Dry fractionation process as an important step in current and future lignocellulose biorefineries: A review. Bioresour Technol 2013;134:362–73. https://doi.org/10.1016/j.biortech.2013.01.169.
[57] Mayer-Laigle C, Rajaonarivony RK, Blanc N, Rouau X. Comminution of dry lignocellulosic biomass: Part II. technologies, improvement of milling performances, and security issues. Bioengineering 2018;5. https://doi.org/10.3390/bioengineering5030050.
[58] Ayrilmis N, Kariž M, Kitek Kuzman M. Effect of wood flour content on surface properties of 3D printed materials produced from wood flour/PLA filament. International Journal of Polymer Analysis and Characterization 2019;24:659–66. https://doi.org/10.1080/1023666X.2019.1651547.
[59] Henke K, Treml S. Wood based bulk material in 3D printing processes for applications in construction. European Journal of Wood and Wood Products 2013;71:139–41. https://doi.org/10.1007/s00107-012-0658-z.

[60] Tao Y, Pan L, Liu D, Li P. A case study: Mechanical modeling optimization of cellular structure fabricated using wood flour-filled polylactic acid composites with fused deposition modeling. Compos Struct 2019;216:360–5. https://doi.org/10.1016/j.compstruct.2019.03.010.
[61] Bi H, Ren Z, Guo R, Xu M, Song Y. Fabrication of flexible wood flour/thermoplastic polyurethane elastomer composites using fused deposition molding. Ind Crops Prod 2018;122:76–84. https://doi.org/10.1016/j.indcrop.2018.05.059.
[62] Chawla K, Singh J, Singh R. On recyclability of thermosetting polymer and wood dust as reinforcement in secondary recycled ABS for nonstructural engineering applications. Journal of Thermoplastic Composite Materials 2022;35:913–37. https://doi.org/10.1177/0892705720925135.
[63] Chen M, Liu B, Li L, Cao L, Huang Y, Wang S, et al. Rheological parameters, thixotropy and creep of 3D-printed calcium sulfoaluminate cement composites modified by bentonite. Compos B Eng 2020;186. https://doi.org/10.1016/j.compositesb.2020.107821.
[64] Peeters J, van der Veen R, Helgers R, Långström O, Bambi M, Papworth N, et al. Resisting Plastics for Ambiguous Results. Delft: 2019.
[65] Tonk R. Natural fibers for sustainable additive manufacturing: A state of the art review. Mater Today Proc, vol. 37, Elsevier Ltd; 2020, p. 3087–90. https://doi.org/10.1016/j.matpr.2020.09.017.
[66] Väisänen T, Das O, Tomppo L. A review on new bio-based constituents for natural fiber-polymer composites. vol. 149. Elsevier Ltd; 2017. https://doi.org/10.1016/j.jclepro.2017.02.132.
[67] Rowell RM. Natural fibres: types and properties. University of Wisconsin 2017:3–66.
[68] Saadi MASR, Maguire A, Pottackal NT, Thakur MSH, Ikram MM, Hart AJ, et al. Direct Ink Writing: A 3D Printing Technology for Diverse Materials. Advanced Materials 2022;34. https://doi.org/10.1002/adma.202108855.
[69] Pulp for paper, board and tissue 2023. https://www.storaenso.com/en/products/market-pulp/pulp-for-paper-board-and-tissue (accessed November 15, 2023).
[70] Sappi Maastricht BV. 2022.
[71] Soda lignin 2023. https://www.biosynth.com/p/FS180396/8068-05-1-soda-lignin (accessed November 15, 2023).
[72] Methocel - Methylcellulose 2023. https://specialingredientseurope.com/products/methyl-cellulose-e461 (accessed November 15, 2023).
[73] Correa D, Papadopoulou A, Guberan C, Jhaveri N, Reichert S, Menges A, et al. 3D-Printed Wood: Programming Hygroscopic Material Transformations. 3D Print Addit Manuf 2015;2:106–16. https://doi.org/10.1089/3dp.2015.0022.
[74] Mineralsplus SE. Portaclay A 90 Sodium bentonite Technical Data CHEMICAL ANALYSIS Mean values. 2012.
[75] 50g Unidirectional Flax Fibre Tape 2023. https://www.easycomposites.eu/50g-unidirectional-flax-fibre-tape (accessed November 15, 2023).
[76] Robotics A. Product specification - IRB 1200. 2014.
[77] DCG140 DCG180. n.d.
[78] NEN-EN 196-1_2016 . n.d.
[79] Een Box- en Whisker-grafiek maken 2023. https://support.microsoft.com/nl-nl/office/een-box-en-whisker-grafiek-maken-62f4219f-db4b-4754-aca8-4743f6190f0d (accessed October 31, 2023).
[80] Materials_ Engineering, Science, Processing and Design (PDFDrive) n.d.
[81] PreethaV, KalaivaniK, NavaneethaS, SenthilkumarV. Buckling Analysis of columns. 2019.

[82] Yoo CH, Lee SC. Buckling of Columns. Stability of Structures, Elsevier; 2011, p. 1–73. https://doi.org/10.1016/b978-0-12-385122-2.10001-6.
[83] Veludurthi A, Bolleddu V. Experimental buckling analysis of NACA 63415 aerofoil wind turbine blade. Mater Today Proc, vol. 46, Elsevier Ltd; 2021, p. 205–11. https://doi.org/10.1016/j.matpr.2020.07.413.
[84] Preisinger C. Welcome to Karamba3D. Linking Structure and Parametric Geometry 2013:110–3. https://manual-1-3.karamba3d.com (accessed October 5, 2023).
[85] Deetman A, Bos D, Ferugson M, Versteege J. 3DCP-TUe / SaladSlicer 2023. https://github.com/3DCP-TUe/SaladSlicer (accessed October 5, 2023).
[86] Azhar AA, Khan A. Shape optimization of compressed members under buckling Master Thesis. 2021.
[87] Custódio J, Broughton J, Cruz H. A review of factors influencing the durability of structural bonded timber joints. Int J Adhes Adhes 2009;29:173–85. https://doi.org/10.1016/j.ijadhadh.2008.03.002.

List of figures and tables

Appendix

Appendix 1 Contact information

Appendix 2 Mix process

Appendix 3 Assessing mixtures

Appendix 4 Product specifications ABB IRB 1200-5/0.9

Appendix 5 RAPID script

Appendix 6 Information printed elements

Appendix 7 Compression tests

Appendix 8 Flexural tests

Appendix 9 Overview Grasshopper scripts

Appendix 10 Technical data sheet PU Bruislijm

Appendix 11 Videos buckling test